5-2019

# Optimal Control of UV-Induced Curing Processes for Layer-by-Layer Manufacturing of Composites

Shiferaw Damtie Beyene
*Clemson University*, shiferawdamtie@gmail.com

# Optimal Control of UV-Induced Curing Processes for Layer-by-Layer Manufacturing of Composites

---

A Dissertation
Presented to
the Graduate School of
Clemson University

---

In Partial Fulfillment
of the Requirements for the Degree
Doctor of Philosophy
Automotive Engineering

---

by
Shiferaw Damtie Beyene
May 2019

---

Accepted by:
Dr. Beshah Ayalew, Committee Chair
Dr. Srikanth Pilla, Co-Chair
Dr. Yunyi Jia
Dr. Matthias Schmid

# Abstract

Composite materials are becoming viable solutions for making safe, yet lighter and more fuel-efficient vehicles in the automotive industry. However, conventional thermal-based composite manufacturing methods are energy intensive. Potential alternatives are radiation-based curing processes which lend themselves to layer-by-layer additive processes that are suitable for making thick structural parts. This dissertation documents an investigation into ultraviolet (UV) induced curing and layering processes including schemes for their optimization and control. First, a curing process model is developed that is comprised of the coupled cure-kinetics and thermal evolution for a cationic polymerization of a single layer of material. This model is then extended to the process of concurrent layering and curing of multiple layers. The model for processing multiple layers is characterized as a multi-mode hybrid system that switches modes both when the UV source is turned off and when a new layer is added. A computational framework is outlined for determining the optimal sequence of switching times that gives a minimal cure level deviation across all layers subjected to the multi-mode hybrid system model of the process. For validation purposes, a one layer material with two mode has been considered. Comparison of the hardness of a sample cured with optimal switching time versus another sample cured for a longer time showed similar hardness values while using energy/ total time.

To improve the interlaminar shear strength, the effect of in-situ consolidation

pressure on the inter-laminar shear strength of the final product is assessed experimentally. Using the optimal time sequence, a fiber-reinforced composite is made with in-situ consolidation and curing. The results showed that thick composite parts fabricated with in-situ consolidation and UV curing process, with the optimal sequence, showed increased inter-laminar shear strength with increases of the consolidation pressure up to a certain point. An increase in consolidation pressure beyond this point decreased the interlaminar-shear strength. Scanning electron microscopy (SEM) is used to investigate the effect of compaction on the microstructure of the final cured product.

For online control, first, a nonlinear model predictive control (NMPC) scheme is outlined for UV-induced acrylate-based curing of a single layer thick composite part. Then, the model is extended for switching nonlinear model predictive control (SNMPC) for layer-by-layer curing process. The key characteristic is that the processes model switches when a new layer is added to the existing layer. Open loop optimal control is used to determine the optimal layering time and temperature profile which give a nearly uniform cure distribution of a thick composite material. Once the temperature trajectory and optimal time sequences are found, the SNMPC is implemented for online control. The objective is to determine theoretical optimal behavior which is then used for online SNMPC for tracking the reference temperature distribution. To demonstrate the effectiveness of the proposed approach a three-layer fiber-reinforced resin is considered and results show a very good agreement between the reference temperature distribution and SNMPC.

# Dedication

This dissertation is dedicated to my parents and siblings, especially to my elder brother Abebe D. Beyene (PhD).

# Acknowledgments

Firstly, I would like to express my sincere gratitude to my advisor Dr. Beshah Ayalew and co-advisor Dr. Srikanth Pilla for the continuous support of my Ph.D study and related research, for their patience, motivation, and immense support. Their guidance helped me in all the time of research. I could not have imagined having a better advisor and co-advisor for my Ph.D study. Besides my advisors, I would like to thank the rest of my dissertation committee: Dr. Yunyi Jia and Dr. Matthias Schmid for their insightful comments and encouragement. Last but not the least, I would like to thank my family: my parents and my siblings for supporting me throughout my PhD study and my life in general.

This dissertation would not have been possible without funding from the National Science Foundation, grant number: CMMI-1537756

# Table of Contents

# List of Tables

# List of Figures

# Chapter 1

# Introduction

## 1.1 Motivation

Composites have become a noteworthy class of structural materials and are either utilized or being considered for use as a substitution for metals in many parts in automotive, aerospace and other similar industries where weight reduction is critical in their structural components. Composites offer a combination of strength and modulus which are equal or better than most metallic materials (Fig. 1.1). This is due to their low density, the high strength to weight ratios and modulus to weight ratios. Moreover, composites have excellent fatigue damage tolerance [1]. Composites can offer a range of mass reductions over steel ranging from $25-30\%$ (glass fiber systems) up to $60-70\%$ (carbon fiber systems). A weight reduction directly minimizes energy consumption as, with the exception of aerodynamic resistance, the energy required to move a vehicle is directly proportional to the vehicle's weight, thus reducing the environmental impact of all upstream activities such as fuel supply, engine energy conversion etc.[2]. A 1% reduction in the gross weight of an empty aircraft will reduce fuel consumption upto 0.75% [3, 4]. This research is motivated by the po-

tential benefit of radiation-based additive manufacturing (AM) for thick composites. AM has transformed into a robust manufacturing paradigm and enabled producing highly customized parts with significantly improved mechanical properties, compared to resin alone. AM of polymers has found their potential application in aerospace industries for creating complex light weight structures [5], structural models [6, 7], for vehicle structures [8] and medical fields for printing tissues and organs [9, 10, 11].

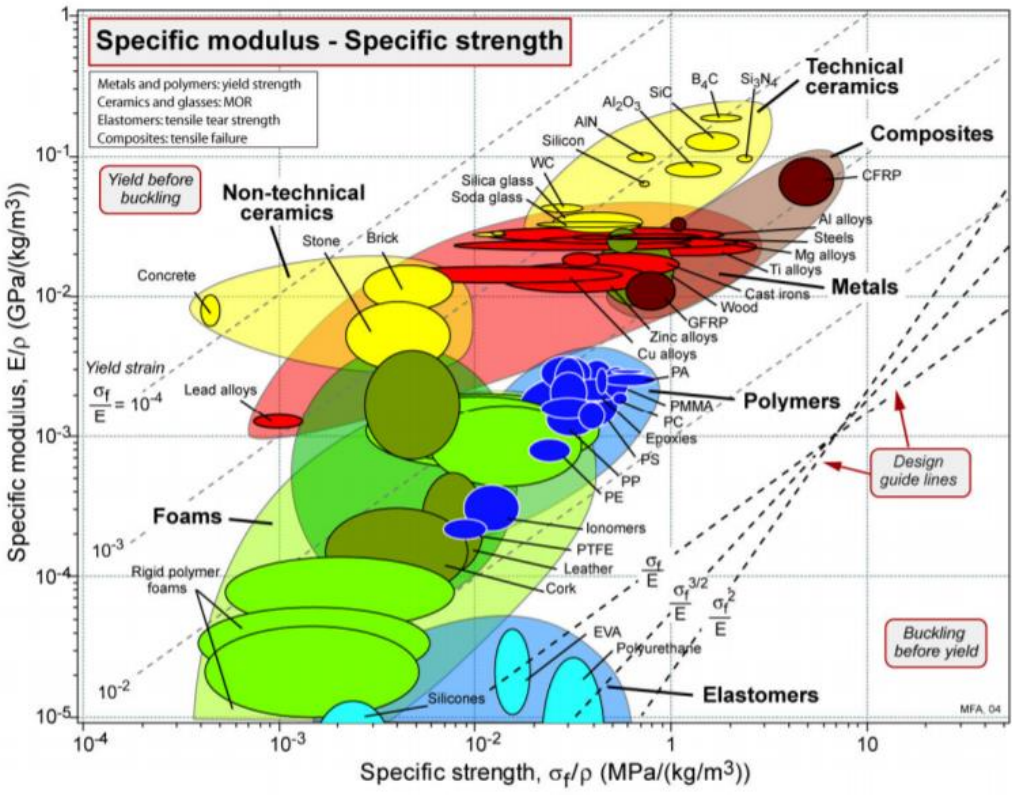


Figure 1.1: Specific stiffness and specific strength for various materials, the figure highlights Carbon Fiber Reinforced Polymer (CFRP) Composites and Glass Fiber Reinforced Polymer (GFRP) Composites [12]

## 1.2 Background

### 1.2.1 Free radical polymerization

Majority of UV cure chemistry is the free radical type which mainly uses acrylate components. There are variety of monomors and oligomers which provide a range of properties are available. The free radicals can be produced by thermal, catalytic or photo-chemical decomposition of organic peroxides, hydroperoxides, azo and diazo compounds. The growth of the polymer chains occur by successive addition of monomers. The general assumption is that the radical reactivity is independent of the chain length and termination occurs via combination or disproportionation. Light induced polymerization stops when light source is off. Free radical polymerization are susceptible to oxygen inhibition where oxygen in the air prevents the molecules at the surface from polymerization. The schematic of free radical polymerization is given Fig. 1.2 and the initation, propagation and termination mechanisms are shown in Fig. 1.3.

The comparision between free radical and cationic photopolymerization is summerized in Table 1.1. There have been few works on free-radical based thick composite

Table 1.1: Comparison between free radical and cationic curing [15]

| | Free-radical | Cationic |
|---|---|---|
| Cost | Low | High |
| Mechanical Properties | Low | High |
| Shrinkage | High | Low |
| Reactivity | High | Low |
| Inhibition | Oxygen | Water |

manufacturing, however there is no work so far which uses cationic based thick composite manufacturing. Therefore , in this dissertation cationc photoinitatiors are used for offline optimal control and free radical photoinitators are used for online control.

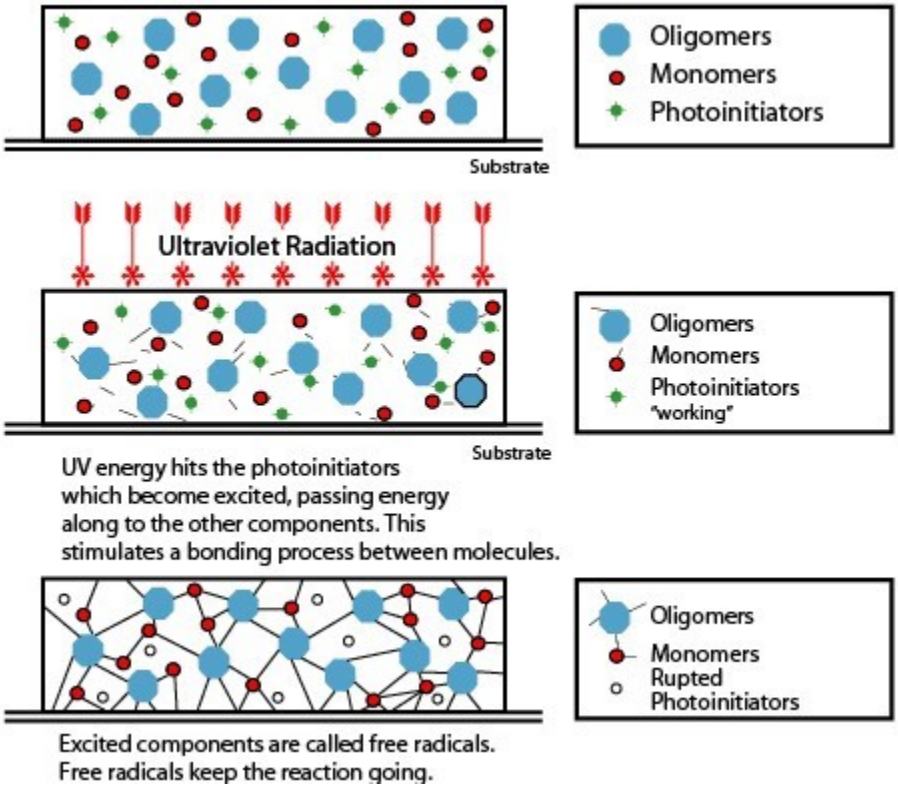


Figure 1.2: Schematic of free radical polymerization [13]

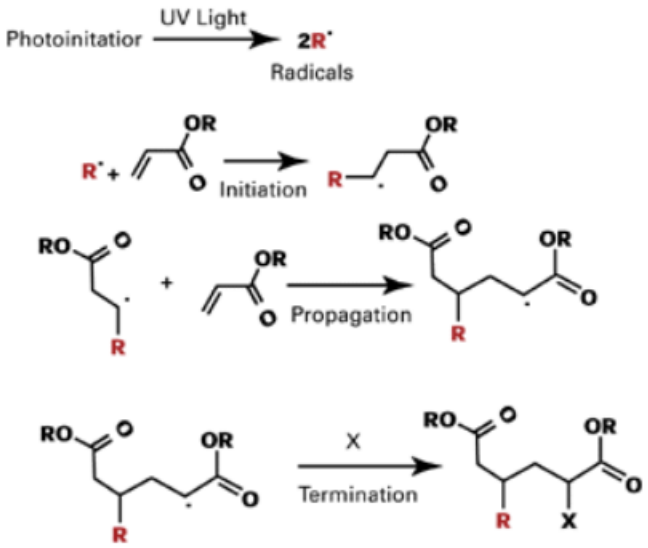


Figure 1.3: Free radical polymerization mechanism[14]

### 1.2.2 Cationic polymerization

Cationic polymerization is a type of chain growth polymerization in which a cationic initiator transfers a proton to a monomer which then becomes reactive. In cationic polymerization mainly contain epoxy and/or vinyl ether components and very small amounts of (strong) Lewis acids. Currently, there is a limited variety of monomers and/or oligomers for cationic polymerization. Once it is exposed to light , curing can continue after the light is off. However, the cure rate is less than as compared to the one with light on and it depends on the temperature. Cationic photoinitiators are humidity vulnerable. The cationic polymerization mechanism is shown in Fig. 1.4.

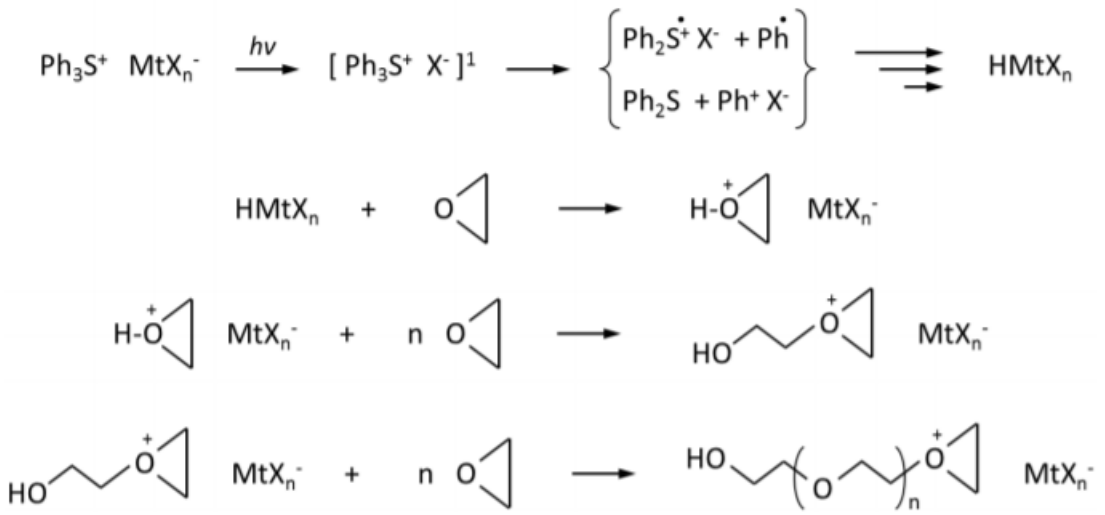


Figure 1.4: Cationic photopolymerization of an epoxy monomer in the presence of a generic triphenyl sulfonium salt[16]

### 1.2.3 Ultraviolet (UV) radiation

In the past, thermal curing had been the sole mechanism for the curing of temperature sensitive substrates, like plastics, papers, woods. However, nowadays,

UV curing has become an alternate curing mechanism to thermal curing. These alternative curing technology uses the energy of photons of radiation sources in the short wavelength region of electromagnetic spectrum in order to form reactive species, which initiate a rapid chain growth curing reaction. Figure 1.5 shows the electromagnetic energy spectrum. It ranges from the near infrared (NIR). To electron beams and X-rays. The UV region is further classified into UV-A, UV-B, and UV-C radiation, is mainly used for this technology. For a resin to fully cured, the resin must receive a sufficient irradiance at the right spectrum. LEDs have a narrow spectral bandwidth, hence it is essential that the UV LED systems wave length matches the absorption spectra of the photo-initiators used. If the spectral absorption of the photo-initiator is different from the UV LED spectral output the resin will not cure. So if the spectral of the two doesnt match the exposure time or irradiance level will not cure the resin.

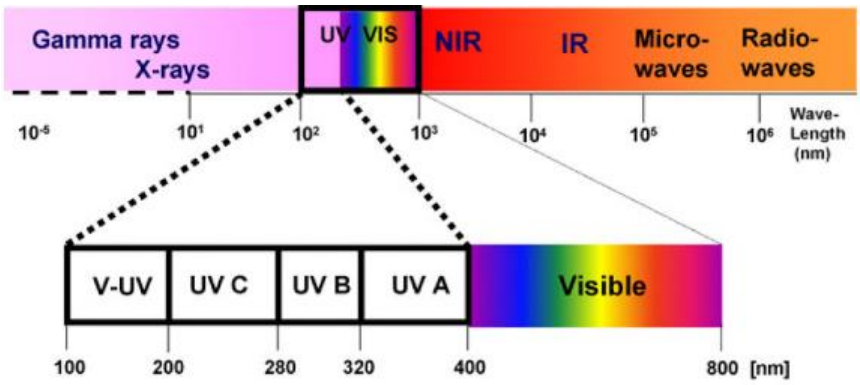


Figure 1.5: Electromagnetic spectrum [15]

## 1.3 Dissertation Outline

The remaining parts of the dissertation are organized as follows: Chapter 2, first describes a curing process model comprised of the coupled cure-kinetics and ther-

mal evolution in a cationic polymerization of a single layer of material and then extends it to the process of concurrent layering and curing of multiple layers. The model for processing multiple layers is characterized as a multi-mode system that switches modes both when the UV source is turned off and when a new layer is added. Therein, the inter-layer and intra-layer mode switching and boundary conditions are explicitly defined. In Chapter 3, an optimal switching time control scheme is proposed for a multi-mode cationic UV curing process of fiber-reinforced epoxy. First, the curing process model for this process is configured as a switching multi-mode system. To show the versatility of the model, the results of five-layer curing are briefly discussed. In chapter 4, first model-based optimal processing time sequence selection scheme for a layer-by-layer additive manufacturing of epoxy-based thick parts via a UV-based cationic curing process is outlined. Fourier Transform Infrared (FTIR) spectroscopy method was used to check the completeness of the final degree of cure. Then, short beam shear (SBS) test is conducted to measure the inter-laminar shear strength of the cured product under different compaction load. Scanning electron microscopy (SEM) images showed that samples made with optimum consolidation pressure had a relatively uniform fiber to resin distribution which results in improved inter-laminar shear strength. In this Chapter 5, online control method with NMPC is proposed for both single layer of material and for multi-layer. First, a nonlinear model predictive control (NMPC) scheme is outlined for UV-induced acrylate-based curing of a single layer thick composite part. Then, the model is extended for switching nonlinear model predictive control (SNMPC) for layer-by-layer curing process. Conclusion and future works are provided in Chapter 6.

## 1.4 Contributions

The main contributions of the researches in this dissertation include:

1. Derivation of cure kinetics model for cationic curing process for thick parts which involves different dynamic model during and after UV irradiation.

2. Experimental verification of UV-induced cationic curing process with optimal switching time.

3. Proposed offline optimal control for UV-induced curing process with switching dynamics.

4. Investigated (experimentally) the effect of consolidation pressure on the inter-laminar shear strength of UV induced thick composite manufactured layer by-layer curing.

5. Proposed a switching nonlinear model predictive control for a single and multi-layer UV-induced curing process.

# Chapter 2

# Optimal Control of Layer by Layer Cationic Curing Process

## 2.1 Abstract

Ultra-Violet (UV) light induced curing involves fast cross-linking of polymer networks starting from a liquid resin comprised of monomers and/or oligomers mixed with photo-initiators. This chapter first describes a curing process model comprised of the coupled cure-kinetics and thermal evolution in a cationic polymerization of a single layer of material and then extends it to the process of concurrent layering and curing of multiple layers. The model for processing multiple layers is characterized as a multi-mode hybrid system that switches modes both when the UV source is turned off and when a new layer is added. Therein, the inter-layer and intra-layer mode switching and boundary conditions are explicitly defined. The optimal mode switching times as well as the final process time are considered as the manipulated control variables that can be selected to optimize the final product quality. A computational framework is outlined for determining the sequence of switching times that gives a minimal cure

level deviation across all layers subjected to the multi-mode hybrid system model of the process. The necessary conditions of optimality are explicitly derived and listed. Results and discussions are included on the different possibilities for the proposed optimal control scheme for this process.

## 2.2 Introduction

Radiation-induced curing allows fast formation of highly cross-linked polymer networks from a liquid resin [17, 18]. Compared to convective or auto-clave processes, which are often referred to as thermal curing processes, radiation curing requires shorter times, reduces emissions of toxic volatile components, and cures at lower temperatures thus reducing energy consumption and associated costs [17]. There are different types of radiation curing technologies such as gamma ray, X-ray, electron beam and ultraviolet (UV) curing. Of these, UV has generally the lowest cost of equipment, lowest energy consumption, less space usage, less environmental pollution and is least hazardous [18, 19, 20]. It is also highly controllable in terms of UV source manipulation. Due to these advantages, UV curing has gained much attention for variety of thin films such as coatings and paints [19, 21]. However, with thicker films and parts, the attenuation of UV with the depth/thickness of the processed material causes a cure level and temperature gradient across the depth that compromises the quality of the end product [19, 22, 23]. This challenge has limited the use of UV curing to the fabrication and repair of relatively thin films and coatings [18]. By processing such thin layers turn by turn, UV curing has immense potential for various emerging additive manufacturing applications. However, since practical layers have some finite thickness for deposition/layering, the attenuation issue cannot be eliminated. Furthermore, with concurrent layering and curing, where a new layer is

added before previous ones cure completely, the attenuation effect will still influence the cure level distribution (measure of product quality) as multiple layers are added.

There has been some recent works that investigate the UV attenuation issue. An approach proposed in [23, 24] and later expanded in [25] offered a model-based compensation scheme for the in-domain attenuation of the UV input. This was then extended for a concurrent curing and layering approach where distinct process optimization opportunities were identified by examining the inter play between the underlying curing kinetics and UV attenuation [19, 26, 27]. The effect of UV exposure and compaction force on inter-laminar shear strength(ILSS) manufacturing was studied by [26]. It was found that improved ILSS of the final product is achieved when the second layer is added before the first layer is completely cured. In [27], the layer-by-layer in-situ UV processing concept was applied to making a thick glass-reinforced polyester composite and has been shown to give improved inter-laminar fracture toughness. These observations have motivated a hybrid system formulation of the layer-by-layer process itself in [19], where the otherwise continuous cure kinetics and thermal evolution are interrupted with discrete layering actions that switch the underlying dynamics. This formulation then facilitated the subsequent optimization of layering times and/or UV inputs in [19, 28]. Further experimental corroborations and control-oriented robustness analyses techniques and results have also been presented in [29].

All of the control-oriented and experimental works cited above dealt with the case of free-radical photo polymerization mechanism. The alternative cationic photo polymerization mechanism has not been addressed. Recent developments in a wide-variety of effective photo initiators and monomers for cationic photo polymerization has generated renewed interest in these processes [30, 31, 15]. Some reasons for the increased interest in cationic UV curing include: the insensitivity of the process to

oxygen inhibition [32]; a lower volumetric shrinkage during the process [32]; better inherent mechanical properties and thermal resistance[32]; operation at lower temperatures; and possibility to use with a wide range of monomer systems including epoxides, vinyl ethers and oxetanes [33]. Moreover, cationic polymerization involves the formation of long-living active centers which leads to a post polymerization (dark cure) after irradiation is stopped, albeit at a reduced rate. In certain systems, it is found that dark cure could account for up to 80% [32] of the whole process. This offers further opportunities for saving processing energy [32, 33]. However, compared to the free-radical polymerization, the model for cationic curing process is relatively more complex. This is because even for curing a single layer, the cationic cure kinetics involves two distinct cure mechanisms and rate equations:one for UV on and the other for UV off (dark cure). The additional switching time within a layer gives further opportunities for optimization of the concurrent layering and curing process, potentially resulting in improved product quality.

This study seeks to model the multilayer cationic polymerization process and develop an optimal control scheme that can be applied to exploit the listed advantages of this alternative process. In this section, we construct a switching hybrid dynamic system model by combining the cure kinetics of cationic photo polymerization during irradiation [33] and the cure kinetics for dark cure [33]. When concurrent layering is considered, then the layering steps also constitute further mode switches. We therefore have two types of mode switches in the whole process: intra-layer switching (turning the UV off at one layering step) and inter-layer switching (between adding layers). We conjecture that despite the UV attenuation through this multilayer process, near through-cure can be achieved by optimizing the UV input and/or the switching time between the modes. In this Chapter, to manage the complexity of the derivations, we opt to work with the mode switching times only even though the simultaneous

optimization of the UV input at each layer can be pursued as was done for the free-radical case in [19]. Specifically, we determine the optimal switching times as well as the final time by explicitly deriving the necessary conditions for optimality given the coupled dynamic constraints describing the cure-kinetics and thermal dynamics involved in the concurrent layering and curing process.

## 2.3 Process Model for Cationic Curing

In this section, we develop a model for the kinetics of cationic curing for a single layer. The schematic of the UV curing set up is shown in Fig. 2.1 below, where the material is exposed to a uniform UV source at the top.

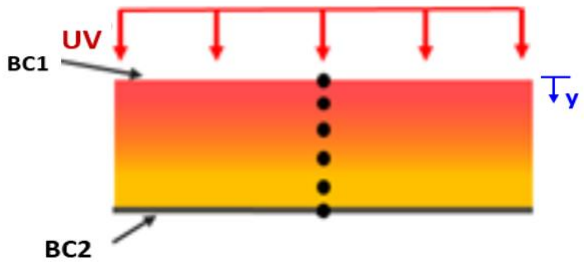


Figure 2.1: Schematic of UV curing process

The evolution of the initiation reaction of radiation-induced cationic polymerization is given by [33].

$$C(t) = C_0[1 - \exp(-k_i t)] \tag{2.1}$$

where $C$ is the concentration of cationic active centers and $C_0$ is the initial concentration of photo-initiators and $k_i$ is the initiation rate constant. The propagation reaction follows the rate expression given by [33]:

$$dM/dt = -k_p MC \tag{2.2}$$

where $M$ is the concentration of monomers and $k_p$ is the propagation rate constant.

The rate equation for the propagation step in the curing polymerization is derived in [29] to be:

$$M/M_0 = \exp\{-k_p C_0 t + \frac{k_p}{k_i} C_0[1 - \exp(-k_i t)]\} \tag{2.3}$$

where $M$ is the concentration of monomers in the resin, and $M_0$ is the initial concentration of monomer. Defining the cure level as:

$$\alpha = (M_0 - M)/M_0 \tag{2.4}$$

Then, combining equations (2.1 - 2.4), the cure rate is given by:

$$d\alpha/dt = k_p C_0[1 - \exp(-k_i t)](1 - \alpha) \tag{2.5}$$

This gives the state equation for cure-level in the first mode (when UV is on) without considering the effect of attenuation and temperature distribution. These effects will be added below. For the second mode, that is when the UV is turned off (referred to as dark cure), the rate equation is observed experimentally to take the form [33]:

$$M/M_{ts} = \exp\{-k_p C_0 t[1 - \exp(-k_i D t_s]\} \tag{2.6}$$

where $t_s$ is time at which UV is turned off and $M_{ts}$ is the monomer concentration at the switching time $t_s$. $D$ is an experimentally estimated constant parameter. From (2.1) and (2.2), we can get the expression for $M_{ts}$ by substituting $t = t_s$ in (2.3). Then, using this in (2.6), the monomer concentration for the dark cure kinetics is given as:

$$M/M_0 = \exp\{-k_p C_0 t_s + \frac{k_p}{k_i} C_0[1 - \exp(-k_i t_s)] - k_p C_0 (t - t_s)[1 - \exp(-k_i t_s D)]\} \tag{2.7}$$

Then, applying the cure level definition (2.4) with (2.7), the cure rate for dark cure

can be written as:

$$d\alpha/dt = k_p C_0[1-\exp(-k_i t_s D)]\exp\{-k_p C_0 t_s + \tfrac{k_p}{k_i} C_0[1-\exp(-k_i t_s)] - k_p C_0(t-t_s)[1-\exp(-k_i t_s D)]\} \tag{2.8}$$

Using (2.4) and (2.6), the cure rate for dark cure (UV off) (2.8) can be rewritten as:

$$d\alpha/dt = -k_p C_0[1-\exp(-k_i t_s D)](1-\alpha) \tag{2.9}$$

Equations (2.5) and (2.9) give the kinetic equation for the UV on and UV off modes without the effects of spatial UV attenuation and temperature distribution. For UV-initiated polymerization, the initiation and propagation parameters $k_i$ and $k_p$ are in general functions of the local UV intensity and temperature, respectively. From Beer Lambert's law, the variation of UV intensity $I$ with depth $y$ into the material is given by [30]:

$$I(y) = I_0 e^{-\lambda y} \tag{2.10}$$

where $I_0$ the intensity at the surface; $y$ is the depth in the direction of radiation and $\lambda$ is the attenuation constant. The initiation rate constant $k_i$ is proportional to the intensity [33] and can be modeled as:

$$k_i = \phi {I_0}^p e^{-\lambda y} \tag{2.11}$$

where $\phi$ and $p$ are constants. The propagation rate constant $k_p$ has the Arrhenius dependence on the local temperature:

$$k_p = k_0 \exp(-E/RT) \tag{2.12}$$

where $k_0$ propagation reaction constant, $E$ is the activation energy, $R$ is the ideal gas constant and $T$ is temperature in Kelvin. Thus, considering the effect of attenuation

and temperature, the cure rate for the UV on case given in (2.5) can be modified as:

$$d\alpha/dt = C_0 k_0 \exp[-E/(RT)](1-\alpha)(1-\exp\{-\phi {I_0}^p [\exp(-\lambda y)]t\}) \tag{2.13}$$

Similarly, the cure rate for the UV off case (dark cure) is given by:

$$d\alpha/dt = C_0 k_0 \exp[-E/(RT)](1-\alpha)(1-\exp(-k_i t_s D)). \tag{2.14}$$

Clearly, the curing kinetics in both cases is a strong function of the local temperature. The temperature distribution in the layer is governed by the contributions of heat generation from cationic polymerization (exothermic reaction), the conductive heat transfer within the material and the (mostly) convective heat transfer at the boundary. These also need to be captured along with other relevant thermal boundary conditions. For the simplified schematic depicted in Fig. 2.1, we consider a convective heat transfer boundary condition at the top (BC1) and an insulated boundary condition at the bottom (BC2). From energy balance, one can write the following partial differential equation (PDE) for the spatial and temporal temperature evolution:

$$\rho c_p \partial T(y,t)/\partial t = k_y(\partial^2 T(y,t))/(\partial y^2) + \rho \Delta H d\alpha(y,t)/dt \tag{2.15}$$

$$-k_y \partial T(y,t)/\partial y + \vartheta I_0 = h(T(y,t) - T_\infty) \tag{2.16}$$

$$\partial T(l,t)/\partial y = 0 \tag{2.17}$$

where $\rho$ and $c_p$ are, respectively, the density and specific heat capacity of the material; $k_y$ is the thermal conductivity of the material along the depth; $T(y,t)$ is the temperature at time $t$ and depth $y$; $\Delta H$ is the enthalpy of polymerization; $\vartheta$ is the

absorptivity constant of UV radiation at the surface; $h$ is the convective heat transfer at the top boundary (BC1) and $T_\infty$ is the ambient temperature. Eq.(2.15) is the general energy balance equation; Eq. (2.16) is convective boundary condition at the top and Eq. (2.17) is insulation boundary condition at the bottom. The coupled evolution of the cure level and temperature for the single layer depicted in Fig. 2.1 is then given by the PDE (2.15) along with the switching cure kinetics given by the ODEs in (2.13) for when UV is on and (2.14) for when the UV is off. The switching is considered to happen at the pre-determined time $t_s$. To facilitate computations and streamline subsequent discussions for the multi-layer process, we discretized the spatial domain in equal intervals across the depth of the layer and convert the temperature PDE in (2.15) (along with the boundary conditions) into a set of ODEs indexed by the discretization. The latter is detailed in the Appendix.

Next, we show typical responses of the coupled cure-kinetics and thermal evolution model derived above. We used model parameters fitted to experimental data from EB radiation-initiated cationic polymerization of Diglycidyl Ether of Bisphenol A (DEBGA) [33, 17], since the cationic polymerization equations are similar for both UV and EB initiated polymerizations [33, 29]. The spatial and temporal evolution of the cure level are shown in the 3D plot of (Fig. 2.2) for a single 5mm thick layer of material. That there is a dramatic change in the cure rate at UV switch off (at $t_s = 300s$) can be seen on the corresponding knee on the cure level state.

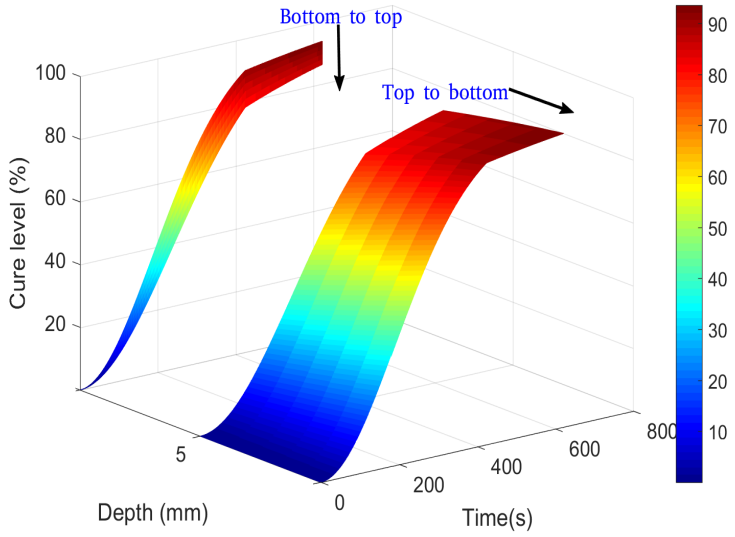


Figure 2.2: 3D plot of cure evolution

## 2.4 Modeling the Layer-by-Layer UV Curing Process for Epoxy Resin

In this section, we outline the model for the concurrent curing and layering process by building on the single layer process model detailed in the previous section. Figure 2.3 shows the schematic and notations we use for describing our model of the concurrent layering and curing process. Here after, $i = 1 : N$ is the layer index, $N$ is total number of layers, $M = 2N$ is total number of modes. We use $ik$ for the mode index, where $i$ stands for the number of layers in the given mode, and $k$ stands for irradiation or post-irradiation ($k = 1$ for UV on, and $k = 2$ for UV off). Hence, we identify the UV on mode in layer i as mode $i1$ and UV off mode as $i2$. Given the coupled cure-kinetics and discretized temperature evolution model described in the previous section for a single layer, we can assemble a state-space model for the

multi-layer case as follows (2.18):

$$\dot{x} = f(x(t), u(t)) \tag{2.18}$$

where $x(t) = [\alpha(t), T(t)]'$ is the state vector comprised of the cure-level and temperature state at each discrete spatial location at any time $t$ or any mode in the layering process. $f((x(t), u(t))$ is a function of the cure-level, temperature state and the UV input for those modes where the UV is on (mode index $i1$ at the $i^{th}$ layer), and it will be a function of only the cure-level and temperature state for those modes where the UV is off (mode index $i2$ at the $i^{th}$ layer).

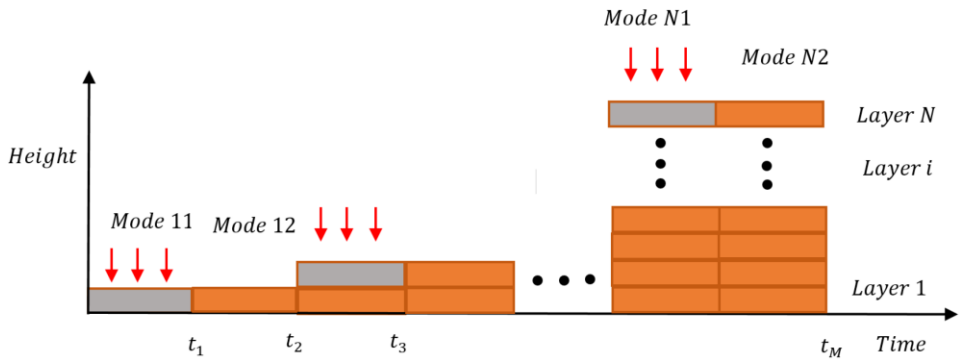


Figure 2.3: Schematic of the concurrent layering and cationic curing process

### 2.4.1 Switching of Modes

As mentioned above, for concurrent layering with cationic curing, there are two types of mode switchings: Intra-layer mode switching and inter-layer mode switching. We now discuss how each of these mode switchings is modeled.

#### 2.4.1.1 Intra-layer switching

Intra-layer switching occurs when the UV is turned off after being initially on at any layering step. During the UV on mode, the temperature of the layers exposed

to UV typically rises to some level higher than the initial ambient temperature. For the subsequent curing in the UV off mode, this change in temperature drives the cure reaction. Hence, the initial values of the temperature at the switch to UV off mode is taken as the final temperature of the UV on mode. The same assumption can be taken for the cure level state. The state transition for intra-layer switching can therefore be described by:

$$x^T_{(j+1)}(t_j^+) = F_j^T(x_j^T(t_j^-)) \tag{2.19}$$

$$x^\alpha_{(j+1)}(t_j^+) = F_j^\alpha(x_j^\alpha(t_j^-)) \tag{2.20}$$

where $x^T_{j+1}(t_j{}^+)$ and $x^\alpha_{j+1}(t_j^+)$ are, respectively, the temperature state and cure level state in UV off mode just after switching to UV off at switching time $t_j^-$. $x_j^T(t_j^-)$ and $x_j^\alpha(t_j^-)$ are the temperature state and cure level in UV on mode just before switching. Here, $j$ is the intra-layer mode index. $F_j$ is a mapping operator and for intra-layer modes it maps to itself. Note that the state vector components are indexed by their discrete spatial location across all layers up to the present processing step.

#### 2.4.1.2 Inter-layer switching

Inter-layer mode switching occurs when a new layer is added on top of the existing layers. The inter-layer mode switch is the same as the case treated for free-radical polymerization detailed in [28]. The state transition in inter-layer switching can be written compactly as:

$$x^T_{(j+1)}(t_j^+) = F_j^T(x_j^T(t_j^-)) \tag{2.21}$$

$$x^\alpha_{j+1}(t_j^+) = F_j^\alpha(x_j^\alpha(t_j^-)) \tag{2.22}$$

where, $x_{j+1}^T(t_j{}^+)$ and $x_{j+1}^\alpha(t_j^+)$ are, respectively, the temperature state and cure level state just after a new layer is added and $x_j^T(t_j^-)$ and $x_j^\alpha(t_j^-)$ are the temperature state and cure level just before layer addition. Here, $j$ is the inter-layer mode index. $F_j$ is mapping operator describing the inter-layer mode switch whose detailed mathematical formulation is given in [28]; we mention only some of the salient aspects and modeling assumptions here. First note that with each layer added, the dimension of the state space increases by the size of the spatial discretization for the added layer. The new layer is assumed to be in ambient condition (uncured state, at ambient temperature). We also assume that for the cationic process we treat here, just before adding a layer, the previous layers were in UV off mode and will be switched to UV on mode simultaneously with the layer addition.

In defining this inter-layer switching, state initializations at interface locations (between the bottom of the new and top of previous layer) need special handling. Since existing layers are likely at relatively at higher temperature, there will be conductive heat transfer between the new layer and existing layers, particularly at the interface location. Here, we take the initial temperature (after layering) at the interface to be the average of the ambient temperature and that at the top of the previous layer. For the cure level state, since the cure level is irreversible for thermoset materials, the cure level of the existing layer will not be instantly affected by the addition of the new layer. Therefore, for the next mode, the cure level at the interface is initialized at the value of the cure level state of the top of the previous layer just before the new layer is added.

Fig. 2.4 illustrates the two kinds of mode switches described above. Here, the top node of the first layer and the bottom node of the second layer temperature evolutions are plotted. Note while some cooling is observed during the intra-layer mode switch, the inter-layer cooling/heating (due to heat conduction) is substantial at the

inter-layer mode switch. This inter-layer cooling/heating is in fact an experimentally observed phenomena in the concurrent layering and curing process [34].

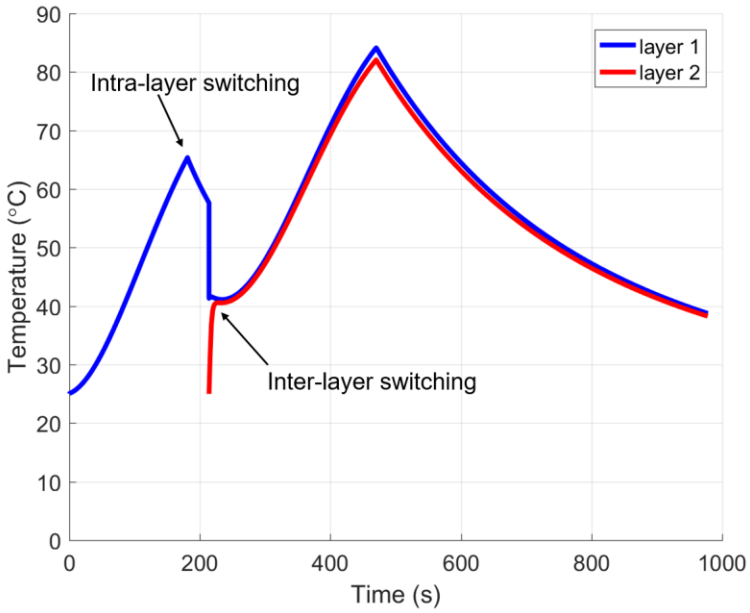


Figure 2.4: Intra-layer and Inter-layer switching modes

## 2.5 Optimal Control of the Multimode Layer-by-Layer Curing Process

In this section, we pose an optimal control problem for the model described by eqs. (2.15) to (2.17) and subsequently derive the necessary conditions for optimality.

### 2.5.1 Problem Formulation

As discussed in the previous section, the multi-mode hybrid system model of the concurrent layering and cationic curing process has time-driven switches. The switching time vector $t = [t_1, t_2 ... t_{M-1}, t_M]'$ is the control parameter. The initial time is zero. However, the final time is free. The sequence of modes (order elements of

the switching time vector) is assumed to be fixed. The state evolution and mode transitions are discussed earlier in 2.18 and (2.19) - (2.22), respectively. The UV input is at each stage is assumed known and the same (for the following analysis, but this could be readily relaxed to be an additional control variable as shown in [19] for the free radical case). Given the above state evolution and transition models and assumptions, the optimal control problem for the present application is to determine the optimal switching time vector $t = [t_1, t_2 ... t_j ... t_{M-1}, t_M]'$ which minimizes cost function:

$$J = \sum_{j=1}^{M} \int_{t_{j-1}}^{t_M} g_j(x_j, u_j)dt + \sum_{j=1}^{M-1} h_j(x_j(t_j^-)) + h(x_M(t_M)) \tag{2.23}$$

where $j = 1, ..., M$ is the (unwrapped, integer) mode number indexing both the inter-layer and intra-layer modes (for example, j=5 refers to layer 2, UV on) $x_j$ is the temperature and cure state at $j$ and $u_j$ is the control input which is the intensity of the UV, $g_j(x_j, u_j)$ is the instantaneous cost in mode $j$, $\phi_j$ is a state transition cost between different modes and $h$ is a terminal cost.

### 2.5.2 Optimality Conditions

For the problem defined in the previous section, the optimality condition for $M$ mode switching system is derived using calculus of variation. Using the cost function given in Eq. 2.23 the optimality condition derived as follows. The Hamiltonian given as:

$$H_j(x_j, \lambda_j, u_j) = g_j(x_j, u_j) + \lambda_j f_j(x_j, u_j) \tag{2.24}$$

By adjoining the state transition constraints: the cost function can be augmented as:

$$\bar{J}_0 = \sum_{j=1}^{M} \int_{t_{j-1}}^{t_j} \left[ H_j \left( x_j, \lambda_j, u_j \right) - \lambda_j \dot{x}_j \right] dt + \sum_{j=1}^{M-1} \mu_j \left[ F_j \left( x_j \left( t_{j^-} \right) \right) - x_{j+1} \left( t_j + \right) \right] \tag{2.25}$$

The first order approximation of the perturbed cost function ,$\bar{J}_\delta$, is given by:

$$\begin{aligned}
&\bar{J}_\delta = \sum_{j=1}^{M} \int_{t_{j-1}}^{t_J} \left[ H_j \left( x_j, \lambda_j, u_j \right) - \lambda_j \dot{x}_j \right] dt + \\
&\sum_{j=1}^{M} \int_{t_j}^{t_j + \delta\theta_i} g_j \left( x_j, u_j \right) dt - \sum_{j=1}^{M} \int_{t_{j-1}}^{t_{j-1} + \delta\theta_{j-1}} g_j \left( x_j, u_j \right) dt + \\
&\delta \sum_{j=1}^{M} \int_{t_{j-1}}^{t_j} \left[ \frac{\partial H_j}{\partial x_j} \eta_j + \frac{\partial H_j}{\partial x_j} \nu_j - \lambda_j \dot{\eta}_j \right] dt + \\
&\sum_{j=1}^{M-1} \mu_j \left[ F_j \left( \left( x_j (t_j + \delta\theta_j)^- \right) - x_{j+1} (t_j + \delta\theta_j)^+ \right] + \right. \\
&\delta \sum_{j=1}^{M-1} \mu_j \left[ \frac{\partial F_j}{\partial x_j} \eta_j \left( t_j^- \right) - \eta_{j+1} \left( t_j^+ \right) \right] + \sum_{j=1}^{M} h_j \left( x_j (t_j + \delta\theta_j)^- \right) + \delta \sum_{j=1}^{M} \frac{\partial h_j}{\partial x_j} \eta \left( t_j^- \right)
\end{aligned} \tag{2.26}$$

It is assumed that in the open intervals $(t_{j-1}, t_{j-1} + \delta\theta_{j-1})$ *and* $(t_j, t_j + \delta\theta_j)$. Now the first variation in the cost function given in eq. 2.23 can be expressed as:

$$\Delta J = \delta \overset{lim}{\to} 0 \frac{\bar{J}_\delta - \bar{J}_0}{\delta} \tag{2.27}$$

Therefore, from 2.25 and 2.26, one can get:

$$\begin{aligned}
&\Delta J = \sum_{j=1}^{M} \int_{t_{j-1}}^{t_j} \left[ \frac{\partial H_j}{\partial x_j} \eta_j + \frac{\partial H_j}{\partial x_j} \nu_j - \lambda_j \dot{\eta}_j \right] dt + \sum_{j=1}^{M} g_j \left( x_j, u_j \right) |_{t_j} \theta_j - g_j \left( x_j, u_j \right) |_{t_{j-1}} \theta_{j-1} \\
&+ \sum_{j=1}^{M-1} \mu_j \left[ \frac{\partial F_j}{\partial x_j} \dot{x}_j \left( t_j^- \right) \theta_j - \dot{x}_{j+1} \left( t_j^+ \right) \theta_j \right] + \sum_{j=1}^{M-1} \mu_j \left[ \frac{\partial F_j}{\partial x_j} \eta_j \left( t_j^- \right) - \eta_{j+1} \left( t_j^+ \right) \right] + \\
&\sum_{j=1}^{M} \left[ \frac{\partial h_j}{\partial x_j} \dot{x}_j \left( t_j^- \right) \theta_j + \frac{\partial h}{\partial x_j} \eta \left( t_j^- \right) \right]
\end{aligned} \tag{2.28}$$

Reordering the sum, reorganizing terms, and remembering that $\theta_0 = 0$ and $\theta_M$=$\theta(t_M)$

one can get :

$$\begin{aligned}\Delta J = &\sum_{j=1}^{M} \int_{t_{j-1}}^{t_j} \left[\frac{\partial H_j}{\partial x_j}\eta_j + \frac{\partial H_j}{\partial x_j}\nu_j - \lambda_j \dot{\eta}_j\right] dt + \sum_{j=1}^{M-1} \left[g_j\left(x_j, u_j\right) - g_{j+1}\left(x_{j+1}, u_{j+1}\right)\right]_{t_j} \theta_j \\ &+ \sum_{j=1}^{M-1} \left[\mu_j \frac{\partial F_j}{\partial x_j} f_j\left(t_j^-\right) - \mu_j f_{j+1}\left(t_j^+\right) + \frac{\partial h_j}{\partial x_j} f_j\left(t_j^-\right)\right] \theta_j \\ &+ \sum_{j=1}^{M-1} \mu_j \left[\frac{\partial F_j}{\partial x_j}\eta_j\left(t_j^-\right) - \eta_{j+1}\left(t_j^+\right)\right] + \sum_{j=1}^{M} \frac{\partial h_j}{\partial x_j}\eta\left(t_j^-\right)\end{aligned} \tag{2.29}$$

Using integration by parts the third term in the integral terms in Eq. 2.29 further reduces to:

$$\sum_{j=1}^{M} \int_{t_{j-1}}^{t_j} \lambda_j \dot{\eta}_j = \sum_{i=1}^{M} \int_{t_{i-1}}^{t_i} \dot{\lambda}_i \eta_i - \sum_{i=1}^{M} \left[\lambda_i\left(t_i^-\right)\eta_i\left(t_i^-\right) - \lambda_i\left(t_{i-1}^+\right)\eta_i\left(t_{i-1}^+\right)\right] \tag{2.30}$$

Substituting Eq. 2.30 and $\Delta J$ and choosing $\lambda_j$ in the intervals $(t_{j-1}, t_j)$ to solve:

$$\dot{\lambda}_j = -\frac{\partial H_j}{\partial x_j}\left(x_j, \lambda_j, u_j\right) \tag{2.31}$$

Which results in:

$$\begin{aligned}\Delta J = &\sum_{j=1}^{M} \int_{t_{j-1}}^{t_j} \gamma_j \nu_j dt + \sum_{j=1}^{M-1} \beta_j \theta_j + \sum_{j=1}^{M-1} \left[\lambda_{j+1}\left(t_j^+\right) - \mu_j\right] \eta_{j+1}\left(t_{j+1}^+\right) \\ &+ \sum_{j=1}^{M-1} \left[\mu_j \frac{\partial F_j}{\partial x_j} + \frac{\partial h_j}{\partial x_j} - \lambda_j\left(t_j^-\right)\right] \eta_j\left(t_j^-\right) \\ &+ \left[\frac{\partial \mathrm{h}}{\partial x_M} - \lambda_M\left(t_M^-\right)\right] \eta_M\left(t_M^-\right)\end{aligned} \tag{2.32}$$

$$\begin{aligned}\gamma_j &= \frac{\partial H_j}{\partial u_j} \\ \beta_j &= \left[g_j\left(x_j, u_j\right) - g_{j+1}\left(x_{j+1}, u_{j+1}\right)\right]_{t_j} + \\ &\left[\mu_j \frac{\partial F_j}{\partial x_j} f_j\left(t_j^-\right) - \mu_j f_{j+1}\left(t_j^+\right) + \frac{\partial h_j}{\partial x_j} f_j\left(t_j^-\right)\right]\end{aligned} \tag{2.33}$$

Considering the fact that $h_M(x_M\left(t_M^-\right) = \mathrm{h}_M\left(x_M\left(t_M\right)\right)$ and $\eta_1\left(0+\right) = 0$ The computation of the perturbations $\eta$ is avoided by choosing:

$$\begin{aligned} \mu_i &= \lambda_{j+1}\left(t_j^+\right) \\ \lambda_j\left(t_j^-\right) &= \mu_j \frac{\partial F_j}{\partial x_j} + \frac{\partial h_j}{\partial x_j} \\ \lambda_M\left(t_M^-\right) &= \frac{\partial h}{\partial x_M} \end{aligned} \tag{2.34}$$

Equations 2.34 describes the boundary conditions of the costate given in Eq. 2.31. Thus the first order variation of $J$ reduces to:

$$\Delta J = \sum_{j=1}^{M} \int_{t_{j-1}}^{t_j} \gamma_j \nu_j dt + \sum_{j=1}^{M-1} \beta_j \theta_j \tag{2.35}$$

Since the control parameters are independent , the necessary conditions for optimality is when the coefficients $\gamma_j$ and $\beta_j$ are zero. By taking $p' = \lambda$, the above equations are summarized as follows:

Euler-langrange Equation:

$$\dot{p'} = -\frac{\partial H_j}{\partial x_j}(x_j, u_j,\ \lambda_j) \tag{2.36}$$

$$p'_M\left(t_M{}^-\right) = \frac{\partial \mathrm{h}}{\partial x_M} \tag{2.37}$$

$$H_j\left(t_j^-\right) - H_{j+1}\left(t_j^+\right) = 0 \tag{2.38}$$

$$H_M\left(t_M^-\right) = 0 \tag{2.39}$$

Supposing that the main goal is to achieve through cure and uniform distribution of cure at the final time, only the terminal cost can be retained in the cost function 2.23 and the optimization problem posed as:

$$\min_t J = \min_t 1/2 \sum_0^n \left(\alpha(y, t_M) - \alpha_{des}\right)^2 \tag{2.40}$$

where $\alpha(y, t_f)$ is the final cure level and $\alpha_{des}$ is the desired cure level. This is subject to the state evolution and mode transition constraints discussed above. The values of the switching and final times in the optimal solution vector $t = [t_1, t_2 ... t_j ... t_{M-1}, t_M]'$ obtained by solving the problem in Eq. 2.40 give the optimum times to turn off the UV, to add each successive new layer, and the final time at which the cure across the depth of the multi-layer part is close to the desired value. For the cost function retaining only the terminal cost, the optimality conditions reduce to:

$$\partial H_j / \partial u_j = 0 \tag{2.41}$$

$$H_j(t_j^-) - H_{j+1}(t_j^+) = 0 \tag{2.42}$$

$$H_M(t_M^-) = 0 \tag{2.43}$$

Note that when we consider the terminal cost only, the instantaneous term in the Hamiltonian (Eq. 2.24) is zero and condition Eq. 2.41 is trivially satisfied. Having derived the necessary conditions for optimality, a steepest descent or some other gradient method can be used to get optimal control values for the switching times. Here , the steepest descent algorithm is used [35] and [36] and detail steps are described below:

1. Choose initial iterate $t_j^0$ for $j = 1, 2, 3 ... M$ and choose a termination tolerance $\varepsilon$
2. Set the iteration counter $k = 0$
3. While $\left| J^k - J^{k-1} \right| > \varepsilon$

4. Compute the state trajectory $x_j(t)$, $t\epsilon[t_{j-1},t_i]$ for $j = 1,2,3...M$ forward in time from $t_0 = 0$ to $t_f = t_M$

5. Compute the adjoining variable $\bar{p}_i(t)$, $for\ j = 1,2,3...M$ backward in time from $t_f = t_M$ to $t_0 = 0$

6. Update the time vector $t_j^{k+1} = t_j^k - \delta_j^k B_j$ , where $j = 1,2,3...M$
   where, $t_M^{k+1} = t_M^k - \delta_M^k C$
   $B_j = H_j(t_j^-) - H_j(t_j^+)$ and
   $C = H_N(t_j^-)$

7. $k = k + 1$

8. *End while*
   Save the optimal switching time vector $[t_1, t_2, t_3...t_M]^T$

A proper step size $\delta_M$ (in step 6) must be selected. Preferably $\delta_M$ should be chosen to reduce the total computational cost; but finding this itself is a challenging problem. To find the proper step size various ad hoc strategies for choosing $\delta_M$ have been proposed. One alternative strategy is Armijo line search method [37].

## 2.6 Results and Discussion

In this section, we apply the framework developed above to cationic curing and layering of a resin. The epoxy resin used for the simulation study is diglycidyl ether of bisphenol A (DGEBA) with density $\rho = 1.17 g/cm^3$, thermal conductivity $k = 0.0025\ w/cm\ k$, and specific heat capacity $C_p = 1.75\ J/g\ k$. Each layer has a thickness of 1mm and six nodes along the depth, five layers are considered to illustrate the method for multi-layer curing. Note that at each spatial node, there are two states

namely, cure-level and temperature. Hence, in one layer there are twelve states (six nodes per layer and two states per node). As depicted in Fig. 2.3 when the number of layers increases from one to five and the size of the state vector increases to 120. The process input, UV intensity is kept on and constant for odd modes ($j = 2i - 1$) and will be off for even modes ($j = 2i$). The inter-layer, intra-layer switching and final times are decided externally. All switching and final times are the control variables, which can be optimized to get minimum cure deviation of the final cure from the desired value of (95 %). The computed optimal switching and final times are shown in Table 2.1.

Table 2.1: Optimal switching and final times

| Mode | 11 | 12 | 21 | 22 | 31 | 32 | 41 | 42 | 51 | 52 |
|---|---|---|---|---|---|---|---|---|---|---|
| Initial switching time | 50 | 100 | 150 | 200 | 250 | 300 | 350 | 400 | 450 | 500 |
| Optimal switching time | 100 | 174 | 365 | 405 | 604 | 754 | 900 | 950 | 1397 | 1452 |

As can be seen in the table, UV is off for substantial amount of time. The total time on which UV is on can be found by adding the duration on which UV was on in all layers, that is: $t_{UV\_on} = 100 + (365 - 174) + (604 - 405) + (900 - 754) + (1379 - 950) =$ 1065 s. As can be seen in Fig. 2.5(a), the temperature of the first layer initially increased from the initial value (25 $^oC$) to about 40 $^oC$, but when UV is turned off at the first switching time ($t = 100$) s, the temperature starts to decrease. However, before it reaches to its initial level a new layer is added with UV turned-on, and the temperature starts to increase. As discussed in Section 2.4.1.2, at the interface initial temperature is taken to be the average of the existing layer, which is relatively at higher temperature and the new layer which is at ambient temperature. This is done by assuming that there will be instant conduction at the interface before transition to the next mode. The same assumption has been considered to upcoming inter-

layer switching. Fig. 2.5(a) shows the details of the temperature evolution, including the changes at the optimal switching times and Fig. 2.5(b) shows the distributed temperature state across all layers at optimal final time ($t$ = 1452 s). The final temperature gradient along the depth is about 9 $^{o}c$ Fig. 2.5(b), which shows that the proposed optimization of the concurrent layering and cationic curing approach reduces the potential of thermal stresses due to large temperature gradients across depth in a thick part.

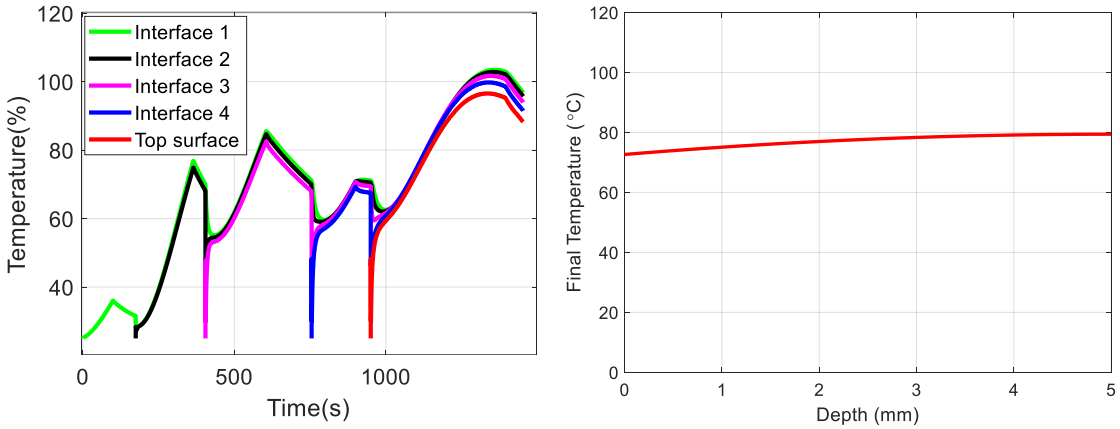


(a) Temperature evolution (b) Final temperature

Figure 2.5: Temperature evolution and final temperature of layer-by-layer curing process

The cure level evolution of at the interfaces and at the top surface is shown in Fig. 2.6(a). The cure level increases by about 60 % in the final mode (without UV input). This shows the advantage of cationic polymerization over free radical. This is because, unlike free radical polymerization, cationic polymerization continues to polymerize after irradiation is stopped [31]. In addition, the cure level of all layers converge to the desired cure level (95 %). The final cure level all layers, as depicted in Fig. 2.6(b), reaches close to the desired target cure level (95 %). The maximum deviation of the final cure level from the desired level is found to be less than 5 %.

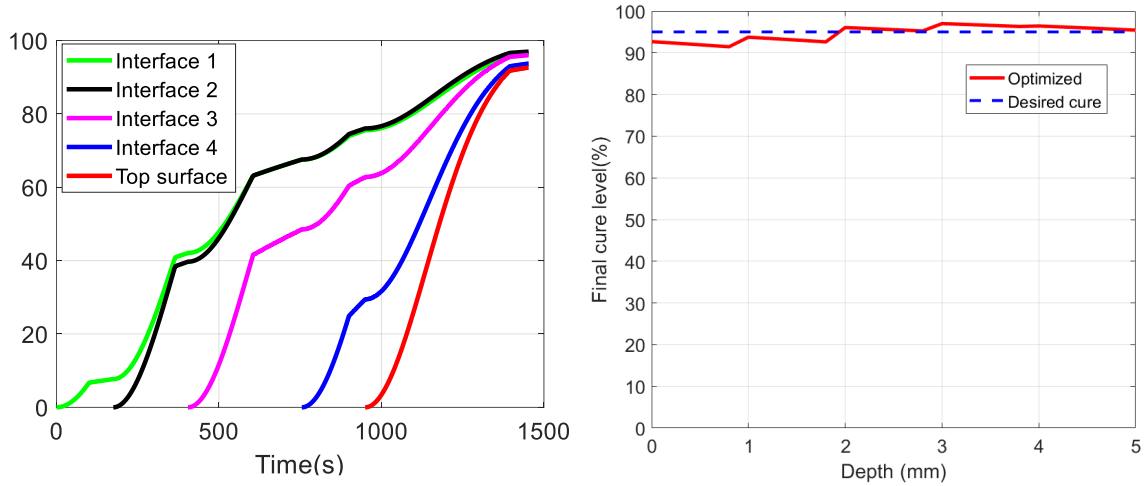


(a) Cure level evolution (b) Final cure level

Figure 2.6: Cure level evolution and Final cure level of layer-by-layer curing process

The proposed approach is then compared to equal time interval curing. This is done by taking the optimized final time and dividing it into equal intervals for all modes. In this case UV will be on for a total of 1331/2=665.5 s, which is much higher than the optimized UV duration of 278 s. Nevertheless, as shown in Fig. 2.7(a) the final cure level is not close to the desired one for most locations in the part, at the final time. The interface temperature evolution of equal time interval curing is depicted in Fig. 2.7(b). As seen in the figure the maximum temperature reached during the process is less than the previously discussed approaches of layer-by-layer and one shot curing. This is because in the case of equal switching time curing, the process more energy is dissipated through convection. The latter is caused by longer duration of the UV off time as compared to the optimized layer-by-layer approach. Hence, we can infer that the optimal layer-by-layer approach outlined in this paper reduces energy loss without compromising through cure and cure-level distribution.

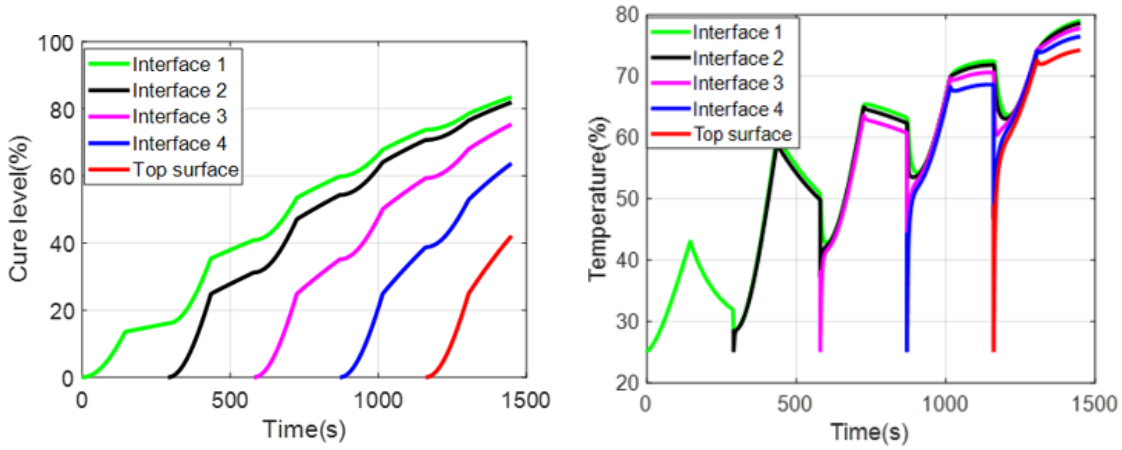


(a) Cure level evolution (b) Temperature evolution

Figure 2.7: Temperature and cure level evolution at equal switching times

## 2.7 Summary and Conclusion

In this chapter, an optimal switching time control scheme is proposed for a multi-layer cationic UV curing process. First, the curing process model for the concurrent layering and cationic curing process is configured as a switching hybrid system. Two conditions for inter-layer and intra-layer switching have been defined. The process model includes UV spatial attenuation effects and spatial temperature distribution that pose a challenge in processing thick layers of material with UV irradiation. The necessary optimality conditions are derived for the switching times and final time that give minimal final cure level deviations from a desired target. It is illustrated how the model-based optimization of the optimal switching times and final time helps to get a near-through cure across a thick part compared with alternative approaches of equal time interval curing and layering with the same final optimized time and all layers cured at once (one shot curing) for the same overall duration. It is also demonstrated that in addition to improving through cure and cure- level distribution, the optimized layer-by-layer approach results in less temperature gradients

as compared with curing of all layers together. This can reduce thermal stresses and hence improve the quality of the final product.

## 2.8 Experimental Verification of Cationic Curing of DGEBA Based Epoxy

In this section, a cure kinetics model is derived for Ultra Violet (UV) induced cationic polymerization of diglycidyl ether bisphenol A (DGEBA). The model is characterized by a two-mode dynamic cure system that switches modes when the UV source is turned off with continued polymerization after UV is off. The model is then used to determine the optimal switching time and the final process time that give a minimal cure level deviation across a layer of material considering the coupled cure-kinetics and the temperature evolution. This is done by explicitly deriving the necessary conditions of optimality for the two-mode dynamic system. The model can be extended to any cationic polymerization process. The effectiveness of the proposed model is assessed by comparing the hardness of the sample cured with optimal switching time with another sample cured for a longer time and showed similar hardness values.

The role of thermosetting materials in applications has increased enormously over the last few decades due to their high flexibility for tailoring desired ultimate properties [38], compactly cross-linked structure [39], durability and resistance towards thermal stress and chemical attacks as provided by their compact cross-linking structure [39]. This dramatic increase is expected to continue in the future. The most commonly used thermosetting resins in the composite industry are epoxy, vinyl

ester, unsaturated polyester, phenolic, polyimides, and cyanate ester. Compared to all other the thermosetting resins, epoxy requires minimum pressure for fabrication of products: has low shrinkage during curing and hence low residual stress in the cured product; available in a wide range from low viscous liquid to tack-free solid. Because of these unique characteristics and useful properties of network polymers, epoxy resins are widely used in structural adhesives, surface coatings, and electrical laminates. The most commonly used epoxy resin is diglycidyl ether of bisphenol-A (DGEBA) [40].

## 2.9 Process Model and Simulation Results

The curing process involves heat generation from cationic polymerization (exothermic reaction), convection heat transfers at the top surface and conduction within the layer. These also need to be captured along with boundary conditions. As depicted in Fig.1, We consider is a convective heat transfer ($BC_1$) at the top and an insulated boundary condition ($BC_2$) at the bottom. As already stated, the UV gets attenuated along the depth and the intensity across the depth is given by Beer-Lamberts law. A one-dimension UV induced cationic curing process model is then summarized in eqs. (2.44) to (2.47).

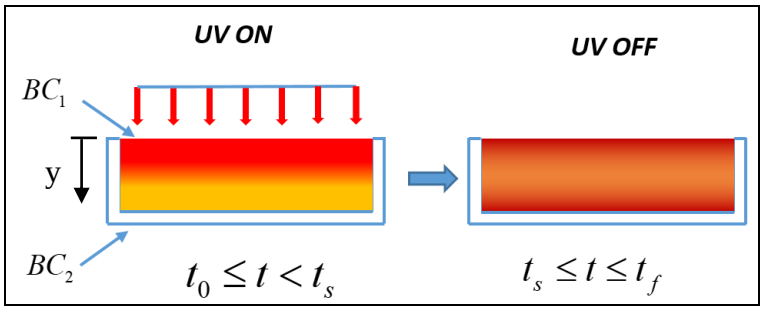


Figure 2.8: Schematic of curing process with UV on and UV off mode

$$\rho c\frac{\partial T(t,y)}{\partial t} = k_y\frac{\partial^2 T(t,y)}{\partial y^2} + \rho\Delta H\frac{d\alpha(t,y)}{dt} \tag{2.44}$$

$$-k_y\frac{\partial T(t,y)}{\partial y} + \vartheta I_0 = h(T(t,y) - T_\infty) \tag{2.45}$$

$$\frac{\partial T(t,l)}{\partial y} = 0 \tag{2.46}$$

$$\frac{\partial \alpha(y,t)}{\partial t} = \begin{cases} A\exp\left(\frac{-E}{RT_{abs}}\right)\left(1 - e^{-\phi I_0(e^{-\lambda y})t}\right)(1-\alpha), & t \in [t_0, t_s) \\ A\exp\left(\frac{-E}{RT_{abs}}\right)\left(1 - e^{-k_i t_s D}\right)(1-\alpha), & t \in [t_s, t_f] \end{cases} \tag{2.47}$$

where $\rho$ and $c$ are the density and specific heat capacity of the epoxy, respectively;$k_y$ is the thermal conductivity of the epoxy across the depth; $T(t,y)$ is the temperature at time $t$ and depth $y$. $\Delta H$ is enthalpy of polymerization;$\alpha(t,y)$ is degree of cure at time $t$ and depth $y$ ; $l$ is the thickness (depth) of the sample; $A$ is pre-exponential constant; $E$ is the activation energy ; $R$ is universal gas constant; $T_{abs}$ the absolute temperature in Kelvin; $I_0$ is the initial UV intensity; $\lambda$ is UV attenuation constant; $k_i$ is initiation rate constant; $t_s$ and $t_f$ are switching and final cure times.

### 2.9.1 Optimal switching time control

An optimal switching time control strategy is designed to manipulate a switching time(s) in such a way that some performance criterion is optimized. In this paper, a specified final cure distribution is desired, the performance index would be related to what extent the actual final cure distribution deviates from the desired cure distribution along the depth. The optimal time control objective would be to minimize this deviation by appropriate manipulation of the switching and final times for a uniform

UV input. The performance index is given in eq. 2.48.

$$J = \frac{1}{2}\sum_{0}^{n}\left(\alpha(t_f) - \alpha_{des}\right)^2 \tag{2.48}$$

A thickness of 2mm DGEBA was considered for this study. The process input, UV intensity, is kept uniform for the first mode and turned off after switching time. A one-dimensional UV-induced cationic polymerization model given in eqs. (2.44) to (2.47) is used to get the temperature and cure distributions along the depth. As discussed earlier, the switching and final time are the control variables that can be optimized to get minimum deviation of the final cure from the desired value (90%). To solve the optimal control problem the necessary conditions for optimality are derived in a similar approach as given in [41] and the coupled PDE-ODE eqs. (2.44) to (2.47) are taken as constraints. Steepest descent algorithm [28] was applied to find the optimal switching and final times. With a predefined tolerance value of the optimal solution is achieved after 185 iterations. The optimal switching and final cure times are found to be 305s and 414s respectively. The simulation result shows that the time for the first mode is higher than the second mode. However, as seen in Fig. 2.9, the degree of cure increases by about 5% in the second mode (without UV input) and as it can be seen on the figure the cure will continue till all the monomers and/or oligomers are polymerized. This shows the advantage of cationic polymerization over free radical polymerization because cationic polymerization continues to polymerize after UV is turned off.

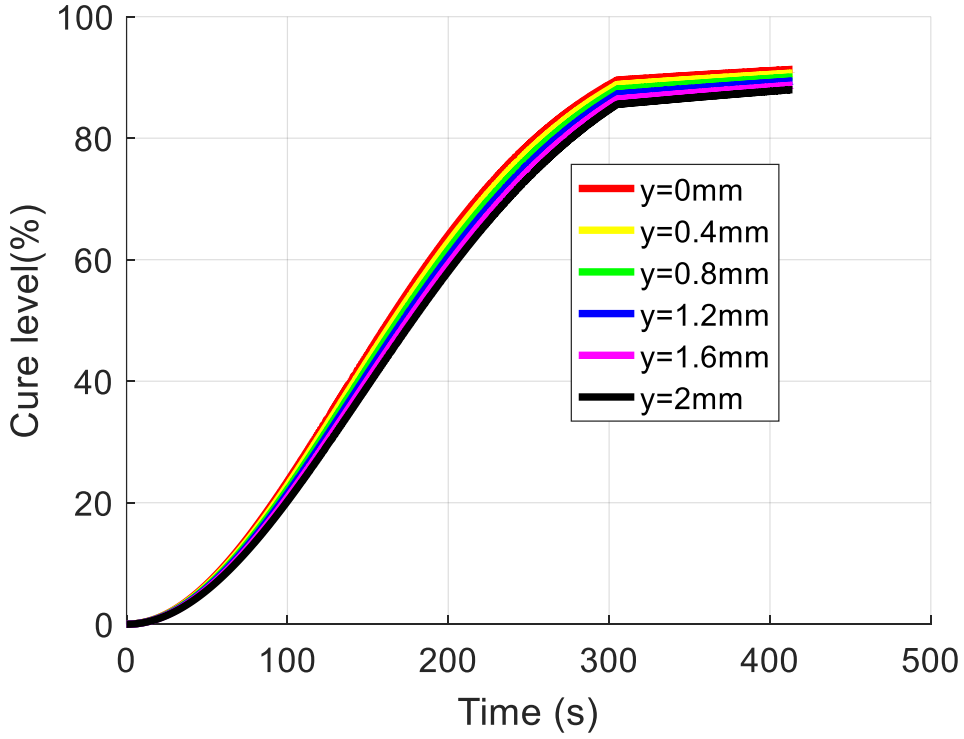


Figure 2.9: Degree of cure evolution

As can be seen in Fig. 2.10 at the switching time, the temperature starts to decrease with time. This is because the increase in temperature comes from the UV input and exothermic reaction. Since the UV is turned off at switching time the temperature decreases. However, it didnt decrease to the initial temperature ($25^oC$) rather decreases to the level which is equal to the contribution of the exothermic reaction.

As expected, initially the temperature at the surface (y=0) is highest but decreases across the depth to the lowest temperature at the bottom (y=2mm). Also, the heat generated from exothermic reaction increases with time and since the lower surface is insulated (no heat loss), the temperature will increase. At the top surface where there is a convection heat transfer, some part of it will be dissipated to the ambient. Hence the temperature of the bottom surface (y = 2 mm) will have the

highest temperature.

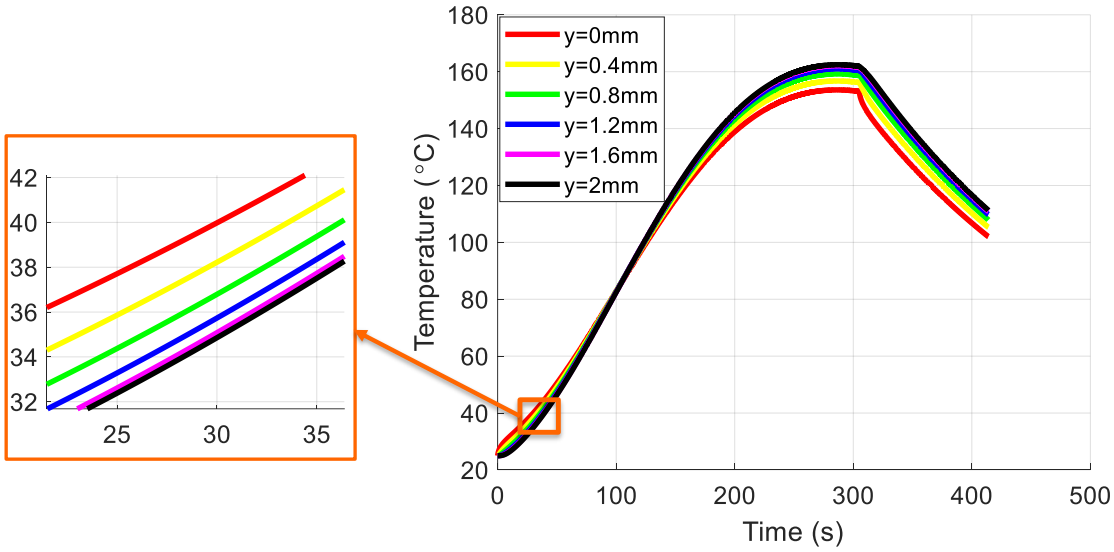


Figure 2.10: Temperature evolution

Figure 2.11 shows the final cure level of all nodes for three cases: the first case is the final cure level, which is less than the desired cure level (under cure). The switching and final times for this case are 225s and 414s respectively. The second case is when the cure level is above the desired value (over cure) which will result in loss of required mechanical properties of the final product. The switching and final times for this case are 400s and 414s respectively. The third case is when the switching and final times are determined by the proposed optimal switching time control approach. The switching and final times for this case are 305s and 414s respectively. As it is seen in Fig. 2.11, final cure level for the optimized switching and the final time case reaches close to the target cure level (90%) and the maximum cur deviation is less than 2 %.

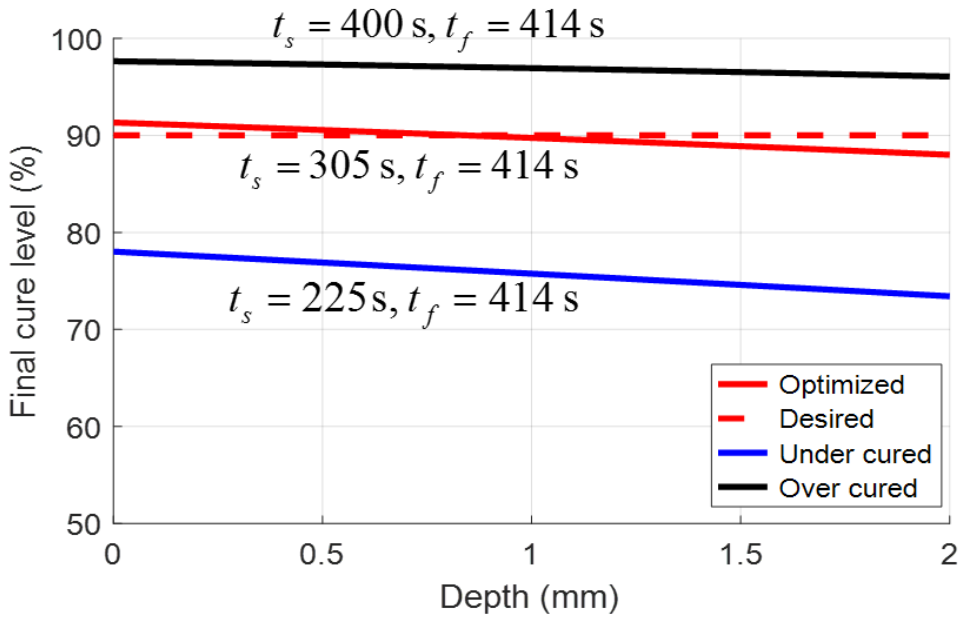


Figure 2.11: Final degree of cure for un-optimized and optimized cases

### 2.9.2 Experimentation

A 16.1W Clearstone UV LED which has UV emission peak wavelength of 365nm was used for irradiating the sample. The amount of UV reaching to the surface of the resin sample is measured by using a digital UV radiometer (Solarmeter) whose resolution is 0.1 mW/cm2. Hardness of the cured sample was assessed by using Vickers digital micro hardness tester (HVD-1000AP Digital Micro hardness tester by Shanghai Jvjing Precision Instrument Mfg. Co., Ltd. China). Bottom insulation was made from polyisocyanurate with thermal conductivity of 0.00024 W/cm$^oC$. The DGEBA epoxy resin was mixed with photo-initiator (Triarylsulfonium hexafluorophosphate salts, mixed with 50 % in propylene carbonate) was used to prepare the samples. Two DGEBA resin samples of equal amount (by weight) were taken for this study. The samples were first mixed with photo-initiator (PI). The optimum amount of photo-initiator was determined by using the method used in [29]

and found to be 3 % by weight. As discussed in the modeling section the materials were thermally insulated at the bottom. The resin was poured on to the insulated mold and let to spread and make a flat surface on the mold. The amount of resin used for each samples were 2.5g. Then the samples were irradiated with 130 mW/cm2 UV cured from the top for 305s (sample 1) and for 420s (sample 2). Note that the first sample was cured for optimal switching time and the second sample was irradiated for about 2 min additional time to compare the hardness the two samples. The cured samples are shown in Fig. 2.12.


Figure 2.12: Cured samples

### 2.9.3 Hardness measurement

Hardness testing was used to assess the effectiveness of the cure with optimal time switching time discussed in the previous section. The Vickers hardness was determined with a micro hardness tester by using a Vickers diamond indenter with a 200g load applied for 10 seconds (dwell time). For each sample, five tests were made on the top and bottom surfaces. All five hardness measurements were taken close to the center (within 1mm diameter). For each specimen, the five Vickers hardness values (HV) were averaged and reported as a single value. The hardness ratio of both specimens were calculated and tabulated using the formula: hardness ratio = mean

HV of top surface/mean HV of bottom surface. The results of the hardness test are summarized in Table2.2.

Table 2.2: Hardness measurment

| Sample | Switching time (s) | Top surface hardness (HV) | | Bottom surface hardness (HV) | | Hardness Ratio |
|---|---|---|---|---|---|---|
| | | Mean | Std. Dev. | Mean | Std. Dev. | |
| 1 | 305 | 21.122 | 0.491422 | 20.232 | 0.72295 | 1.04399 |
| 2 | 420 | 20.654 | 0.612163 | 20.644 | 1.02156 | 1.000484 |

.

As can be seen in Table 2.2 the hardness values of the samples cured with optimal switching time is similar to the sample irradiated with longer time which shows that the proposed model saves considerable amount of time and therefore curing energy. Moreover, optimal times will help finding the better quality of the product which otherwise would be compromised. This is because if it is under cured obviously the required property of the product will not be achieved and if it is over-cured the final product will be brittle [42].

### 2.9.4 Summary and Conclusion

In this section, an optimal switching time control scheme is proposed for a cationic UV curing process. First, the curing process model for this process is configured as a switching system. The kinetics model includes UV spatial attenuation effects and spatial temperature distribution that pose a challenge in manufacturing thick layers with UV. The necessary optimality conditions are then derived and used for the switching and final time that give minimal cure level deviations across the thick layer. The maximum deviation of final cure from the desired one is less than 2%. It is also illustrated how the model-based optimization of the optimal switch-

ing and final time help to get a near through cure across a 2mm part compared is arbitrary selections of the same. To assess the performance of the proposed method samples was prepared as used in simulation and cured with optimal switching time and higher switching time. The hardness of both samples were measured and showed that both samples have comparable hardness on both top and bottom surfaces. The optimal switching time control strategy used in this paper can be applied to any cationic curing process and composite laminates which are made from epoxy and UV transparent fibers such as fiber glass.

# Chapter 3

# Modeling the Layer-by-Layer UV Curing Process for Fiber-Reinforced Composite

## 3.1 Abstract

This chapter first describes a curing process model comprised of the coupled cure-kinetics and thermal evolution in a cationic polymerization of a single layer of material and then extends it to multi-mode curing of multiple layers. The model is characterized as a switching multi-mode dynamic system that switches when the UV source is turned off and when a new layer is added to the existing layer. These two switching conditions are explicitly defined. The model is then used to determine the optimal mode switching times and the final process time which are considered as manipulated control variables. This is done by explicitly deriving the necessary conditions of optimality for the multi-mode switching system. The results are first illustrated for a two-layer composite laminate and then the results of five-layer curing

are briefly discussed to show the versatility of the proposed approach. The optimal switching times and final time result in minimal cure level deviation across the thick composite material.

## 3.2 Introduction

The optimal switching time control of a multi-mode, ultraviolet induced fiber-reinforced composite part is considered. There are different methods of thermal based curing of thermo-set fiber-reinforced composites. Of which, the most widely used is autoclave or oven processing [43], which applies heat and pressure to combine resin and fiber to form a composite part. However, autoclaves require high capital for equipment and operation costs and have limited space. This and other associated disadvantages make out-of-autoclave methods such as Ultraviolet (UV) radiation more attractive to composite manufacturers.

UV curing is non-conventional, non-thermal radiation-based process offering several advantages: improved resin stability, handling flexibility, fast curing speed, fewer emissions of toxic volatile components, lower curing temperature thus reducing energy consumption. Due to these advantages, UV curing has gained much attention as an alternative to conventional thermal based curing [19, 23]. However, since the light penetration is not good enough to undergo complete cure in thick samples, UV and other light-induced polymerization reactions are currently restricted to the area of coatings, clear coats or varnishes and paints where the light penetration is high enough for these thin samples to ensure a fast and efficient curing [44, 18, 26]. Moreover, with thicker films and parts, the attenuation of UV with thickness causes a cure level and temperature gradient across the depth which compromises the quality of the end product [45, 24, 28, 25].

There are few research works focused on UV induced thick layer manufacturing. A 2 mm thick laminate of epoxy acrylate-modified unsaturated polyester composite was cured using UV irradiation at room temperature in air [20]. UV curing technology was combined with a fiber placement process to fabricate acrylate/glass-fiber composites [26] and the effect of UV exposure dose and compaction force on the performance of thick acrylate/glass-fiber composites was also studied. A layer-by-layer manufacturing approach proposed in [28, 41] showed that for acrylate/glass-fiber composites by partially curing a thin layer and adding new layer will help minimize the cure deviation across thickness/depth.

Thick composite manufacturing approaches are all focused on acrylate based matrix with free radical photo-initiator, which cures during irradiation and stops curing once UV is off. Unlike free radical polymerization mostly acrylate based, epoxy with cationic photo-initiator continues polymerization post-irradiation, albeit at a slower rate.

Epoxy resins are by far the most used materials in conventional, thermal curing process [46]. However, an epoxy-based matrix with cationic photo-initiators, which cures during irradiation and continues to cure at a slower rate after UV is off, has received relatively little attention, particularly for manufacturing of thick parts. The post-irradiation curing makes cationic polymerization more attractive as compared to the free-radical polymerization. However, as the modeling and control problem becomes more challenging due to change in the cure dynamics of the process from UV on to UV off mode and vice versa. This chapter seeks to model the multilayer cationic polymerization process and develop an optimal control scheme that can be applied to exploit the aformentioned advantages of UV curing process. A switching multi-mode dynamic system is modeled by combining the cure kinetics of cationic photopolymerization during irradiation [30, 28] and the cure kinetics for dark cure

[33]. The model is characterized by two types of switching modes in each layer: mode switch one ($MS1$) and mode switch two ($MS2$). $MS1$ happens when UV is turned off from UV on mode and $MS2$ occurs when UV is on from UV off mode (when a new layer is added to the existing one). Despite the UV attenuation across depth/thickness, near through-cure can be achieved by optimizing the switching times between the modes and final process time. In this chapter, the mode switching times and final time are optimized even though the simultaneous optimization of the UV input at each layer can be pursued as was done for the free-radical case in [19]. Optimal switching times, as well as the final time, are determined by explicitly deriving the necessary conditions for optimality given the coupled dynamic constraints describing the cure-kinetics and thermal dynamics involved in the multi-mode curing process.

## 3.3 Curing Process for Cationic Polymerization

In this section the cure kinetics of a 1D cationic curing process is discussed. We consider a 1D process for UV induced cationic curing of a fiber glass reinforced composite. The process set up is shown in Fig. 3.11, where a single layer of material is cured with a uniform UV source at the top from initial time to switching time ($t_0 \leq \mathrm{t} < t_s$) and then left to cure by itself without UV till final time ($t_s \leq \mathrm{t} \leq t_f$). The curing process involves heat generation from cationic polymerization (exothermic reaction), convection heat transfers at the top surface and conduction within the layer. These also need to be captured along with boundary conditions. As depicted in Fig. 3.11, we consider a convective heat transfer (BC1) at the top and an insulated boundary condition (BC2) at the bottom. From the low of energy, a one dimensional transient heat conduction which includes internal heat generation due to exothermic

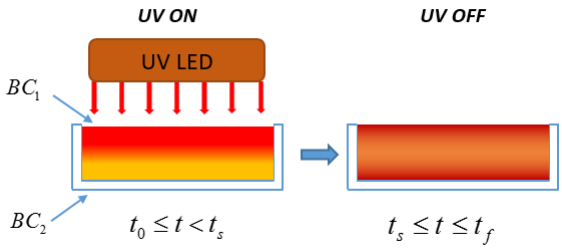


Figure 3.1: Schematic of 1D curing process

cure reaction equation can be written as [47].

$$\rho c \frac{\partial T(t,y)}{\partial t} = k_y \frac{\partial^2 T(t,y)}{\partial y^2} + \rho_r \Delta H_r \frac{d\alpha(t,y)}{dt} \tag{3.1}$$

where $\rho$ and $c$ are the density and specific heat capacity of the composie, respectively; $k_y$ is the thermal conductivity of the composite across the depth; $T(t,y)$ is the temperature at time $t$ and depth $y$. $\Delta H_r$ is enthalpy of polymerization; $\alpha(t,y)$ is degree of cure at time $t$ and depth $y$ ; $l$ is the thickness (depth) of the layer(s). Equation (3.1) is coupled with the cure rate equation for UV on and UV off modes. The cure rate equation for UV on mode derived in the previous section Eq. 2.14 is highly nonlinear and the fact the cure rate equation for UV on mode is well established for both acrylate resin [28, 30] and epoxy resin [30, 48] , we opt to use the already avialable equation for UV ON mode and is given as follows:

$$\frac{d\alpha(t,y)}{dt} = A \exp\left(\frac{-E}{RT_{abs}}\right) I(y) \alpha^m (1-\alpha)^n \tag{3.2}$$

where, $A$ is pre-exponential constant; $E$ is the activation energy ; $R$ is universal gas constant; $T_{abs}$ is the absolute temperature in Kelvin and $I(y)$ is the UV intensity at depth $y$ from the top surface. From Beer Lambert's law, the variation of the UV

intensity with depth is studied in [30] and is given by Eqn. (3.3 ).

$$I(y) = I_0 e^{-\mu y} \tag{3.3}$$

where $I_0$ is the intensity at the top surface; $y$ is the depth in the direction of radiation and $\mu$ is attenuation constant. As stated earlier, cationic polymerization continues after UV is off but with a slower rate. The cure kinetics for UV off mode (dark cure) determined experimentally in [33] and is given by Eqn. (3.4).

$$\frac{d\alpha}{dt} = d \exp\left(\frac{-E}{RT_{abs}}\right)(1 - \exp(-k_i t_s D))(1 - \alpha) \tag{3.4}$$

where $k_i$ is initiation rate constant and $t_s$ is switching time.
The convective boundary conditions (BC1) shown in Fig. 3.11 can be given as:

$$-k_y \frac{\partial T(t,y)}{\partial y} + \vartheta I_0 = h(T(t,y) - T_\infty) \tag{3.5}$$

where $T_\infty$ is the ambient temperature; $h$ is the convective heat transfer coefficient; $\vartheta$ is the UV absorptivity constant at the top surface. A one dimensional UV curing process model is then summarized as:

$$\begin{cases} \rho c \frac{\partial T(t,y)}{\partial t} = k_y \frac{\partial^2 T(t,y)}{\partial y^2} + \rho_r \Delta H_r \frac{d\alpha(t,y)}{dt} \\ -k_y \frac{\partial T(t,y)}{\partial y} + \vartheta I_0 = h(T(t,y) - T_\infty) \\ \frac{\partial T(t,l)}{\partial y} = 0 \\ \frac{d\alpha(t,y)}{dt} = \begin{cases} A \exp\left(\frac{-E}{RT_{abs}}\right) I_0 e^{-\mu y} \alpha^m (1-\alpha)^n, & t \in [t_0, t_s) \\ d \exp\left(\frac{-E}{RT_{abs}}\right)\left(1 - e^{-k_i t_s D}\right)(1-\alpha), & t \in [t_s, t_f] \end{cases} \end{cases} \tag{3.6}$$

Note that the control input is uniform UV which is given in Eqn. (3.3) and the optimization parameters are switching and final curing times.

## 3.4 Multi-Mode Layer-by-Layer Curing Process

For layer-by-layer additive manufacturing process the switching sequence is fixed. And the initial time is known ($t_0$), but the final time is relaxed and is free to be optimized. The dimensions of states,control spaces and system dynamics vary when switching from UV off mode to UV on mode and control space and system dynamics will vary when switching from UV on to UV off mode. Now, for a single layers, the state evolution during time interval $[t_0, t_s]$ is given by the following equation.

$$\dot{x} = f_1(x(t), u(t)), \qquad t_0 \leq t \leq t_s \tag{3.7}$$

And the state evolution for UV off mode that is on the interval $(t_s, t_f]$ is given as :

$$\dot{x} = f_2(x(t)), \qquad t_s < t \leq t_f \tag{3.8}$$

where $x(t) = [\alpha(t), T(t)]'$ is the augmented state vector comprised of the cure-level and temperature state at each discrete spatial location at any time $t$ or any mode in the layering process. $f_1(x(t), u(t))$ is a function of the cure-level, temperature state and the UV input, and $f_2(x(t))$ is a function of only the cure-level and temperature state. As stated earlier, the switching mult-mode system considered in this study involves two types of switching: the first one is when UV is off and the other is when a new layer is added on the previous layer. The details of the two switching modes are discussed as follows:

### 3.4.1 Mode Switch One (MS1)

Mode switch one occurs when the UV is turned off after being initially on at any layering step. During the UV on mode, the temperature of the layers exposed to UV rises to some level higher than the initial ambient temperature. For the subsequent curing in the UV off mode, this change in temperature drives the cure reaction. Hence, the initial values of the temperature at the switch to UV off mode is taken as the final temperature of the UV on mode.The same assumption can be taken for the cure level state. The state transition for mode switch one can therefore be described by eqs. (3.9) and (3.10).

$$x_{j+1}^{T}(t_j^{+}) = \Gamma_j^{T}(x_j^{T}(t_j^{-})) \tag{3.9}$$

$$x_{j+1}^{\alpha}(t_j^{+}) = \Gamma_j^{\alpha}(x_j^{\alpha}(t_j^{-})) \tag{3.10}$$

where $x_{j+1}^{T}(t_j{}^{+})$ and $x_{j+1}^{\alpha}(t_j^{+})$ are, respectively, the temperature state and cure level state in UV off mode just after switching to UV off at switching time $t_j^{-}$. $x_j^{T}(t_j^{-})$ and $x_j^{\alpha}(t_j^{-})$ are the temperature state and cure level in UV on mode just before switching. Here, $j$ is the index of mode switch one . $\Gamma_j$ is a mapping operator and for inter-layer modes it maps to itself. Note that the state vector components are indexed by their discrete spatial location across all layers up to the present processing step.

### 3.4.2 Mode Switch Two (MS2)

Mode switch two occurs when a new layer is added to the existing layer. This mode switch is the same as the case treated for free-radical polymerization detailed in [28]. In defining this inter-layer switching, state initializations at interface locations (between the bottom of the new and top of previous layer) need special

handling. Since existing layers are likely at relatively at higher temperature, there will be conductive heat transfer between the new layer and existing layers, particularly at the interface location. Here, we take the initial temperature (after layering) at the interface to be the average of the ambient temperature and that at the top of the previous layer. For the cure level state, since the cure level is irreversible for thermo-set materials, the cure level of the existing layer will not be instantly affected by the addition of the new layer. Therefore, for the next mode, the cure level at the interface is initialized at the value of the cure level state of the top of the previous layer just before the new layer is added. The state transition for mode switch two can therefore be described by Eqns. (3.11) and (3.12 ) :

$$x^T_{j+1}(t_j^+) = \Gamma^T_j(x^T_j(t_j^-)) \tag{3.11}$$

$$x^\alpha_{j+1}(t_j^+) = \Gamma^\alpha_j(x^\alpha_j(t_j^-)) \tag{3.12}$$

where, $x^T_{j+1}(t_j{}^+)$ and $x^\alpha_{j+1}(t_j^+)$ are, respectively, the temperature state and cure level state just after a new layer is added and $x^T_j(t_j^-)$ and $x^\alpha_j(t_j^-)$ are the temperature state and cure level just before layer addition. Here, $j$ is the inter-layer mode index. $\Gamma_j$ is mapping operator describing the mode switch two whose detailed mathematical formulation is given in [28]; we mention only some of the salient aspects and modeling assumptions here. First note that with each layer added, the dimension of the state space increases by the size of the spatial discretization for the added layer. The new layer is assumed to be in ambient condition (uncured state, at ambient temperature). The schematic of mode switch one and mode switch two is illustrated in Fig. 3.2.

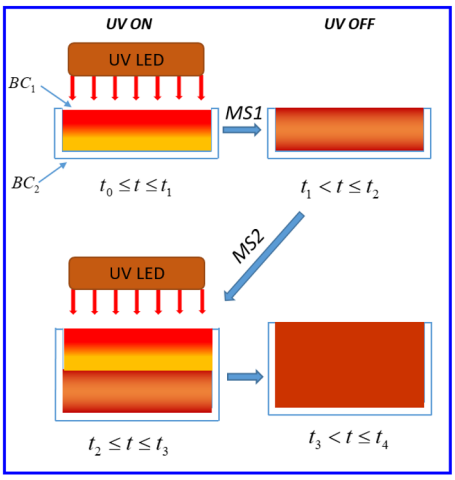


Figure 3.2: Layer-by-Layer Cationic Curing Process.

## 3.5 Optimal Control of Multimode Switching System

In this section we pose an optimal control problem for the model described in Eqn. 3.6 and subsequently derive the necessary conditions of optimality for the given problem.

### 3.5.1 Problem Formulation

To have a successful curing, the process must allow full cure of the whole resin in the composite material and there should be full consolidation within a laminate and between layers. Therefore, the UV induced cationic curing process system discussed in the previous section can be controlled by fixing the switching time for each mode and manipulating the UV intensity or by keeping the UV constant and find the optimal switching times and final time. The process is dependent on UV for only half of the modes (UV on modes) and the rest (UV off modes) are obviously not dependent on

it, but both modes are dependent on switching times. Hence, we opt for optimizing the switching and final times and apply uniform UV during UV on mode. Therefore, assuming that switching between the different dynamics is time-driven, the switching-time vector $\bar{t} = [t_1, t_2 ... t_M]$ will be the only control parameter. For a given UV input the optimal problem is to determine the optimal switching time vector $\bar{t} = [t_1, t_2 ... t_M]$ which minimizes the cost function given in Eqn. (3.13)

$$J = \sum_{j=1}^{M} \int_{t_{j-1}}^{t_M} g_j(x_j, u_j)dt + \sum_{j=1}^{M-1} \phi_j(x_j(t_j^-)) + \Phi(x_f(t_f)) \tag{3.13}$$

where $j = 1, ..., M$ is the mode index, $g_j(x_j, u_j)$ is the instantaneous cost in mode $j$, $\phi_j$ is a state transition cost between different modes and $\Phi$ is a terminal cost.

### 3.5.2 Optimality Conditions

The optimality condition is derived based on variational approach [49]. Here we will present only the summarized optimality conditions, a full derivation of a similar approach for different hybrid problems can be found in [36, 19]. By adjoining the dynamical constraints in eqs. (3.7) and (3.8) to the cost function eq. (3.13) via different Lagrange multipliers, $\lambda_j(t)$, defined over the interval $(t_{j-1}, t_j)$, will not change the value of the cost function. In addition , by adjoining the state transition constraints at the switching times given in eqs. (3.9) to (3.12) via Lagrange multipliers $\mu_j$ .

To get through cure and uniform distribution of cure the terminal cost is taken and the optimal control is, therefore, posed as one of optimizing the time vector $[t_1, t_2, ..., t_M]$ , which minimize the cost function. The values of the switching and final times will give the optimum time to turn off the UV, to add a new layer and the final time at which the cure at all depth is close to the desired value. Since our

interest is in achieving uniform cure distribution across layers, the cost function takes only the terminal cost. Hence , the optimization problem can be posed as :

$$J = 1/2 \sum_{0}^{n} (\alpha(y, t_M) - \alpha_{des})^2 \tag{3.14}$$

subjected to the state evolution given in ens. (3.7) and (3.8), and mode switching constraint given in eqs. (3.9) and (3.12). In Eqn. (3.14), $\alpha(y, t_M)$ is the final degree of cure , $\alpha_{des}$ is the desired degree of cure and $N$ is the number of discretization points along the depth. The necessary condition for first order equation is Euler Lagrange equation and is given in eq. 3.15.

$$\dot{\lambda}_j = -\frac{\partial H_j}{\partial x_j}(x_j, u_j, \ \lambda_j) \tag{3.15}$$

where $H$ is the Hamiltonian and is given in Eqn. (3.16)

$$H_j(x_j, u_j, \lambda_j) = L_j(x_j, u_j) + \lambda_j f_j(x_j(t)) \tag{3.16}$$

where $f$ is defined in eqs. (3.7) and (3.8), $j = 1, 2..., M$ is the mode index. Moreover, the boundary conditions for the given model is given in eqs. (3.17) to (3.19).

$$\mu_j = \lambda_{j+1}({t_j}^+) \tag{3.17}$$

$$\lambda_j({t_j}^-) = \mu_j(\partial F_j/\partial x_j) \tag{3.18}$$

$$\lambda_M({t_M}^-) = \partial\Phi/\partial x_M \tag{3.19}$$

For a given cost function, the optimality conditions are given in Eqns. (3.20) - (3.22).

$$\partial H_j/\partial u_j = 0 \tag{3.20}$$

$$H_j(t_j^-) - H_{j+1}(t_j^+) = 0 \tag{3.21}$$

$$H_M(t_M^-) = 0 \tag{3.22}$$

Note that for simulation, as we considered only the terminal cost the instantaneous term in the Hamiltonian defined in (3.16) is therefore zero. More over as discussed earlier, since UV is uinform, the optimality condition in eq. (3.20) is not required. Thus Equations (3.21) and (3.22) are used to determine the switching and final times. Having derived the necessary conditions for optimality, a steepest descent or gradient method is used to get optimal control values. The detail procedure of the numerical algorithm can be found [49] and [36] .

## 3.6 Results and Discussions

In this section, the main purpose is to discuss the results of a two-layer composite with each layer 1mm thickness and then the results of five-layer composite laminates are briefly discussed to show the versatility of the proposed approach.

### 3.6.1 Two-Layer Curing

The one-dimensional UV-induced cationic polymerization model summarized in the PDE-ODE eq. 3.6, is used to generate the temperature and cure state evo-

lutions. We select six discretization nodes along the depth and since there are two states for each node, namely cure state and temperature state, the system has 12 states. The process input, UV intensity is kept uniform for the first mode and the UV is turned off after a specified or optimal switching time ($t_s$). The switching and final time are the control variables that can be optimized to get minimum cure deviation of the final cure from the desired value, which is selected to be 90% in the simulation analyses to follow. Each layer has six nodes along the depth, two layers are considered to show the method for multi-mode curing. In each node there are two states namely, cure and temperature state. In one layer, there are twelve states (six nodes per layer and two states per node). As depicted in Fig. 3.2 when a layer is added on the previous layer (switching mode two) , the size of the sample increases and hence the size of state increases accordingly.Therefore, in two layer a total of up to 24 states are processed. The process input, UV intensity is kept uniform for UV on modes and will be off for UV off modes. All switching and final times are the control variables, which can be optimized to get minimum cure deviation of the final degree of cure from the desired value (90%). The optimal switching and final times are shown in Table. 3.1.

Table 3.1: Optimal switching and final times

| Mode | 1 | 2 | 3 | 4 |
|---|---|---|---|---|
| Initial switching time (s) | 120 | 250 | 350 | 400 |
| Optimal switching time (s) | 85 | 187 | 350 | 676 |
| Equal interval switching time (s) | 169 | 338 | 507 | 676 |

As seen in the table, for optimal switching time case, UV is ON until $85s$ and

then dark cure continued till the next layer addition/UV on time ($187s$) and then curing with UV resumes till the next UV off time ($350s$) then dark cure continues until the final optimal time ($676s$). This is depicted in Fig. 3.3 and show that significant cure happened during dark curing. The total time on which UV is on can be found by adding the durations on which UV was on, that is $t_{UV\_ON} = 85 + (350 - 187) = 248s$.

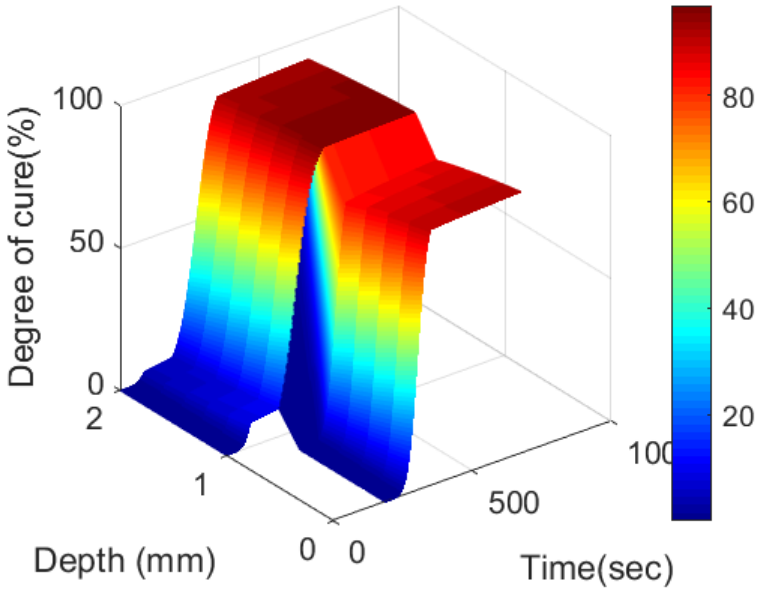


Figure 3.3: Degree of cure evolution with optimal switching times

As can be seen in Fig. 3.4 and Fig. 3.5, the temperature of the first layer initially increased from its initial value ($25\,^oc$) to about $40\,^oc$ and UV is turned off at the first switching time ($t_s = 85s$) then the temperature starts to decrease till a new layer is added. As stated earlier, at the interface (mode switch two) initial temperature is taken to be the average of the existing layer which is relatively at higher temperature and the new layer which is at ambient temperature (Fig. 3.5 ).This is done by assuming that there will be instant conduction at interface before transition to the next mode. However, for switch mode one, that is when UV is off the final temperature of the previous mode is taken as initial temperature for the next

mode. Fig. 3.5 shows the details of the temperature evolution at optimal switching times and optimal final time ($t_f = 676$).

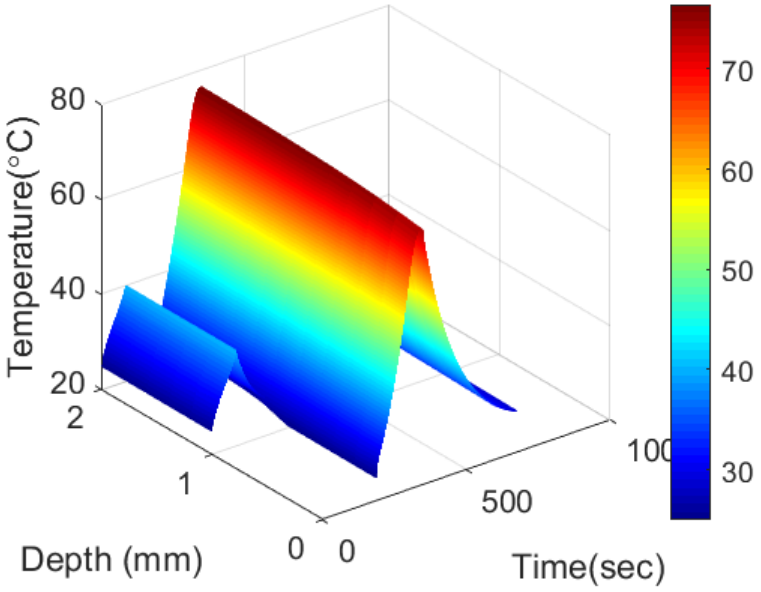


Figure 3.4: Temperature evolution with optimal switching times for two layer curing

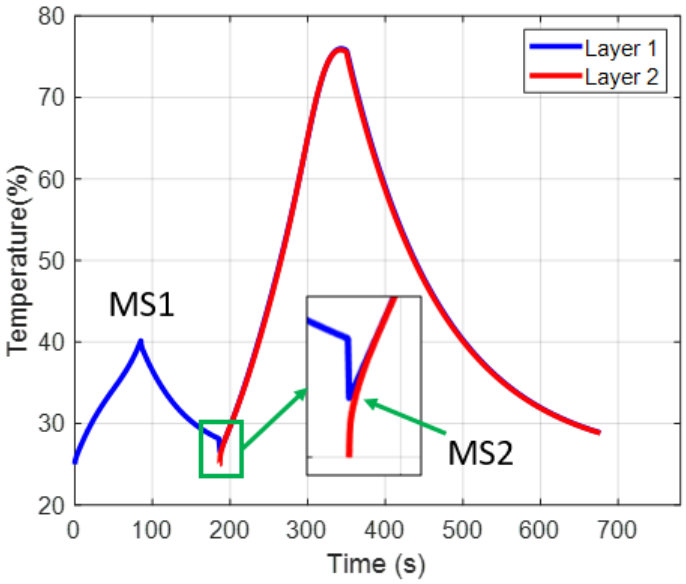


Figure 3.5: Interface temperature evolution for two layer curing

The proposed approach is then compared with equal time interval curing. This is done by taking the optimized total process time duration ($t_f$) and dividing by the total number of modes (for two-layer curing number of modes is four), so that all modes will have equal duration. In this case UV will be on for 676/2=338s, which is much higher than the optimized UV duration that is 248s. Moreover, as shown in Fig. 3.6 and Fig. 3.7, the final cure level is not close to the desired one, it has more than 25% deviation from the desired value which shows the importance of our approach in which case as dipicted in Fig. 3.7 the maximum deviation is not more than 5% .

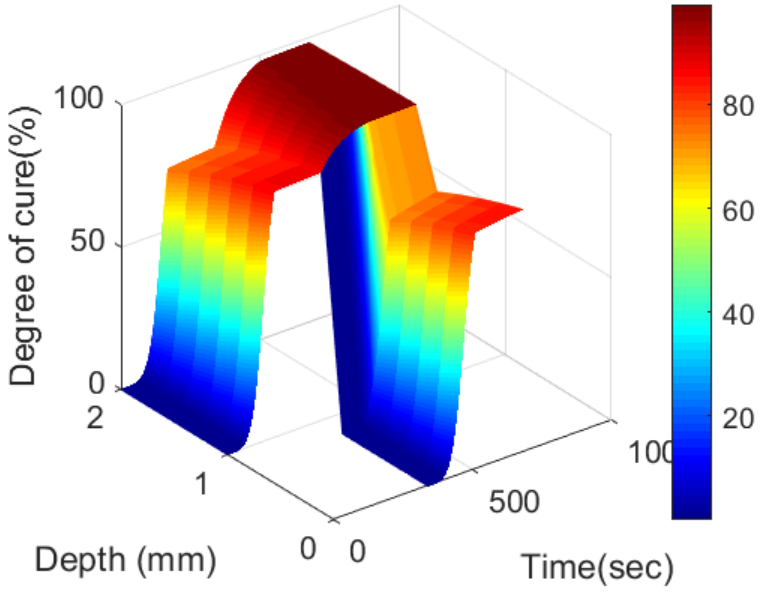


Figure 3.6: Degree of cure evolution with equal switching time in each mode

Figure 3.7 depicts the final degree of cure for with optimal switching times and the result is compared with equal time curing, under cure (less UV on time than optimized) and over cure (more UV on time ). For all cases considered, final time is the same and is taken from the optimal final process time. The switching times for

Table 3.2: Different switching times for two layer curing

| Curing type | $t_1(s)$ | $t_2(s)$ | $t_3(s)$ | $t_4(s)$ | UV ON time (s) |
|---|---|---|---|---|---|
| Optimal time | 85 | 187 | 350 | 676 | 248 |
| Equal time | 169 | 338 | 507 | 676 | 338 |
| Over cure | 151 | 226 | 500 | 676 | 425 |
| Under cure | 85 | 200 | 300 | 676 | 185 |

all cases are summerized in Table 3.2.

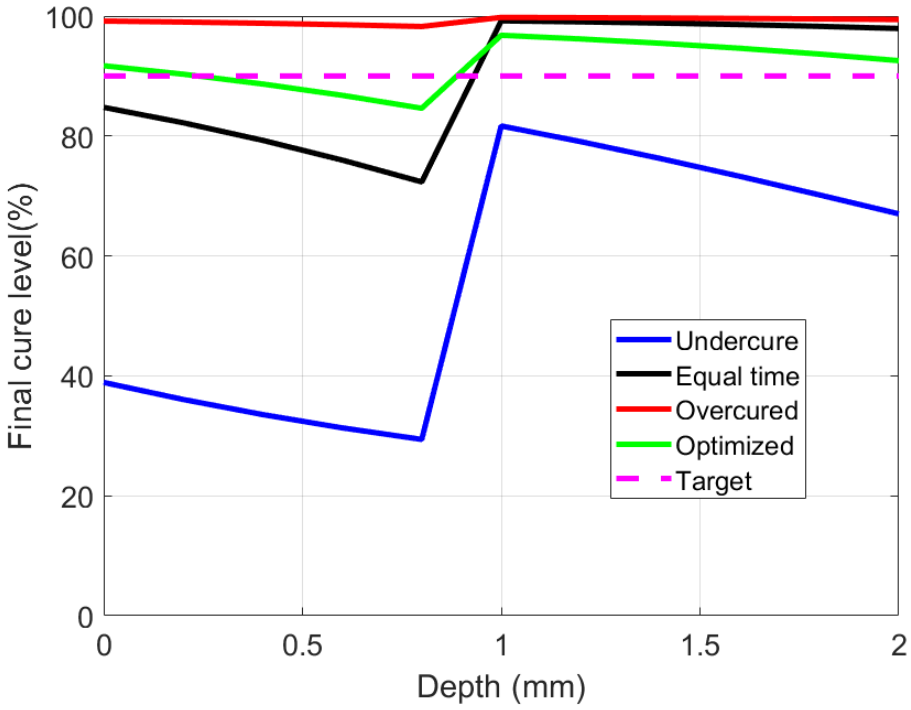


Figure 3.7: Comparison of final degree of cure

### 3.6.2 Five-Layer Curing

To show that our proposed approach, multi-mode swiching time optimal control, can work for any number of layers (part thickness), in this section we breifly discuss the results of a five layer curing. Figure 3.8 shows the degree of cure evolution for five layer curing. As can be seen in this figure and later in Fig. 3.9 and Fig. 3.10,

the final degree is close to the desired value. The degree of cure evolutions at the

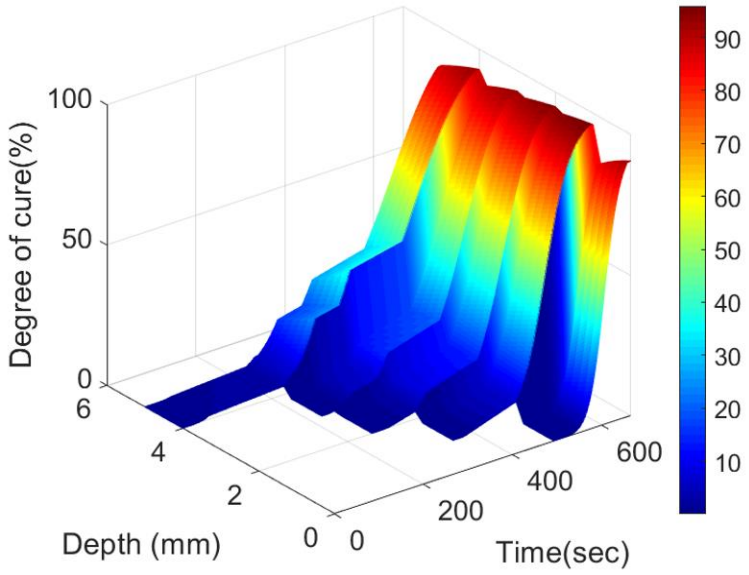


Figure 3.8: Degree of cure evolution of five layers

interfaces, at the top and bottom surfaces are shown in Fig. 3.9. As discussed earlier the degree of cure has zero initial value at interface. As illustrated in Fig. 3.9, unlike free radical polymerization the cure level increases by significant amount during the UV off mode (dark cure). This shows the advantage of cationic polymerization over free radical which do not polymerize after irradiation is stopped [31]. In addition, the final degree of cure of all layers, as depicted in Fig. 3.9 and Fig. 3.10 , reaches close to the target degree of cure (90 %).

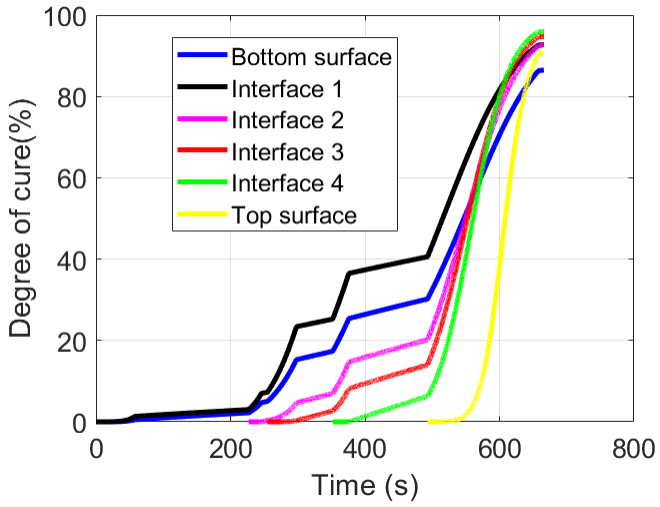


Figure 3.9: Degree of cure evolution at interfaces

As can be seen in Fig. 3.10, the maximum deviation of the final degree of cure as compared to the desired target is about 5% which is similar to the result found for two layer curing discussed in the previous section. This shows that the proposed approach can be used for any number of layers (thickness). The temperature evolution

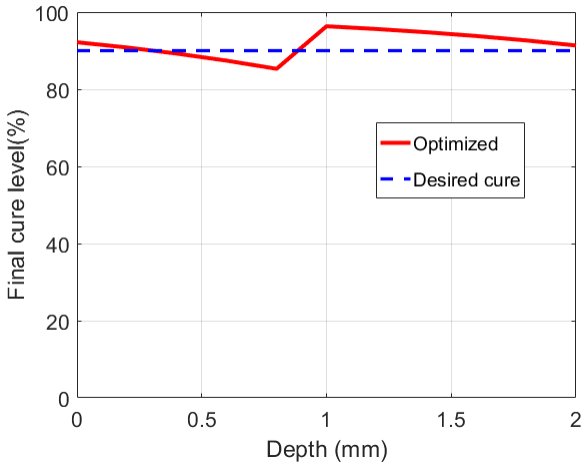


Figure 3.10: Final degree of cure

of five layers of composite laminates are shown in Fig. 3.11(a) and as can be seen in

Fig. 3.11(b) the final temperature gradient along the depth is about 10 °c, which shows that the proposed optimization of multi-mode curing approach reduces the potential of thermal stresses due to large temperature gradients across depth in a thick part. Figure 3.12 shows the degree of cure evolution using randomly selected switching time

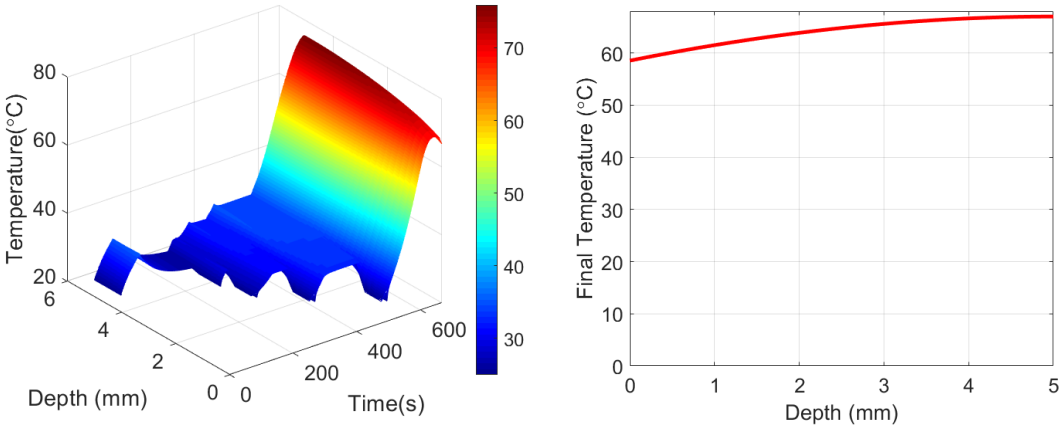


(a) Temperature evolution of five layers (b) Final temperature of five layers

Figure 3.11: Temperature evolution and final temperature

sequences, and Fig. 3.13 shows the degree of cure evolution using optimal switching time sequence.

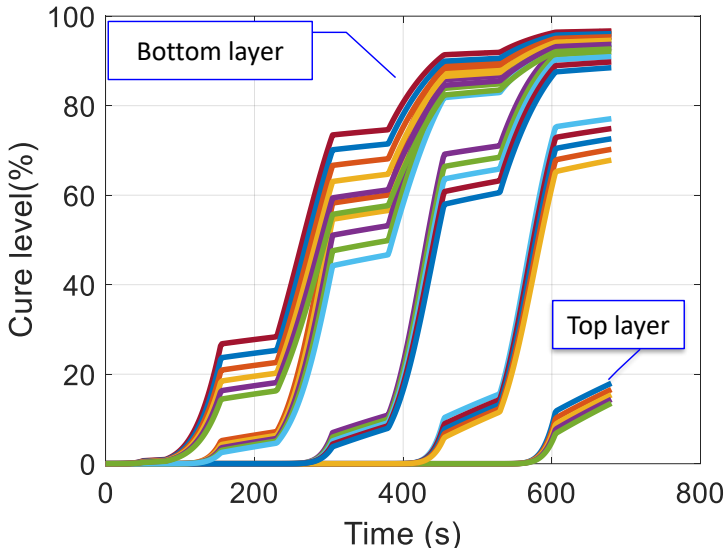


Figure 3.12: Degree of cure evolution with initial switching times

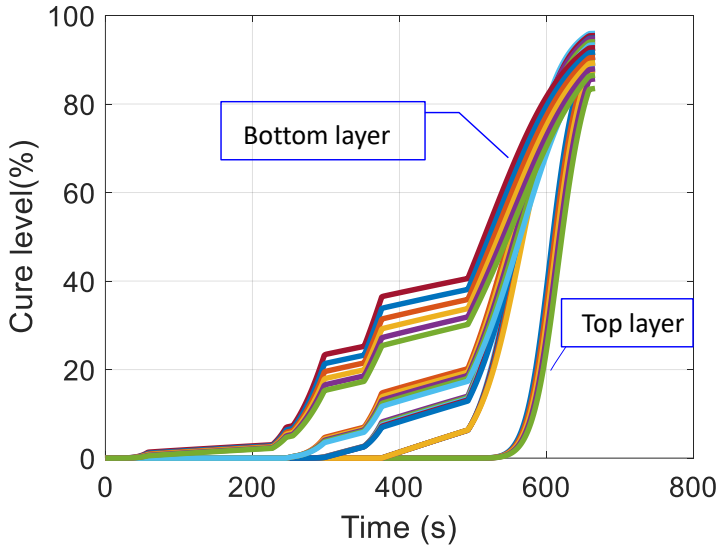


Figure 3.13: Degree of cure evolution wth optimal switching times

## 3.7 Conclusion

In this chapter, an optimal switching time control scheme is proposed for a multi-mode cationic UV curing process. First, the curing process model for this process is configured as a switching multi-mode system. The kinetics model includes UV spatial attenuation effects and spatial temperature distribution that pose a challenge in processing thick layers of material with UV. The two mode switching types are explicitly defined. The necessary optimality conditions are outlined for mode switching and final time that give a minimal final degree of cure deviations from the desired target. It is illustrated how the model-based optimization of the optimal switching times and final time helps to get near through cure across thick composites parts as compared to curing by taking equal time interval with the same final optimized time. The proposed approach is compared with equal time interval curing, which is determined by dividing the optimized final time by the number of modes. This comparison showed that the proposed approach in addition to achieving the targeted degree of cure, reduces the total amount of time UV is on and hence reduces the associated cost. To show the versatility of the model, the results of five-layer curing are briefly discussed.

# Chapter 4

# Effect of Consolidation Pressure on the Inter−laminar Shear Strength of Thick Composites Manufactured Layer−by−Layer

## 4.1 Abstract

In this chapter, we set to examine the Inter-Laminar Shear Strength (ILSS) of a fiber-reinforced composite part manufactured via a stepped-concurrent ultra-violet (UV) curing and layering process. This process was specifically proposed for making epoxy-based thick parts whereby a layer-by-layer, model-based, optimal layering time and UV control scheme is set up with the objective of minimizing the degree of cure deviation across the final thick part. We focus on a cationic curing process wherein additional energy savings are possible by switching off the UV source after initiating the curing reaction with the UV source at each layer addition. Since the

inter-laminar sheer strength of parts made via a layering process is often a concern, we consider the application of in-situ consolidation pressure in the layering process. We then characterize the inter-laminar shear strength by manufacturing samples with application of different in-situ consolidation pressures and measuring the inter-laminar shear strength of each sample by the short beam shear test. The results showed that the inter-laminar shear strength of composite parts fabricated with the proposed stepped-concurrent curing and layering process increases with the applied consolidation pressure up to a point. Scanning electron microscopy (SEM) of samples cured at different in-situ consolidation pressure showed that the sample with optimum consolidation pressure has relatively uniform fiber to resin distribution and hence improved inter-laminar shear strength.

## 4.2 Introduction

Additive manufacturing (AM) of fiber-reinforced composites is currently conducted by stereolithography, layer-by-layer, fused deposition modeling, selective laser sintering, and extrusion [50]. Layer by layer also called laminated object manufacturing (LOM) manufacturing is a type of additive manufacturing process which uses sheet of material and adhesive to make thick part [6]. Due to its inherent capability for handling sheet materials such as fiber reinforced composite prepregs, for producing geometrically complex near net shape objects , LOM is preferred is preferred manufacturing process among others [51]. Therefore, in the last two decades there has been a growing interest in layer-by-layer method for composite manufacturing. The interfacial characteristics of composites fabricated by LOM was investigated by [51] and reported that interlaminar shear strength is one of the main factors affecting the overall performance of the final product. C-shaped panels, made from polymer

matrix composites, were directly fabricated by curved LOM [52]. A vacuum thermoforming apparatus was applied to bond commercial prepregs. In other research, model based UV-induced stepped-concurrent curing approach for manufacturing of thick acrylate based composites was proposed [28, 41] and later validated with experiment [34]. The major issue for layer by layer manufacturing process is the difficulty of bringing adjacent layers to fully consolidate and cure [52]. It is quite important to increase the interlayer strength and reduce the void content as low as possible. A handful researchers have been studying to address this issue, [26] studied the effect of compaction and UV exposure on the inter-laminar shear strength (ILSS) and reported that improved ILSS of the final product is achieved when the optimum ILSS and UV intensity is chosen. The concept of layer-by-layer in-situ UV processing concept to make a thick glass fiber reinforced polyester composite was studied by [27]. The effect of layer thickness on the inter-laminar shear strength on achieving better ILSS is studied. The LOM system used in previous studies require post processing operation to increase the bonding between layers [53].

In this chapter, the main objective is to experimentally characterize the ILSS for parts manufactured with the layer-by-layer approach that uses the model-based optimization results. Furthermore, unlike the cited works above, which focused on free-radical UV polymerization (Curing) processes ,here we focus on cationic polymerization based curing processes. Recently, the availability of different photo-initiators and monomers for cationic curing has increased interest in their use. As discussed in the previous chapters , one of the main advantages of cationic polymerization is that once it is exposed to UV for sometime, it coutinues curing after UV is off. Hence, additional energy savings are possible by switching the UV source off after curing reactions are initiated after each layer addition. These switching times make for additional optimization variables in the layer-by-layer scheme. Researchers have indeed

investigated how to improve the ILSS of fiber-reinforced composites in thermal-based curing and have proposed different approaches [54, 55, 26, ?, 56]. In [54], the effects of exothermic overheating on the ILSS of a composite part is studied. They produced high thickness laminates and intentionally overheated it to induce thermal damage. From ILSS test results, authors claimed that the ILSS is lower for thicker samples that were overheated.

There has not been much work on characterizing the inter-laminar shear strength with radiation-based curing processes, partly since the processes are relatively new for thick composites manufacturing. The effect of irradiance on the intra-laminar shear strength was investigated in [43], which found that high UV and poor adhesion (ILSS). On the other hand, insufficient UV lowers ILSS. The work in [26] studied the effect of UV dosage and cure gradient on the ILSS of stepwise-curing of fiber-reinforced acrylates and reported that with an increase in UV, cure uniformity increases but the ILSS reduced. The effect of UV intensity on the curing uniformity and inter-laminar shear strength was assesed in [54] . The cure uniformity increased with increasing UV intensity, but higher UV intensity decreases ILSS. The effect of UV intensity and compaction force on intra-laminar shear strength of an automatic fiber placement composite manufacturing process was studied [54]. It was found in that work that the compaction force increases the infiltration of the resin and the distribution of the resin around the fiber becomes uniform, which makes the final product capable of resisting more load and so have better ILSS. However, the effect of compaction on ILSS have not been studied in a stepped-concurrent layer by layer thick composite manufacturing process.

The present study is motivated, in part, by these observations and aims at characterizing the ILSS when applying the stepped-concurrent curing, switching and layering process for making an epoxy resin-infused fiber-reinforced composite. First,

the optimal processing time sequence, which is composed of the UV switching times (off/on), the layering times, and the final time, is determined by posing and solving a model-based optimal control problem. The optimization objective is set us minimizing the cure deviation across all layers at the final time. Then, using the obtained optimal processing time sequence, two-layer composite samples were made by in-situ curing with varying consolidation pressures. The final degree of cure of these samples were analyzed by FTIR-ATR spectroscopy. We then experimentally characterize the inter-laminar shear strength and study the effects of in-situ consolidation pressure on the inter-laminar shear strength as measured by the short beam shear test. The SEM images of the cured samples were also analyzed.

## 4.3 Process Modeling

### 4.3.1 Modle for Cationic UV Curing Process (Single Layer)

Fig.1 shows a basic set up for a cationic UV curing of a single layer of material. We consider one dimensional heat conduction, where the boundary conditions are the insulation boundary condition at the bottom (BC1) and convective boundary condition at the top surface (BC2). The model for the cationic polymerization is comprised of the cure kinetics model for curing under UV (with UV ON) and for the subsequent curing without UV (with UV OFF). The attenuation of the UV intensity along the depth is modeled by the Beer-Lamberts Law [54, 55, 26].

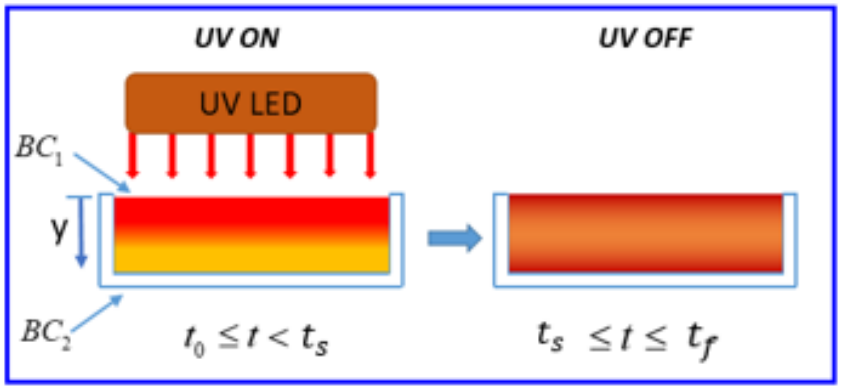


Figure 4.1: 1D concurrent layering and cationic curing process

Bringing all of these together, the curing process model is summarized as follows [28, 57, 58]:

$$\rho c \frac{\partial T(t,y)}{\partial t} = k_y \frac{\partial^2 T(t,y)}{\partial y^2} + \rho_r \Delta H_r \frac{d\alpha(t,y)}{dt} \tag{4.1}$$

$$-k_y \frac{\partial T(t,0)}{\partial y} + \vartheta I_0 = h(T(t,0) - T_\infty) \tag{4.2}$$

$$\frac{\partial T(t,l)}{\partial y} = 0 \tag{4.3}$$

$$\frac{d\alpha\left(y,t\right)}{dt} = \begin{cases} A\exp\left(\frac{-E}{RT_{abs}}\right) I_0^p \exp\left(-\lambda y\right) \alpha\left(y,t\right)^m \times \\ \left[1-\alpha\left(y,t\right)\right]^n, \ t\epsilon\left[t_0 t_s\right) \\ d\exp\left(\frac{-E}{RT_{abs}}\right) \left[1-\exp\left(-k_i t_s D\right)\right] \times \\ \left[1-\alpha\left(y,t\right)\right], \quad t\epsilon\left[t_s, t_f\right] \end{cases} \tag{4.4}$$

where $\rho$ and $c$ are the density and specific heat capacity of the epoxy, respectively; $k_y$ is the thermal conductivity of the epoxy across the depth; $T(t,y)$ is the temperature at time $t$ and depth $h$ . $\Delta H_r$ is enthalpy of polymerization; $\alpha(t,y)$ is

Table 4.1: Physical parameters for the numerical simulation

| | Volume fraction | $\rho[cm/cm^3]$ | $c[J/(kgK)]$ | $k_y[W/(cm^o c)]$ | $\Delta H[J/g]$ |
|---|---|---|---|---|---|
| Resin | 0.4 | 1.15 | 1.75 | 0.0025 | 332 |
| Glass fiber | 0.6 | 2.575 | 0.80 | 0.01275 | - |
| Composite | 1 | 2 | 1.02 | 0.0037 | 332 |

degree of cure at time and depth $y$ ; $l$ is the thickness (depth) of the sample; $A$ is pre-exponential constant; $E$ is the activation energy; $R$ is universal gas constant; $T_{abs}$ the absolute temperature in Kelvin; $I_0$ is the initial UV intensity; $\mu$ is UV attenuation constant; $k_i$ is initiation rate constant; $t_s$ and $t_f$ are switching (UV off) and final cure times. The switching in eq. (4.4) captures the different curing kinetics with UV ON/OFF in cationic curing. The above model shall be implemented by adopting a spatial discretization of the domain and forward in-time central difference in space (FTCS) approximation [59] of the coupled partial/ordinary differential equations and the boundary conditions listed in eqs. (4.1) to (4.4) .

### 4.3.2 Model for the Layer-by-Layer Process

In this section, we outline the model for the stepped concurrent curing, layering and switching process. We build on the single layer cationic cure process model detailed above. The stepped concurrent curing (SCC) and layering approach for UV-induced thick composite manufacturing is first proposed in [41] assuming free radical polymerization. In this paper, we extend this to the cationic polymerization where the resin continues to cure even after UV is turned OFF, albeit at a different rate. The specific addition is the presence of the UV switching (ON to OFF) time, even before another layer is added, which now makes for another controllable variable. The schematic of stepped concurrent curing, switching and layering process is shown in

Fig. 2.3.

One simplification we consider is that UV turns ON concurrently with the addition of each layer. The UV intensity itself could vary between layers, but this case is not considered in the present work. For the mathematical formulation involving these cases the reader is referred to [28].

Given the coupled cure-kinetics and discretized temperature evolution model described in the previous section for a single layer, we can assemble a state-space model for the multi-layer case as follows:

$$\dot{x} = f(x(t), u(t)) \tag{4.5}$$

where $x(t) = [\alpha(t), T(t)]$ is the state vector comprised of the cure-level and temperature state at each discrete spatial location at any time $t$ or any mode in the layering process. $f(x(t), u(t))$ is a function of the cure-level, temperature state and the UV input for those modes where the UV is on (mode index $i1$ at the $i^{th}$ layer), and a function of only the cure-level and temperature state for those modes where the UV is off (mode index $i2$ at the $i^{th}$ layer).The details of eq. (4.5) can be found in our previous work [28, 57].

In the next section, we demonstrate the stepped concurrent curing and layering process for making a two-layer part. As mentioned earlier, we use model based optimal control to determine the optimal processing time sequence (comprised of layering time, UV switch OFF time, and final times), which gives uniform cure distribution across both layers. This still will not guarantee the complete bonding between layers as it doesnt explicitly deal with this issue. Therefore, to improve the bonding between adjacent layers, we consider the effect of applying in situ consolidation pressure on the inter-laminar shear strength; therein, our approach is purely experimental.

### 4.3.3 Optimal processing time control

Optimal control of switching systems are designed get optimal switching and final times which optimize the given performance criterion. This criterion considers the deviation of final degree of cure from targeted degree of cure. The optimal time control objective is thus to minimize this deviation by choosing the optimal switching and final times for a uniform UV input. The objective function is given by:

$$J = 1/2 \sum_{0}^{n} \left(\alpha(y, t_M) - \alpha_{des}\right)^2 \tag{4.6}$$

where $J$ is the cost function; $\alpha(t_f)$ is the distributed cure state for the final degree of cure along the depth and is the desired degree of cure along the depth at the final time, is the thickness (depth) of the sample. eq. (4.6) is subjected to the state evolution model depicted in Figure 2.3 and given compactly in eq. (4.5). The cost function as well as the evolution model in eq. (4.5) are converted to discretized forms for computation. Taking the optimality condition given in the previous chapter and the cost function , the numerical algorithm to solve the optimal time sequence is given by Steepest descent algorithm and the steps are shown below [35, 28].

1. Choose initial iterate $\tau_i^0$ for $i = 1, 2, 3, 4$ and choose a termination tolerance $\varepsilon$
2. Set the iteration counter $k = 0$
3. While $\left|J^k - J^{k-1}\right| > \varepsilon$
4. Compute the state trajectory $x_i(t)$, $t\epsilon\left[\tau_{i-1,}\tau_i\right]$ for $i = 1, 2, 3, 4$ forward in time from $t_0 = 0$ to $t_f = \tau_N$
5. Compute the adjoining variable $\bar{p}_i(t)$, $for\ i = 1, 2, 3, 4$ backward in time from $t_f = \tau_N$ to $t_0 = 0$

6. Update the time vector $\tau_i^{k+1} = \tau_i^k - \delta_i^k B_i$ , where $i = 1, 2, 3$ and $N = 4$

7. $\tau_N^{k+1} = \tau_N^k - \delta_N^k C \;\; B_i = H_i(\tau_i^-) - H_i(\tau_i^+)$ and $C = H_N(\tau_i^-)$

8. $k = k + 1$

9. *End while*

10. Save the optimal switching time vector $[\tau_1, \tau_2, \tau_3, \tau_4]^T$

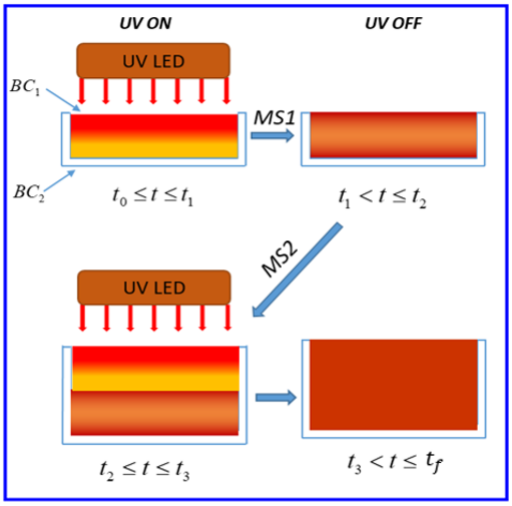


Figure 4.2: Two-layer four-mode cationic curing process

The computational framework for solving the optimization problem involves the derivation of the necessary conditions of optimality using traditional optimal control approaches, where the system/process model in eq. (4.5) serve as constraints to the objective function in eq. (4.6). The necessary conditions for optimality are derived and outlined in our previous work [57] and similar derivations for acrylate based composites can be found in [23, 28, 19] . For brevity, we skip those derivations here and discuss some typical outcomes from the model-based optimal control. Using the necessary conditions of optimality, we apply the steepest descent algorithm to

find the optimal solutions for the processing time sequence [35, 41]. For the two-layer part, for which the four-mode cationic curing process is depicted in Figure 4.2, we seek to achieve minimal cure-level deviation (across the part) from the desired target by computing the optimal processing times ($t_1$, $t_2$,$t_3$ and $t_f$ ) that minimize the objective function in eq. (4.6). The values of $t_1$, $t_2$,$t_3$ and $t_f$ give the optimum times, respectively, to switch the UV OFF with just the first layer, to layering and turn the UV ON for second layer, and to switch the UV OFF on the second layer, and to stop the process at the final time. If the optimizations are successful (i.e., solutions are found), at the final time, the cure at all depths will be the closest to the desired degree of cure.

For the results below, we set the target cure level at 98%, for two-layer composite with each layer being 2mm thick. The computed optimal processing and final times are shown in Table 4.2. Figure 4.3 depicts the degree of cure evolution showing that this is indeed achieved in the two-layer part. Figure 4.4 shows temperature evolution. As can be seen there, the peak temperature is less than $70^o$C, which is quite low compared to other curing methods such as autoclave curing processes, in which the cure process temperature rages in general from $121^o$C or $180^o$C for epoxy-based prepregs [60]. The optimal processing times for making a two-layer part are shown in Table 4.2.

Table 4.2: Optimal switching and final times

| Mode | 11 | 12 | 21 | 22 |
|---|---|---|---|---|
| Optimal switching time (s) | 288 | 505 | 800 | 884 |

Table 4.3: Optimal curing time

| Mode | 11 | 12 | 21 | 22 |
|---|---|---|---|---|
| | UV-ON in $1^{st}$ layer | UV-OFF in $1^{st}$ layer | UV-ON in $2^{nd}$ layer | UV-OFF in $2^{nd}$ layer |
| Optimal curing time (s) | 0- 288 | 288-505 | 505-800 | 800-884 |

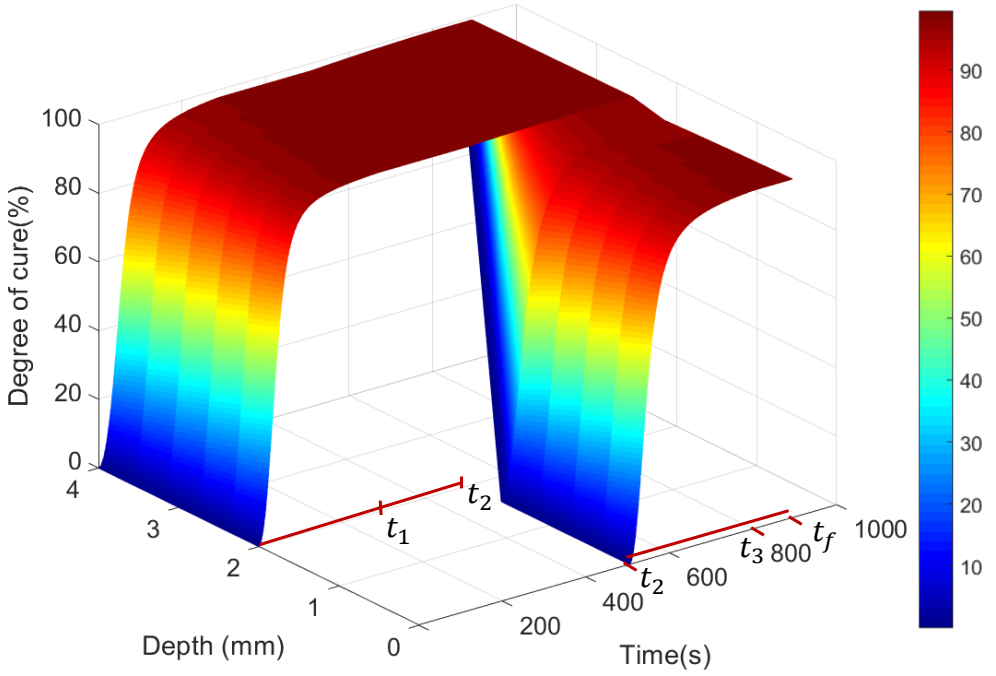


Figure 4.3: Degree of cure profile with optimized processing times

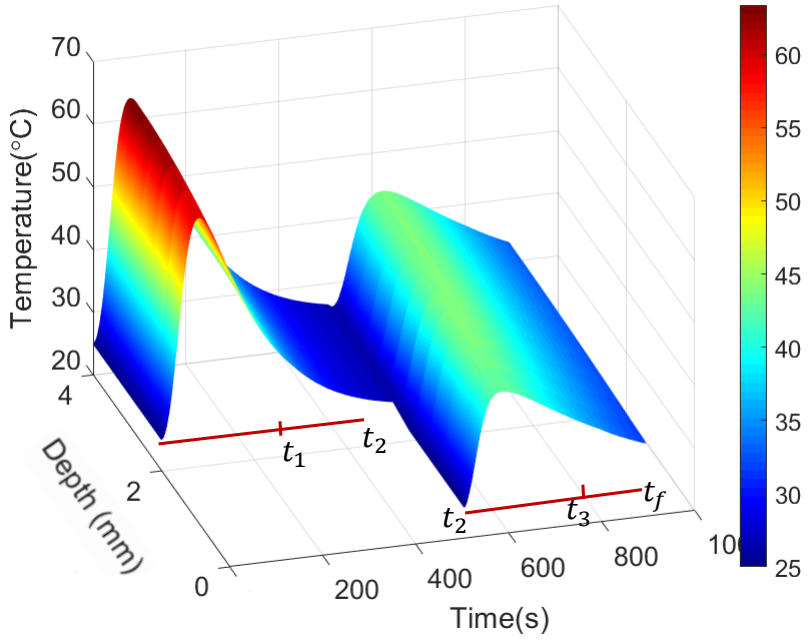


Figure 4.4: Temperature profile with optimized processing times

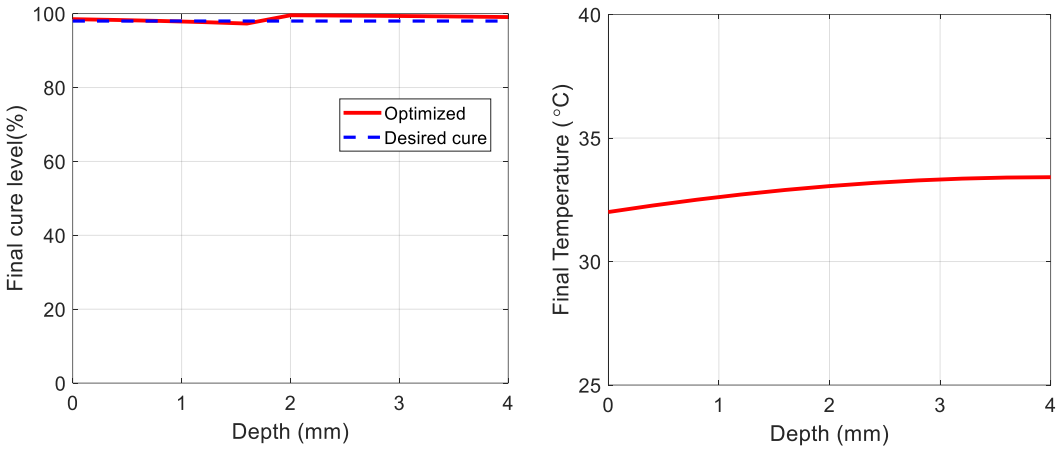


(a) (b)

Figure 4.5: Final degree of cure (a) and final temperature (b)

### 4.3.4 Interface condition

The interface condition is crucial for the mechanical property of the composites. For an optimum crosslinking between adjacent layers intimate contact is required [61]. In our model, the temperature at the interface is taken to be the average of the existing layer and the new layer which was at ambient temperature (initial temperature). As can be seen in Fig. 4.6, following the UV-OFF instant ($t_1$), the temperature starts to decrease with time, caused by an increase in temperature from the UV input and exothermic reaction. Since the UV is turned OFF at switching time ($t_1$ or $t_3$) which a temperature decrease. Rather than decreasing to the initial temperature ($25^oC$) the temperature decreases to that which is equal to the contribution of the exothermic reaction. The fact that the layering happens at a relatively lower temperature may have an adverse effect on the crosslinking between adjacent layers and reduce the bonding strength [61].

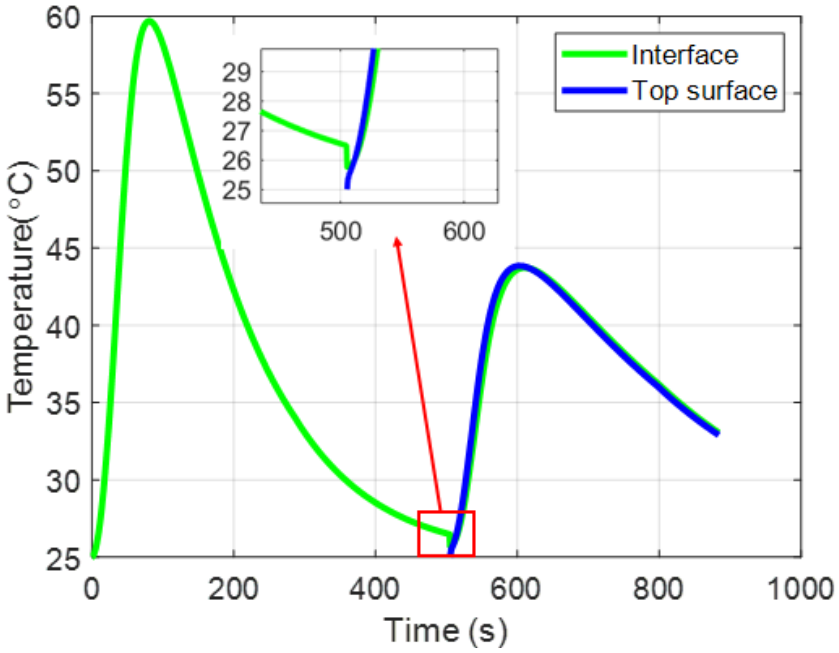


Figure 4.6: Temperature profile with optimal switching times

## 4.4 Expermental Work

### 4.4.1 Materials

Commercially-available diglycidyl ether bisphenol A (DGEBA) based epoxy, 105 Epoxy resin was purchased from West Systems Epoxy, USA . As per the manufacturers claim this resin is designed specifically to wet out and bond with fiberglass, wood fiber, reinforcing fabrics and a variety of metals. Triarylsulfonium hexafluorophosphate salts, mixed with 50 % in propylene carbonate was obtained from Sigma Aldrich, USA and used as photo-initiator (PI). The DGEBA epoxy resin was mixed with 3 % (by weight) of photo-initiator and steered till it mixes completely. Fiberglass cloth was used as the reinforcement.

### 4.4.2 Photoinitatior Concentration

The amount of photoinitator (PI) concentration used in cataionic polymerization varies from 3% to 5% by weight [62]. To determine the proper amount of PI, we measured the UV transmission of DGEBA based epoxy. This is done by comparing the UV intensity applied at the surface and the amount or UV intensity measured at the bottom of the sample. The UV intensity measurement set up is shown in Fig. 4.7 and the UV transmission for PI concentration of 1% to 5% is shown in Fig. 4.8. The UV intensity on the surface of sample is 35 $mw/cm^2$, one can take a different UV intensity, however, the corresponding optimal curing time will different accordingly. The UV intensity is kept constant through out the whole experiment and intensity transmitted through the sample were recorded every 30 s. As seen in Fig. 4.8, the UV absorbance for 3%, 4% and 5% are not significantly different ( $< 1mW/cm^2$). The maximum absorbance is at 5% for about $60s$ and at 4% PI concentration for the

rest of the time, although the absorbance for 3% ,4% and 5% PI are not significantly different. We chose the PI concentration to be 3% as it has also be considered optimal in most other works [21, 63].

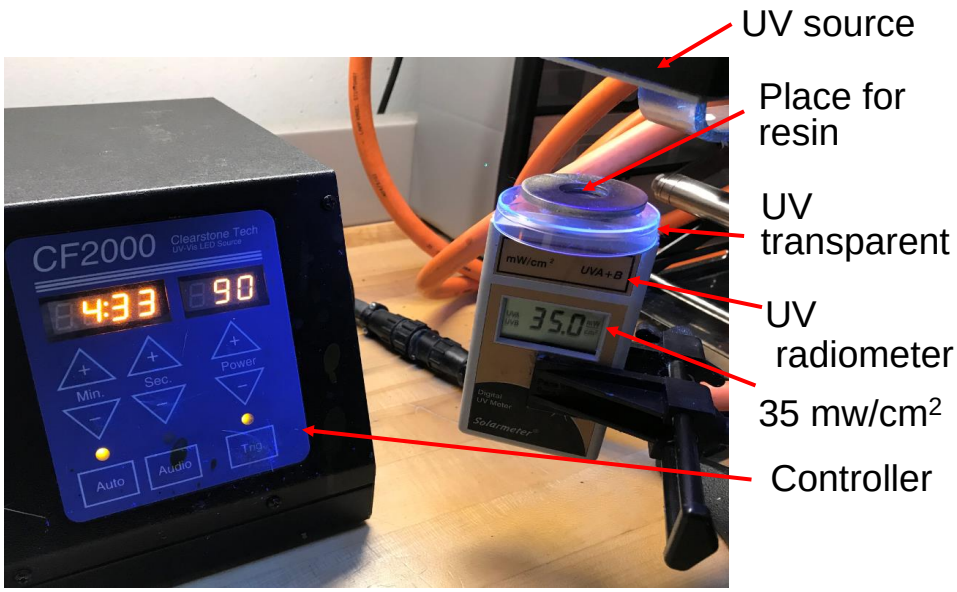


Figure 4.7: UV intensity measurment setup

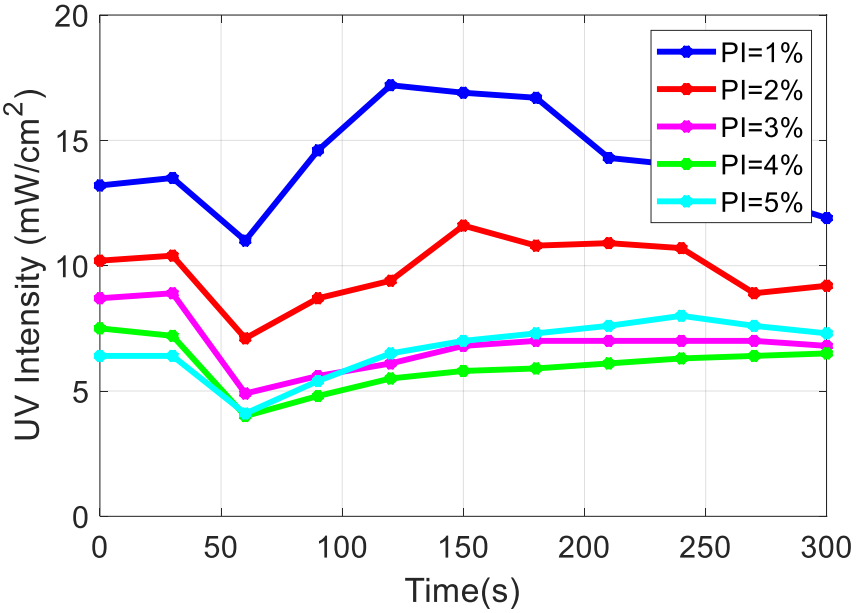


Figure 4.8: Temperature profile with optimized processing times

### 4.4.3 Composite preparation process

The prepreg was made by mixing approximately 60% of fiber glass with 40% of resin by weight. Three fiber glass mats were used to prepare a laminate. The hand layup process was used to carefully prepare the prepreg and the composition ratio of the resin to the fiber was determined by measuring the glass fiber alone and again in the final cured product. The schematic of a single laminate curing is shown in Fig. 4.9

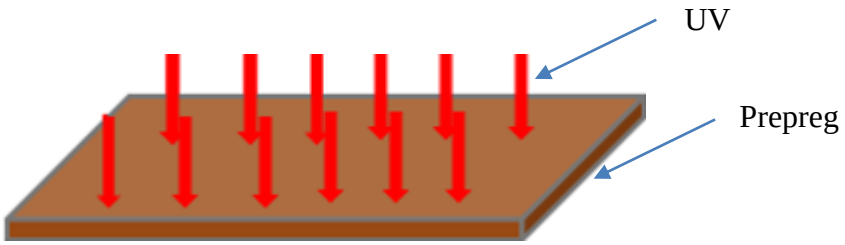


Figure 4.9: Schematic of a single laminate curing

### 4.4.4 In-situ curing and consolidation

Composites were fabricated by irradiating the prepreg samples using a 16.1W Clearstone UV LED with a UV emission peak wavelength of 365nm. A digital UV radiometer (Solarmeter) with a 0.1 mW/cm2 resolution was used to measure the amount of UV reaching the surface of the resin sample. All samples were placed at the same depth from the UV LED. As discussed in the previous section UV attenuates with material depth, hence thickness of a layer has to be limited. Previously, we experimentally verified the optimal switching times from our simulation that were most effective in curing a 2mm thick epoxy [64, 57]. Based upon those results, 2mm thick material was used as the single layer in the present study. Fig. 4.10 shows a

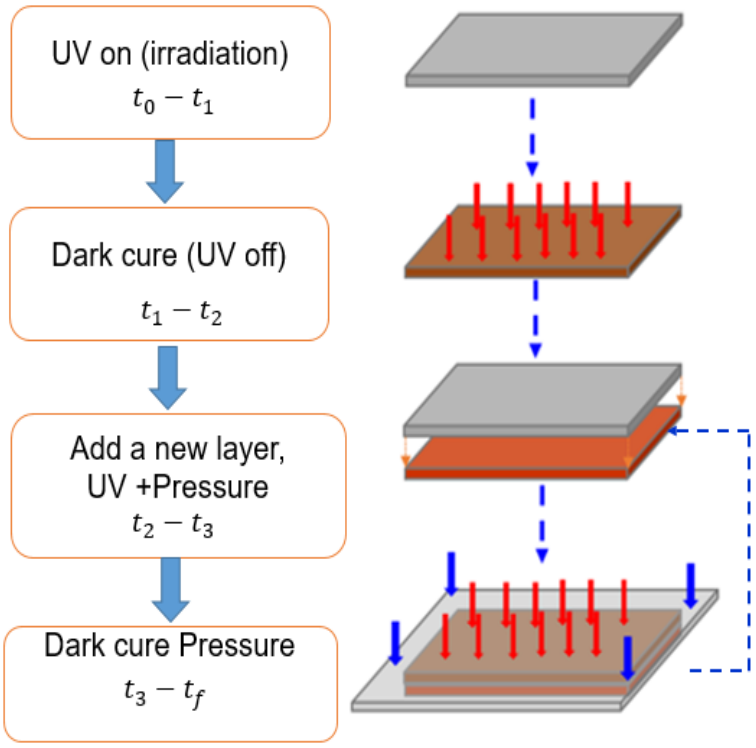


Figure 4.10: Schematic of in-situ compaction

schematic of the in-situ compaction or consolidation process investigated here. The first layer is cured followed by the addition of a new layer with a clear glass sheet on top to facilitate the application of pressure. Based on the amount of load/pressure applied during curing, we considered four samples as summarized in Table 4.4.

Table 4.4: Samples cured with different load

| Name | Sample 1 | Sample 2 | Sample 3 | Sample 4 |
|---|---|---|---|---|
| Load (N) | 0 | 6.8 | 18.2 | 33.9 |

### 4.4.5 Degree of cure

Thermo-Nicolet Magna 550 FTIR spectrometer in combination with a Thermo-SpectraTech Foundation Series Diamond ATR accessory was used to measure degree of cure. To make sure that the samples were completely cured, we recorded the FTIR of all cured samples and compared with the FTIR of the uncured epoxy resin. Each spectrum of the samples was collected in the 500 to 4000 $cm^{-1}$ region with $2cm^{-1}$ resolution and averaging of 64 scans. In the FTIR spectrum of epoxy resin, the peak around 915 (shown in Figure 4.11) is characteristic absorption of epoxy groups. Figure 4.11 shows the spectrum of samples recorded in the 525 to $1650cm^{-1}$ range. As seen in figure, the characteristic absorptions of oxirane ring approximately at $915cm^{-1}$ is observed in the epoxy resin (before curing). This is attributed to the C-O deformation of oxirane group [65, 66, 67]. The disappearance of this band in all samples shows that all samples, which were made with different in-situ consolidation pressures, are completely cured[66, 68, 69].

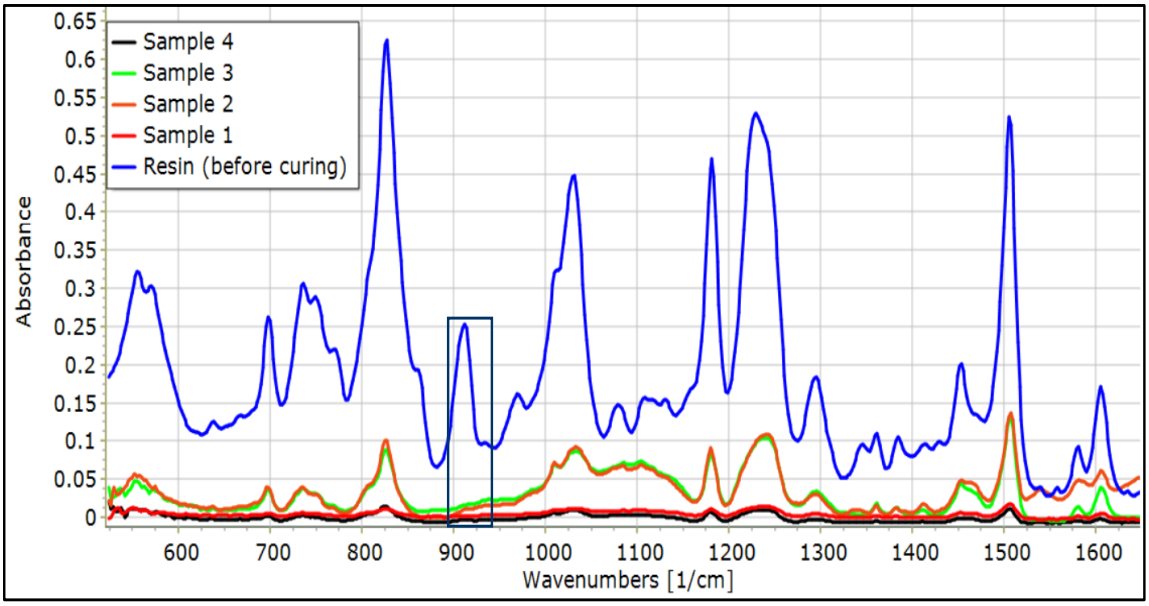


Figure 4.11: FTIR-ATR Spectroscopy of before and after curing

### 4.4.6 Inter-laminar shear strength

Shear strength of composite materials is a mechanical property that mainly depends on the resin [70]. The shear strength of composite materials is governed by the adhesion between fibers and resin (intra-layer shear strength) and, if there is more than one layer involved, the bonding of adjacent laminates (inter-layer shear strength) needs to be considered. Different approaches and devices have been proposed for determining the sheer strength of composites [56]. To choose the ideal shear test method one should consider: simplicity to perform, size, preparation required to get the specimen for the test and accuracy of measurement [70, 56]. The short beam shear test (SBS) has been used widely for measuring the interlaminar shear strength of fiber reinforced composites [70]. It has similarities to a flexural test method, but the specimen in SBS has a very small height to thickness ratio [71].

In this work, the inter-laminar shear strength (ILSS) of the fiber-reinforced composite was analyzed on a universal testing machine (Instron Model 5582). Specifically, the short beam bending test method was adopted as described in American Society for Testing and Materials (ASTM) standard D2344[71]. Crosshead speed of 1.27mm/min was used for the specimen test. Based upon the ASTM standards, five specimens were tested with the results averaged to report each ILSS. SBS tests were carried out on specimens having span length ($L$ ) to thickness ($h$ ) ratio equal to 4 [71]. The short beam bending test setup is depicted in Fig. 4.12.

The inter-laminar shear strength is given as follows [72]:

$$ILSS = 0.75 \times \frac{P_m}{b \times h} \tag{4.7}$$

where the ILSS is the short-beam shear strength in MPa; $P_m$ is the maximum load recorded during the test in Newton (N); b is the measured specimen width in mm; and

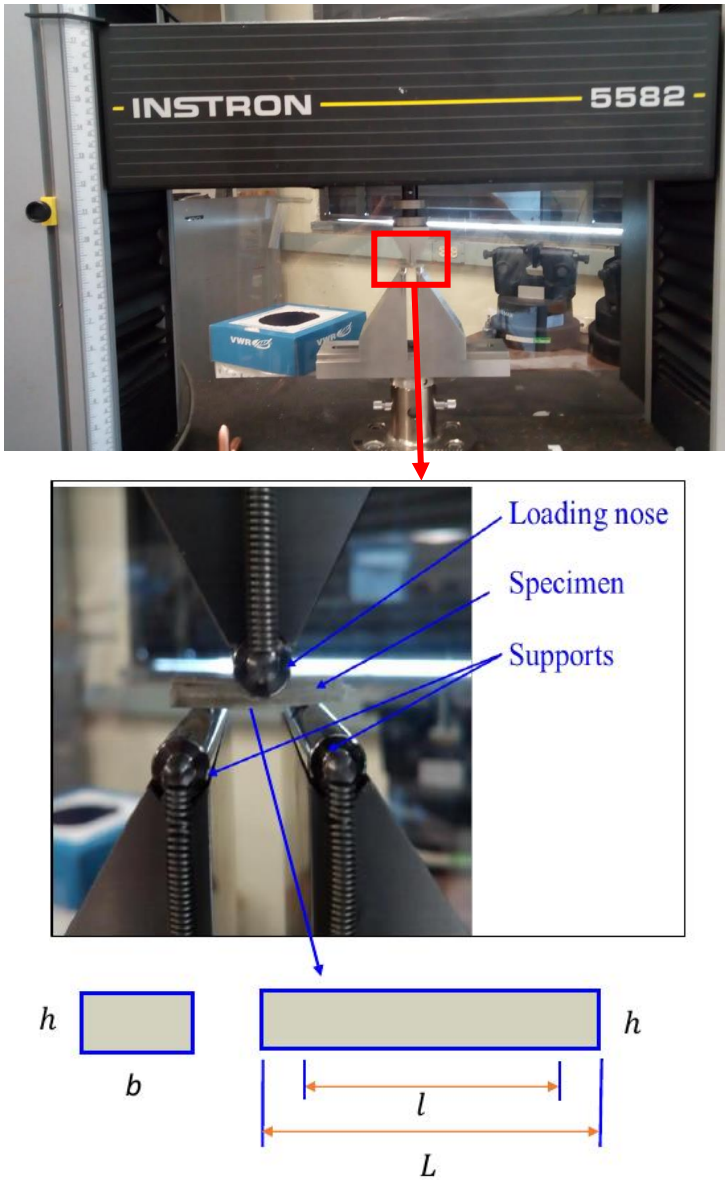


Figure 4.12: Picture of short beam shear (SBS) test

h is the measured specimen thickness in mm. For this study, samples with dimensions 24 X 8 X 4 mm were tested over 16 mm span.

## 4.5 Experimental Results and Discussion

In the previous sections, we showed that the optimal process times determined using optimal process control helped to get a uniform cure. The final degree of cure was also verified experimentally by FTIR-ATR spectroscopy. However, this does not guarantee that there is complete cross linking between adjacent layers when two or more layers involved in the cure process. This is because each layer can be cured uniformly but the cross-linking between layers at the interface cannot be verified from the final degree of cure experiment. In this section, the effect of in-situ consolidation pressure on the inter-laminar shear strength is investigated by using inter-laminar shear strength. Fiber reinforced matrix samples with a 60% glass fiber by weight. According to the standard [71] for each sample five tests were made.

### 4.5.1 Effect of pressure on the Inter-Laminar Shear Strength (ILSS)

Samples were fabricated by the in-situ curing method with varying pressures applied to each, followed by an analysis of the inter-laminar shear strengths to determine optimal consolidation pressure. For each case, we conducted five experiments and averaged the results. Figure 4.13 shows the maximum load observed for different loading conditions and Fig. 4.14 shows the correlation between ILSS and the load applied during in-situ curing. Note the substantial increase in the ILSS 40.63 % with an increase in the applied load from 0 to 18.2 N and decreases when a sample is cured under higher load. This shows that an optimum pressure is required to get better inter-laminar shear strength.

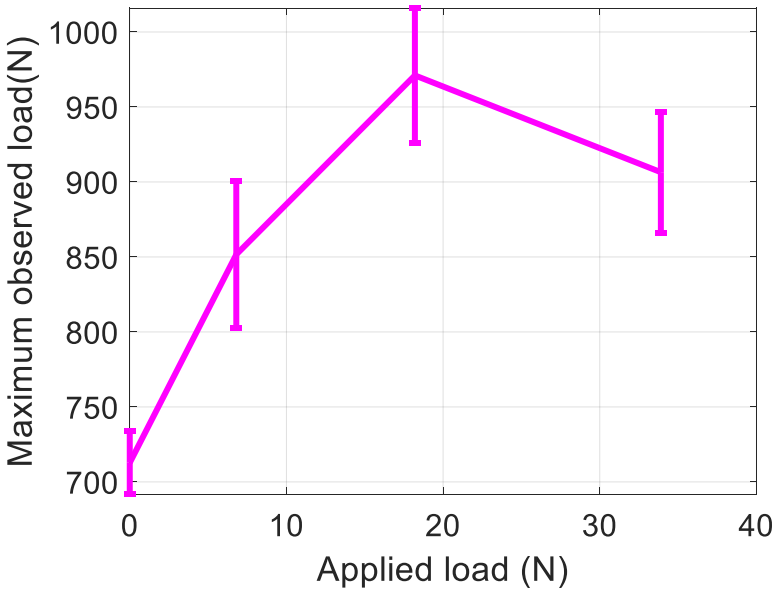


Figure 4.13: Maximum observed load for different loading condition

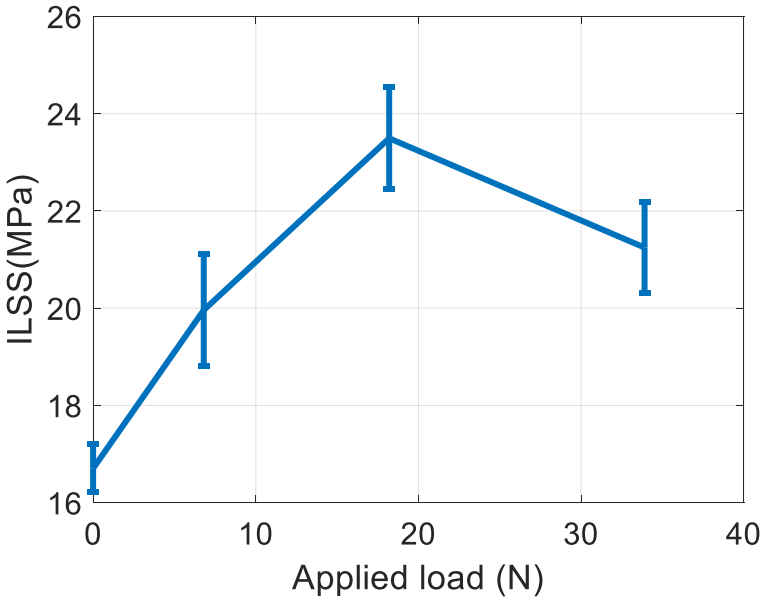


Figure 4.14: ILSS for different loading conditions.

Scanning electron microscope (SEM) images were obtained using Hitachi S3400N Variable Pressure Scanning Electron Microscope (VPSEM). The SEM images shown in Fig. 4.15 are that of samples cured under different loading variances from 34N

to 0. These images clearly indicate that a higher consolidation pressure will lessen the amount of resin between the fibers (see Fig. 4.15 a ) and thus reduce the shear strength. This is inline with the effect of higher fiber volume fraction on the ILSS reported in [73, 74]. Therein, it is found that when the fiber volume fraction exceeds 60% the ILSS of the composite decreased . On the other hand, more resin is evident in the presence of a reduced consolidation pressure or an absence of consolidation pressure altogether as seen in Fig. 4.15 d. As compared to other loading conditions, the one with high ILSS has relatively uniform distribution of epoxy resin around glass fiber as is clearly evident in Fig. 4.15 b.

Table 4.5: Load applied during curing

| Name | Load applied (N) |
|---|---|
| Load 1 | 0 |
| Load 2 | 6.8 |
| Load 3 | 18.2 |
| Load 4 | 33.9 |

### 4.5.2 Effect of pressure to Inter Laminar Shear Strength (ILSS)

Four samples were fabricated by the in-situ curing method with varying pressure applied to the samples and inter-laminar shear strengths were tested to find out the optimal pressure. The applied load and maximum load observed are summarized in Table 4.6..

Table 4.6: Correlation between applied load and maximum load observed

| Applied load (N) | Maximum observed load(N) | ILLS(MPa) |
|---|---|---|
| 0 | 712.8 | 16.7 |
| 6.8 | 779.8 | 18.3 |
| 18.2 | 916.5 | 21.5 |
| 33.9 | 864.5 | 20.3 |

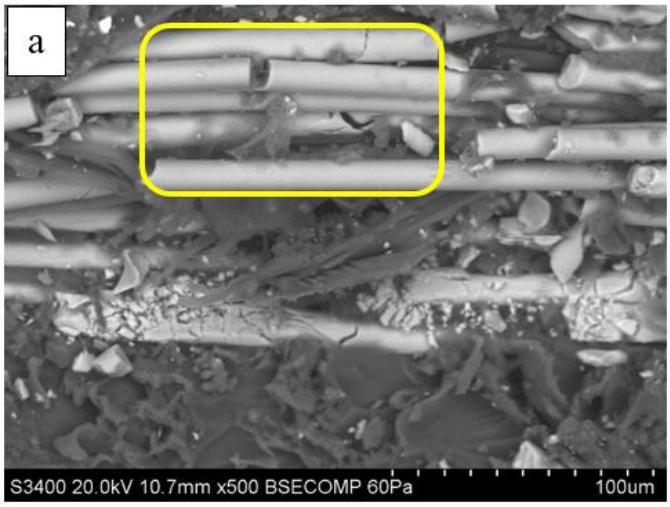


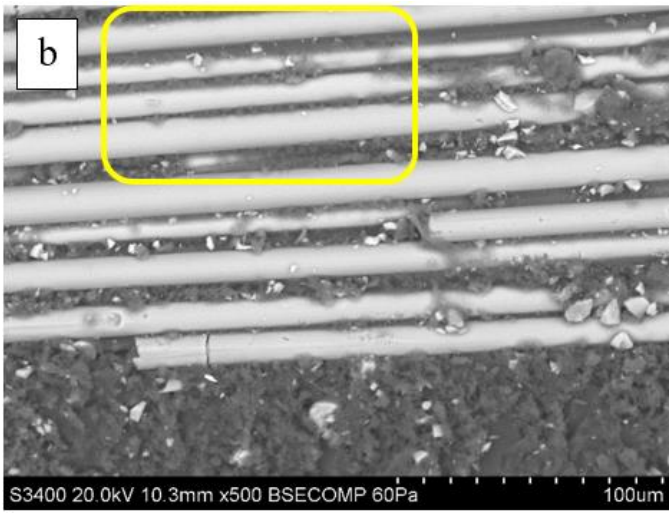

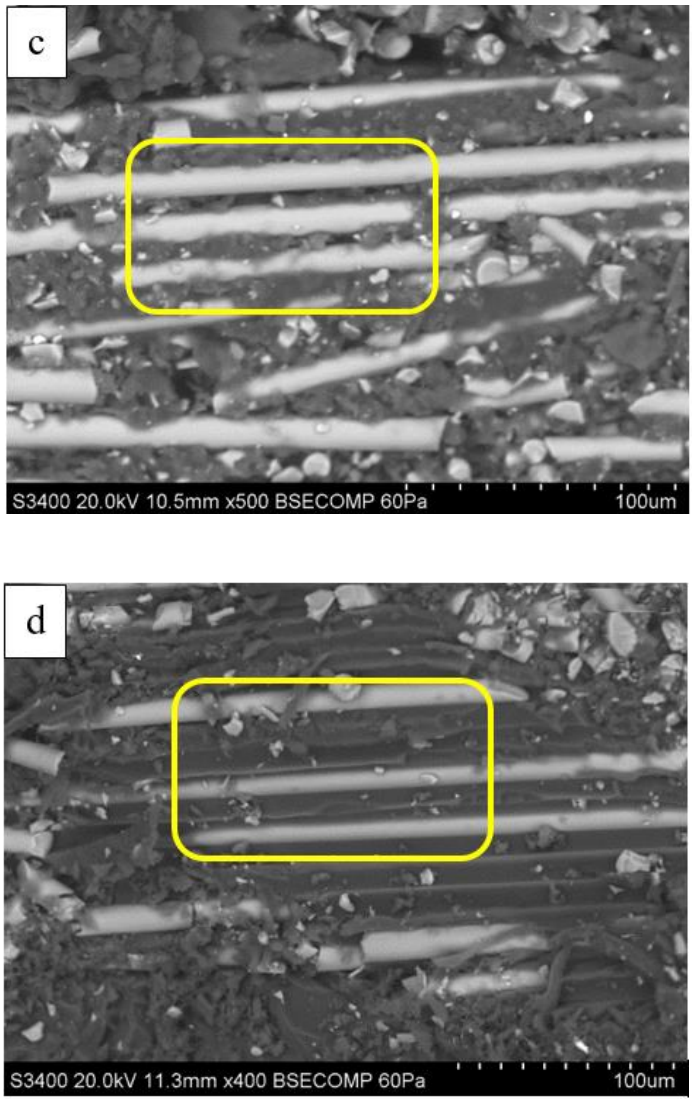


Figure 4.15: SEM images of cross sections from fiber reinforced composites fabricated at different pressure a) 34N b) 18N c) 7N and d) No load

## 4.6 Conclusion

In this chapter, first model-based optimal processing time sequence selection scheme for a layer-by-layer additive manufacturing of epoxy-based thick parts via a UV-based cationic curing process outlined. The temperature evolution showed that the layering the temperature is relatively low and hence less bonding between layers.

To improve the inter-laminar shear strength, we then assessed the effect of in-situ consolidation pressure on the inter-laminar shear strength. The optimum percentage of photo-initiator concentration is chosen for a given UV-intensity by conducting different experiment. Fourier Transform Infrared (FTIR) spectroscopy method was used to check the completeness of the final degree of cure. Then, short beam shear (SBS) test is conducted to measure the inter-laminar shear strength of the cured product under different compaction load. The curing times were found from optimal switching time control and the UV intensity and photo-initiator concentration were similar for all samples. The result showed that thick composite parts fabricated with in-situ compaction and UV curing process have showed increased inter-laminar shear strength with increased compaction load up to a certain point. An increase in compaction beyond this point decreased the inter-laminar shear strength. Scanning electron microscopy (SEM) images showed that samples made with optimum consolidation pressure had a relatively uniform fiber to resin distribution which results in improved inter-laminar shear strength.

# Chapter 5

# Nonlinear Model Predictive Control of UV-Induced Curing Process for Thick Composite Manufacturing

## 5.1 Abstract

In this chapter, first the nonlinear model predictive control (NMPC) of UV-induced curing for manufacturing of thick composite parts is proposed and then we extend the model for switching layer-by-layer curing process. The process involves layer-by-layer curing of thin composite laminates to form thick part. The model for NMPC switches when a new layer is added to the existing layer. The layer addition times are determined externally. The offline optimal control is used to determine the optimal time and temperature profile which will give uniform cure distribution of a thick composite material. Once the temperature trajectory and optimal time

sequences are found, the NMPC is implemented for online control. The objective is to determine theoretical optimal behavior (assuming the process measurement is available) which will be used for online switching NMPC for tracking the reference temperature of switching layer-by-layer manufacturing process. To demonstrate the effectiveness of the proposed approach three layer fiber-reinforced resin is considered and results show a very good agreement between the temperature of the reference and NMPC.

## 5.2 Introduction

Lightweight materials have a great potential for improving vehicle performance, it can improve the passenger vehicle fuel efficiency six to eight percent for each ten percent reduction in weight [75]. Fiber reinforced polymer composites are one of the most promising weight reduction technologies available today [75]. The manufacturing process of these composites are mainly thermal based curing process. However, recently radiation based curing process have shown a great potential for thick composites manufacturing.

As discussed in the previous sections UV has limited penetration, this challenge has limited the application of UV to thin polymer films in applications such as printing inks and adhesives, printing plates, microcircuits and production of thin composite parts [18].

To overcome the cure depth limitation, a layer-by-layer deposition was recently introduced and have been implemented for production of thick composite parts manufacturing using UV as radiation source and acrylate matrix [28] and epoxy matrix [57]. This was then extended for a concurrent curing and layering approach where distinct process optimization opportunities were identified by examining the inter

play between the underlying curing kinetics and UV attenuation [28, 57]. All the recent proposed approaches focused on the offline optimal time control for determining the optimal input and or layering time with the objective of uniform final cure distribution across the finished product. However, these approaches assume a uniform UV intensity in optimizing the layering time and hence the optimal layering times are optimal for the given input only. In this chapter, we propose a model predictive control strategy for online control of UV-induced curing process.

Model predictive control (MPC) also referred to as receding or moving horizon control has been widely used in industry as an effective approach to deal with large multi-variable constrained control problems. It is a well established control strategy in the chemical process industry which are typically characterized by a longer sampling periods. In recent years, however, the improvement in the processor speed and the development of new algorithms has extended the application of MPC to other applications such as automotive [76, 77, 78], aerospace [79, 80, 81, 82] where typical sampling is in the order of milliseconds [83, 84, 85, 86]. The main advantage of MPC controller as compared to traditional proportional, integral and derivative (PID) is that it allows taking constraints on states, inputs and outputs of the system. Moreover, multivariable feedback control can be designed with similar procedural complexity as of single variable ones [83].

The main idea of MPC is to choose control actions by repeatedly solving an online constrained optimization problem, which aims at minimizing a cost function over a finite prediction horizon based on predictions obtained by a system model [87, 88]. In general, an MPC design is composed of three components: 1) A model of the system. This model is used to predict the future evolution of the system in open-loop and the efficiency of the calculated control actions of an MPC depends highly on the accuracy of the model and the amount of noise/disturbance . 2) A

cost function over a finite horizon. This cost will be minimized subject to constraints imposed by the system model, restrictions on control inputs and system state and other considerations at each sampling time to obtain a trajectory of future control inputs. 3) A receding horizon scheme. This scheme introduces feedback into the control law to compensate for disturbances and modeling errors [89]. In Fig. 5.1 $k-1$, $k$ and $k+1$ represents the past , current and future time indexes respectively. The prediction horizon Np is the time range on which state prediction is made. The control horizon Nu denotes the duration on which the control input is optimized. The prediction and optimization preformed at time k provide the open-loop optimal control sequence over the current control horizon Nu. The first control input will be implemented to the system till the next sampling instant $k+1$. At time k + 1 the computation is repeated with the horizon moved by one sampling time.

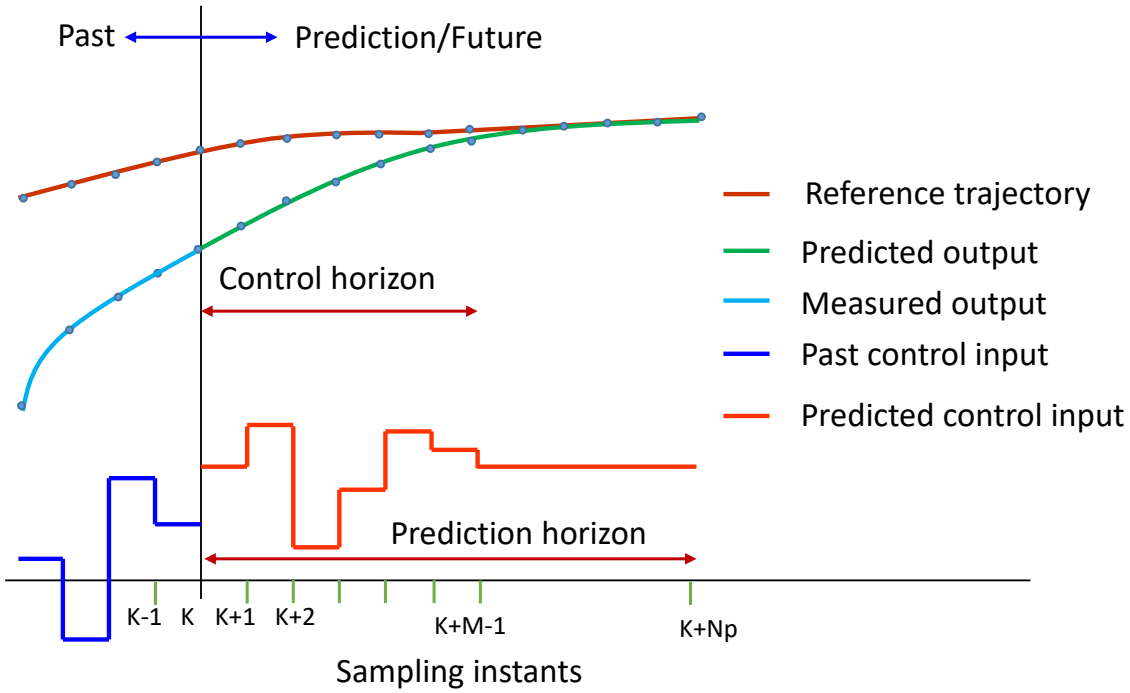


Figure 5.1: Principle of model predictive control

There are few papers where MPC has been applied for distributed parameter systems such as curing process of thick composites [90, 91, 92]. In these works, distribute parameter systems with high order dimension models are considered. However, the dimension of states is constant i.e. there is no change in dimension throughout the process. In our study first we discuss on the distributed parameter NMPC which is highly nonlinear UV-induced curing of composites with UV intensity as a control input and process temperature and degree of cure considered as state.

### 5.2.1 Curing Process Model

Considering the 1D curing set up shown in Fig. 5.2 below, a single layer of material is exposed to a uniform UV source at the top.

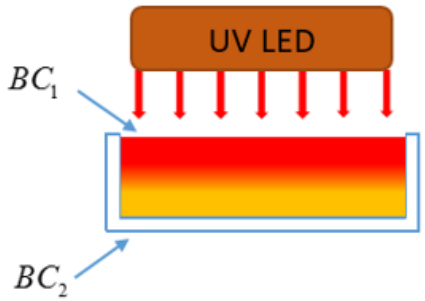


Figure 5.2: Schematic of UV-curing process

The curing process involves heat generation from polymerization (exothermic reaction), convection heat transfers at the top surface and conduction within the layer. These also need to be captured along with boundary conditions. The convective boundary condition (BC1) at the top and insulation boundary condition (BC2) at the bottom. The UV gets attenuated as it passes through the material and the intensity across the depth is given by Beer-Lamberts law [30, 93]. The temperature within the fiber-reinforced composites can be calculated using the law of conservation of energy together with a model for cure kinetics. By neglecting the energy transfer by

convention, the energy conservation equation can be described as:

$$\rho c_p \frac{\partial T(y,t)}{\partial t} = k_y \frac{\partial^2 T(y,t)}{\partial y^2} + \rho_r \Delta H_r \frac{d\alpha(y,t)}{dt} \tag{5.1}$$

where $\rho$ and $\rho_r$ are density of the composites and resin respectively, $c_p$ is the specific heat capacity of composites, $\Delta H_r$ is the enthalpy of polymerization of the resin, $k_y$ is the thermal conductivity in the direction perpendicular to the plane of the composite, $T(y,t)$ is the temperature at time $t$ and depth $y$, $\alpha(y,t)$ is the degree of cure of the resin at depth $y$ and time $t$. Equation 5.1 is coupled with the exothermic reaction (cure) rate equation of the unsaturated polyester resin which is given in Eq. 5.2

$$\frac{d\alpha(y,t)}{dt} = \varphi S^q I_0^p \exp(-\lambda_c y)\, exp\left(\frac{-E}{RT_{abs}(y,t)}\right) \alpha^m(y,t)\left(1-\alpha(y,t)\right)^n \tag{5.2}$$

where, $\phi$ is pre-exponential rate constant $S$ is photo-initiator concentration, $\lambda_c$ UV attenuation constant, $E$ is activation energy ,$R$ is gas constant [28].

The convection and insulation boundary conditions (BC1 and BC2) are given in Eq. 5.3 and Eq. 5.4 respectively.

$$-k_y \frac{\partial T(y,t)}{\partial y} + \vartheta I_0 = h\left(T(y,t) - T_\infty\right) \tag{5.3}$$

$$\frac{\partial T(y_{max},t)}{\partial y} = 0 \tag{5.4}$$

where, $y_{max}$ is the thickness of the fiber-reinforced resin.

## 5.3 Nonlinear Model Predictive Control of Thick Composite Laminate

For a single layer thick composite manufacturing, the schematic of NMPC is shown in Fig. 5.3. As mentioned previously, the reference temperature is taken from offline optimal control. Therein, the optimal switching times and temperature profile are determined. As seen in Fig. 5.3, the optimal times are used for the NMPC model and for the plant.

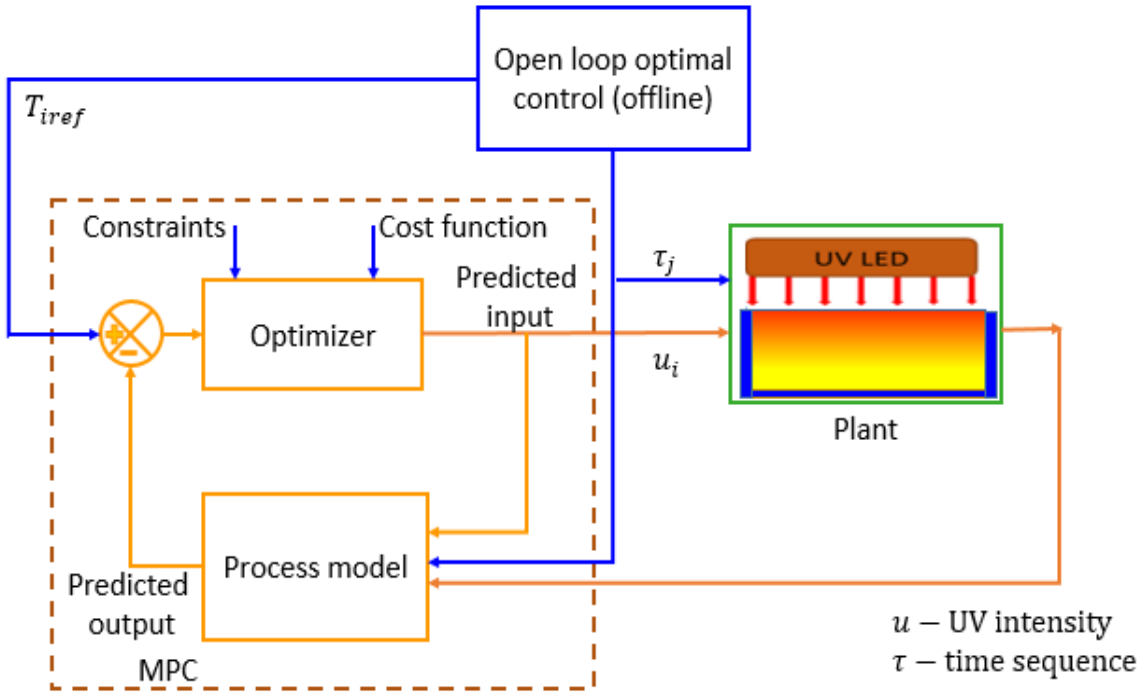


Figure 5.3: Schematic of NMPC

### 5.3.1 Objective Function

One of the advantages of NMPC formulation as constrained optimization problem is a large number of problems can be stated. It can be used in trajectory tracking for controlled variables , minimization of any economic function, minimization of en-

ergy supply under technical specifications, etc. In optimizing the cure it is desired to use the PDE-ODE model outlined above to get an optimal temperature profile [94].

$$J = Q \sum_{k=1}^{N_p} \left(T(k) - r(k)\right)^2 + R \sum_{k=1}^{N_p} u(k)^2 \tag{5.5}$$

subjected to:

$$u_{\min} \leq u \leq u_{\max}$$
$$x_{k+1} = f(x_k, u_k)$$
$$x(0) = x_0$$

where $f$ is system dynamics and is given as follows:

$$\rho c_p \frac{\partial T\left(y,t\right)}{\partial t} = k_y \frac{\partial^2 T\left(y,t\right)}{\partial y^2} + \rho_r \Delta H_r \frac{d\alpha\left(y,t\right)}{dt} \tag{5.6}$$

$$-k_y \frac{\partial T\left(y,t\right)}{\partial y} + \vartheta I_0 = h\left(T\left(y,t\right) - T_\infty\right) \tag{5.7}$$

$$\frac{d\alpha\left(y,t\right)}{dt} = \varphi S^q I_0^p \exp\left(-\lambda_c y\right) exp\left(\frac{-E}{RT_{abs}\left(y,t\right)}\right) \alpha^m\left(y,t\right)\left(1-\alpha\left(y,t\right)\right)^n \tag{5.8}$$

$$\frac{\partial T\left(y_{max},t\right)}{\partial y} = 0 \tag{5.9}$$

$k$ is the NMPC step index, $N_p$ is the receding horizon , $T$ is the process control variable and $u$ is the sought optimal control sequence and $r$ is the reference temperature ($T_{ref}$). The result shown in Fig. 5.4 is in a good agreement with the reference temperature.

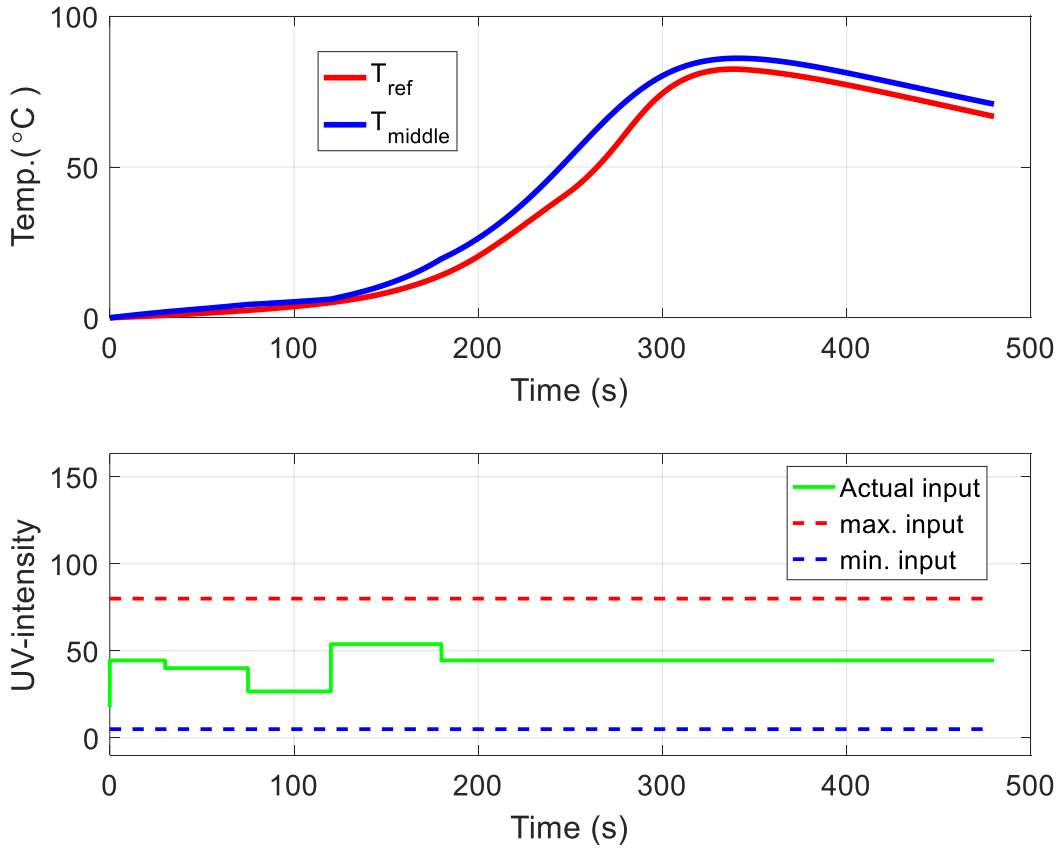


Figure 5.4: NMPC singlelayer result

## 5.4 Nonlinear Model Predictive Control of Layer by Layer Curing Process

### 5.4.1 Offline Optimal Control

In this section we pose an optimal control problem for the model described in eqs. (5.1) to (5.4) to find the optimal layering time which will be used as a reference for NMPC. Here, cost function is outlined. Readers are referred to Section 2.5.2 for the derivation of optimality conditions and details of the offline optimal control

procedure used [28]. The cost function for free radical polymerization is given by:

$$J = 1/2 \sum_{0}^{n} (\alpha(y, t_N) - \alpha_{des})^2 \tag{5.10}$$

Here, unlike the previous sections , the system has $N$ modes, this is because it is free radical polymerization (there is no cure after UV is off ). So in this case the number of modes of the system is $N$ not $M$ which was used in the previous chapters. Note that $M = 2N$ for cationic polymerization. For illustration three layer free radical polymerization , depicted in Fig. reffig:1schfree, is used. Using eq. 5.10 and optimality conditions discussed in Section 2.5.2 the following steepest descent numerical algorithm is used to compute the optimal solution. The parameter values used in the numerical solution are given in Table 5.1.

1. Choose initial iterate $\tau_i^0$ for $i = 1, 2, 3$ and choose a termination tolerance $\varepsilon$
2. Set the iteration counter $k = 0$
3. While $\left|J^k - J^{k-1}\right| > \varepsilon$
4. Compute the state trajectory $x_i(t)$, $t\epsilon[\tau_{i-1}, \tau_i]$ for $i = 1, 2, 3$ forward in time from $t_0 = 0$ to $t_f = \tau_N$
5. Compute the adjoining variable $\bar{p}_i(t)$, $for\ i = 1, 2, 3$ backward in time from $t_f = \tau_N$ to $t_0 = 0$
6. Update the time vector $\tau_i^{k+1} = \tau_i^k - \delta_i^k B_i$ , where $i = 1, 2, 3$ and $N = 3$
7. $\tau_N^{k+1} = \tau_N^k - \delta_N^k C$
8. $B_i = H_i(\tau_i^-) - H_i(\tau_i^+)$ and $C = H_N(\tau_i^-)$
9. $k = k + 1$

Table 5.1: Parameter values used for numerical simulation [28]

| Parameter | Variable | Value |
|---|---|---|
| Density of resin | $\rho_r$ | 1.1 g/cm3 |
| Specific heat of resin | $c_{pr}$ | 1.674 J/g°C |
| Thermal conductivity of resin | $k_r$ | 0.0017W/cm°C |
| Density of composite | $\rho$ | 1.69 g/cm3 |
| Specific heat of composite | $c$ | 1.14 J/g°C |
| Thermal conductivity of composite | $k$ | 0.0035w/cm°C |
| Convective heat transfer | $h$ | 0.002 w/cm$^2$ °C |
| Volumetric fraction of resin | $v_r$ | 0.6 |
| Polymerization enthalpy of resin | $\Delta H_r$ | 335 J/g |
| Photoinitiator concentration | $s$ | 0.05% wt |
| Activation energy | $E$ | 12.7 KJ/mol |
| Gas constant | $R$ | 8.314 J/mol K |
| Pre-exponential factor of rate constant | $\Phi$ | 0.631 $s^{-1}$ |
| Reaction orders | $m$ | 0.7 |
| Constants exponents | p | 0.8 |
| Absorptivity UV radiation at surface | $\nu$ | 0.85 |
| UV attenuation constant | $\lambda_c$ | 2cm-1 |

10. *End while*

11. Save the optimal switching time vector $[\tau_1, \tau_2, \tau_3]^T$

As seen in Fig. 5.6 the final cure is close the desired value and the maximum error is less than 1% hence the proposed approach gives the optimal time which result in uniform final cure distribution. Fig. 5.7 shows the temperature evolution of the bottom (layer-1) middle (layer-2) and top(layer-3) layers. These temperature profiles will be used as a reference for the NMPC.

Model predictive control refers to a class of control algorithm in which a dynamic process model is used to predict and optimize process performance. The idea is to solve, at each sample time, an open-loop optimization in order to find the value of the manipulated variable is reiterated at the next sample time with the update of the process measurement. Today, MPC has become a control strategy widely used in

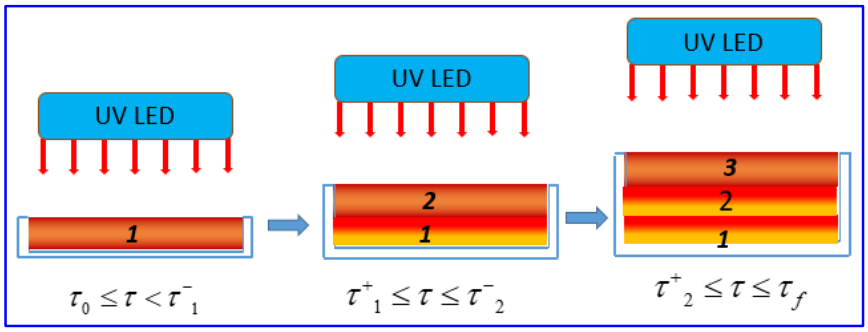


Figure 5.5: Schematic of layer-by-layer curing process

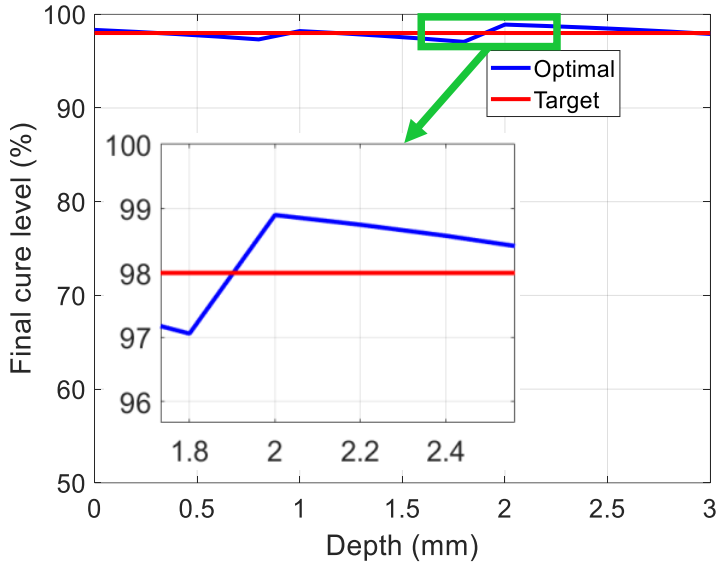


Figure 5.6: Final degree of cure with optimal processing times

industry. Indeed, MPC is well suited for high performance control since constraints can be explicitly incorporated into the formulation of the control problem[95].

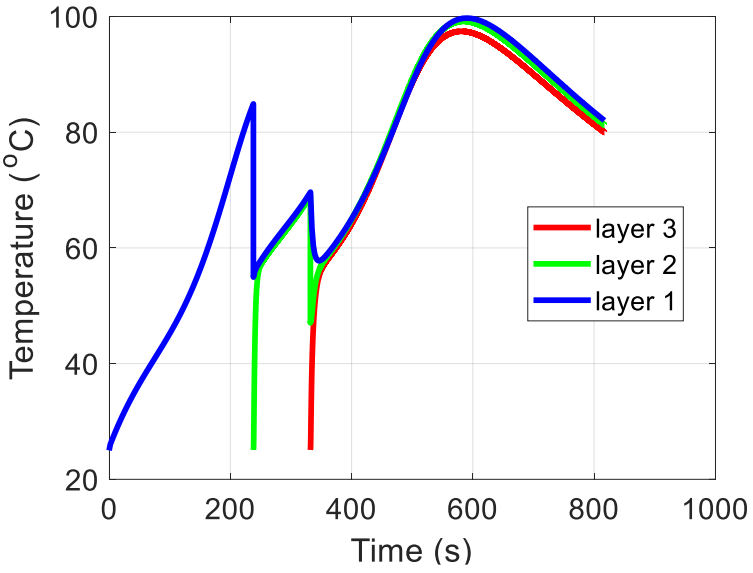


Figure 5.7: Temperature evolution of three layer.

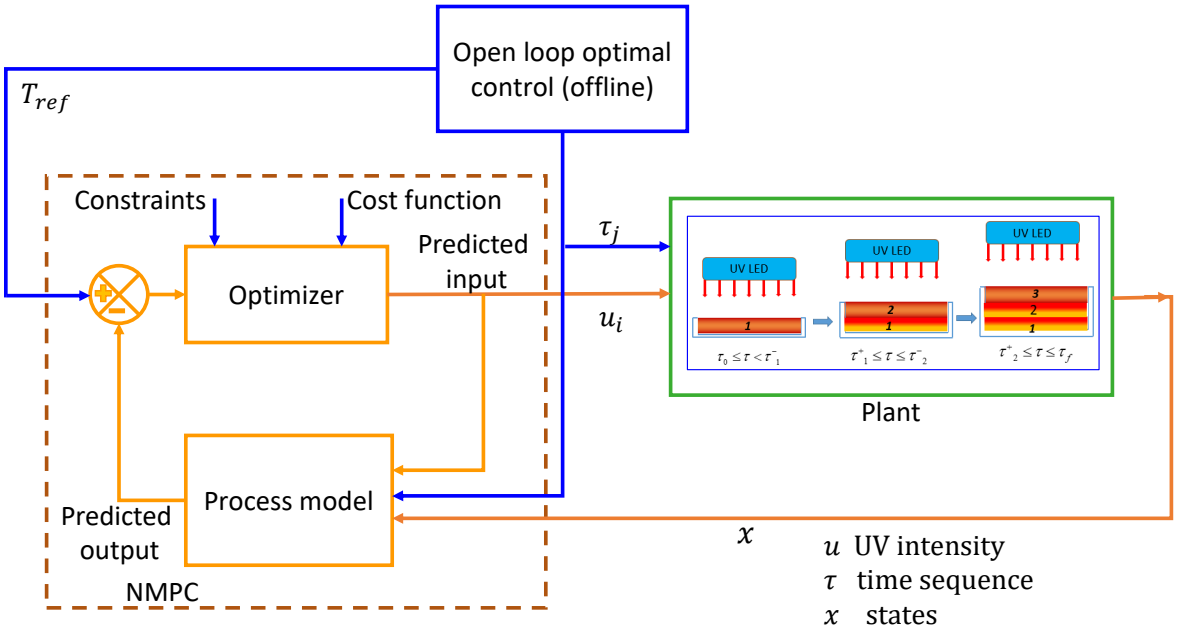


Figure 5.8: Schematic of SNMPC

### 5.4.2 Control objective

Thermal based curing of composites have to follow a specif temperature profile (called cure cycle) to achieve a required quality of final product. Hence, researchers have been using temperature as a reference to control the curing process [94, 96, 97]. In radiation based curing such as UV the initiation comes mainly from the photo-initators which absorbs light. However, the propagation strongly dependent on temperature. As seen in the previous section the optimal switching times chosen with the objective of minimizing final cure deviation resulted in near uniform final temperature. Therefore, for the NMPC the offline temperature profile which is found from offline optimal control with the objective of uniform cure distribution is used. The control problem considered here is the tracking of a reference temperature ($T_{ref}$) and minimizing the control effort. The NMPC technique solves the optimal control problems repeatedly from the current measured state by online computation. After giving the initial control input $u(t)$ and states $x(t)$; the current control input at time $t$ is found by determining the optimal control solution online over the interval $[t, t+Tp]$ with the objective of minimizing the temperature difference from a given reference and control input. As depicted in Fig. 5.9 the system involves mode change. The mode change times are as discussed earlier determined from offline optimal control with the objective of minimizing final degree of cure deviation across layers. In SNMPC the horizon may range from one mode to the next higher mode. In that case, the number of states increase and hence the cost function before and after the switching instant within that horizon is different. The ideal cost function should switch at the switching time however, it may pose computational challenge. Therefore, two cases are considered: 1) the cost function which switches within the horizon when a switching instant falls in the horizon and when mode is changed (i.e when a layer

is added) and 2) the cost function does not switch considers one model in the given horizon and the switching happens only when the mode is changed.

#### 5.4.2.1 Case 1

As mentioned in the previous section, the first case considered is when the cost function is able to switch and increase its dimension to predict the upcoming layer (s). This will occur when the switching time (layer addition time) lies within the prediction horizon. In that case, the cost function will add one more layer to the existing layer(s). The cost function which includes the mode switching within the horizon is given in Eq. 5.11.

$$J_S = Q\left\{\sum_{k=1}^{N_s}\sum_{i=1}^{N_z(l_n)}\left(T(k,i)-r(k,i)\right)^2+\sum_{k=N_s}^{N_p}\sum_{i=1}^{N_z(l_{n+1})}\left(T(k,i)-r(k,i)\right)^2\right\}+R\sum_{k=1}^{N_p}u(k)^2 \tag{5.11}$$

subjected to:

$$\begin{aligned} x_{k+1} &= f(x_k, u_k) \\ u_{\min} &\leq u \leq u_{\max} \\ x(0) &= x_0 \end{aligned} \tag{5.12}$$

where $f$ is as given in section 5.3.1, $N_p$ is the prediction horizon (number of predictions), $M_p \leq Np$ is the control horizon , in this study the control horizon taken to be the prediction horizon (i.e $M_p = N_p$), $T$ is the temperature from SNMPC and $r = T_{ref}$ is reference temperature from the open loop offline optimal control (see Fig. 5.8), $Q$ is the weighting matrix for predicted errors ($Q \geq 0$) and $R$ is the weighting matrix for control moves ($R \geq 0$). $N_z$ is the number of nodes in the given mode which is defined as described in Fig. 5.9. Herein, $l_n$ is the number of layers in mode $N$. For NMPC model the number of nodes considered are three therefore, the total number

of nodes in mode $n$ is: $N_z = 3l_n$.

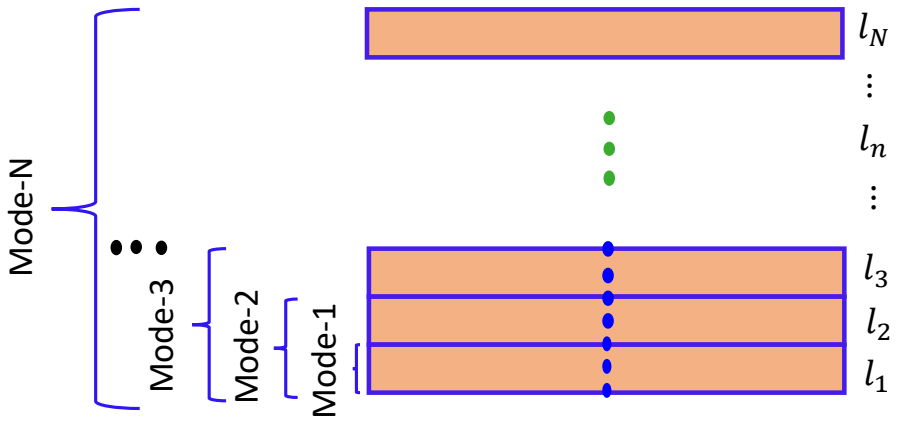


Figure 5.9: Reduced model for MPC

#### 5.4.2.2 Case 2

In this case, when the switching time (layer addition time) lies with in the prediction horizon the cost function does not switch to add the next layer. The switching occurs on the next step. Therefore, in case 2 only one model is used in a given prediction horizon. The cost function for case 2 is therefore given by:

$$J = Q\sum_{k=1}^{N_p}\sum_{i=1}^{N_z(l_n)}\left(T(k,i) - r(k,i)\right)^2 + R\sum_{k=1}^{N_p}u(k)^2 \tag{5.13}$$

subjected to:

$$\begin{aligned} x_{k+1} &= f(x_k, u_k) \\ u_{\min} &\leq u \leq u_{\max} \\ x(0) &= x_0 \end{aligned} \tag{5.14}$$

Here, all the parameters are as defined in 5.3.1 and 5.4.2.1

### 5.4.3 SNMPC algorithm for switching system

The algorithms for the SNMPC for case 1 and case 2 are as follows:

#### 5.4.3.1 SNMPC algorithm for case 1

1. Compute the switching instants (from offline open loop optimal control as described in the previous section)

2. At the k-th sampling instant, the values of the manipulated variables, u, at the next $M_p$ sampling instants, u(k), u(k+1), , u(k+$N_P$ -1) are calculated. The control inputs are calculated to minimize the deviations from the reference temperature over the next $N_P$ sampling instants while satisfying the constraints.

3. When the sampling instant is equal to the switching time (new layer addition) the cost function switches from tracking temperature of the existing layers to tracking existing layers and the new layer (the size of the states being tracked increased). From this time to next switching instant the dimension of the states used in the objective function and constraints will be constant.

4. Then the first control move, u(k), is implemented.

5. At the next sampling instant, k+1, the $N_P$ -step control policy is re-calculated for the next $N_P$ sampling instants, k+1 to k+$N_P$ , and implement the first control move, u(k+1).

6. Then Steps 2 and 3 are repeated for subsequent sampling instants.

#### 5.4.3.2 SNMPC algorithm for case 2

1. Compute the switching instants (from offline open loop optimal control as described in the previous section)

2. At the k-th sampling instant, the values of the manipulated variables, u, at the next $M_P$ sampling instants, u(k), u(k+1), , u(k+$N_P$ -1) are calculated.

3. The set of $N_P$ control inputs is calculated to minimize the deviations from the reference temperature over the next $N_P$ sampling instants while satisfying the constraints.

4. When the sampling instant is equal to the switching time (new layer addition) the cost function does not switch (unlike case 1) rather it continues to track the temperatures of the existing layers. It switches from tracking temperature of the existing layers to tracking existing layers and the new layer at the next instant. From this time to next switching instant the dimension of the states used in the cost function and constraints will be constant.

5. Then the first control move, u(k), is implemented.

6. At the next sampling instant, k+1, the $N_P$ -step control policy is re-calculated for the next $N_P$ sampling instants, k+1 to k+$N_P$ , and implement the first control move, u(k+1).

7. Then Steps 2 and 3 are repeated for subsequent sampling instants.

### 5.4.4 Results and Discussion

To demonstrate the effectiveness of the proposed SNMPC approch, three layer fiber-reinforced composite is considered. A prediction horizon of 100s and 10 steps is taken. Following the algorithms for case 1 and case 2 given above, first the results for case 1 is given and later these results will be compared with case 2 results. Figures 5.10 to 5.12 show the reference temperature tracking and the corresponding control effort of bottom layer , middle layer and top layer respectively.

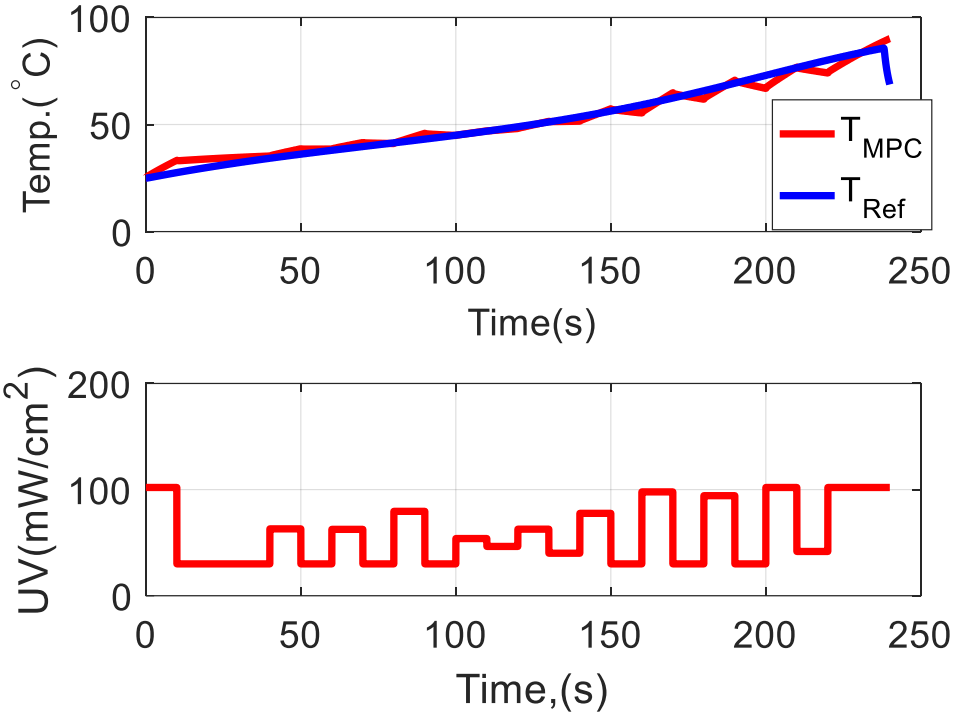


Figure 5.10: Layer 1 temperature tracking and control input

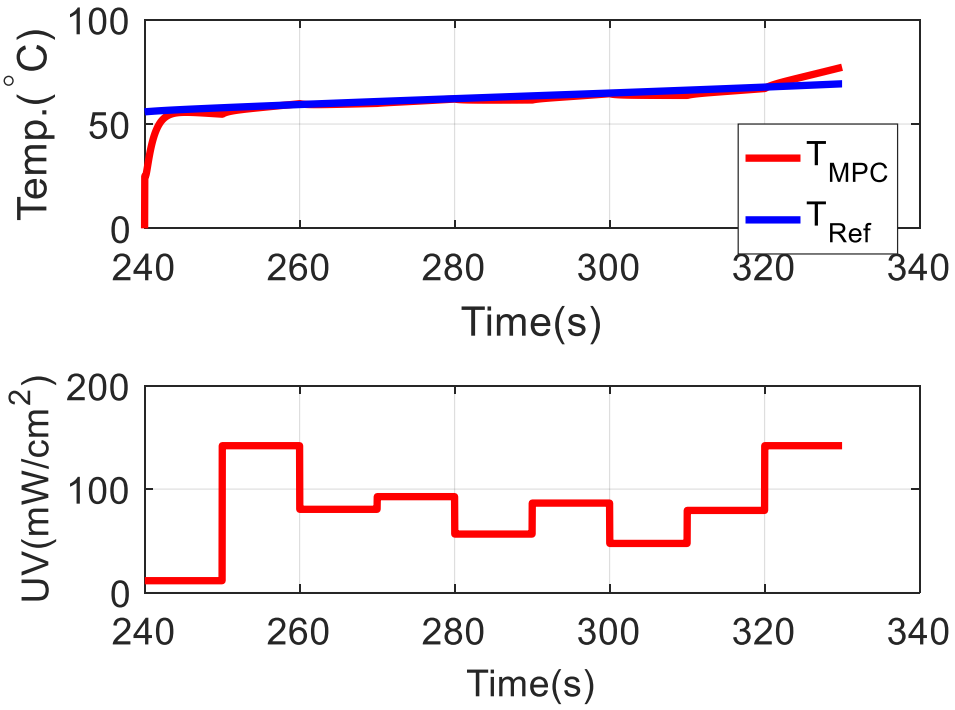


Figure 5.11: Layer 2 temperature tracking and control input

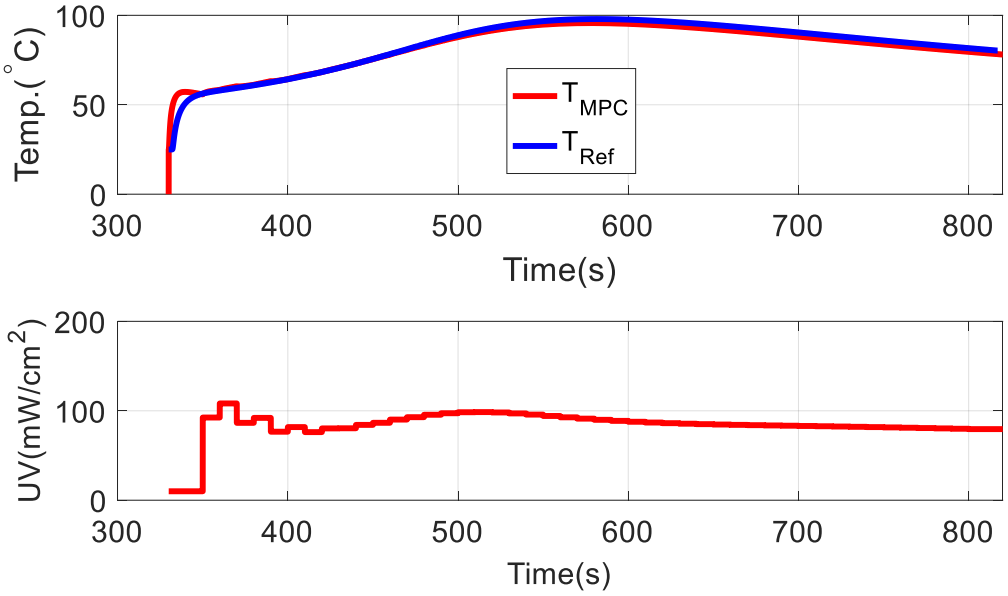


Figure 5.12: Layer 3 temperature tracking and control input

Figure 5.13 depicts the bottom layer reference temperature and the results of

SNMPC for all layers for the case 1. As can be seen in the figure, there is a very good agreement of the reference temperature and the SNMPC temperatures. To avoid confusion, the temperatures from SNMPC of all layers are compared with the bottom reference temperature, so the deviation seen close to the end is mainly from the spacial difference of the nodes considered.

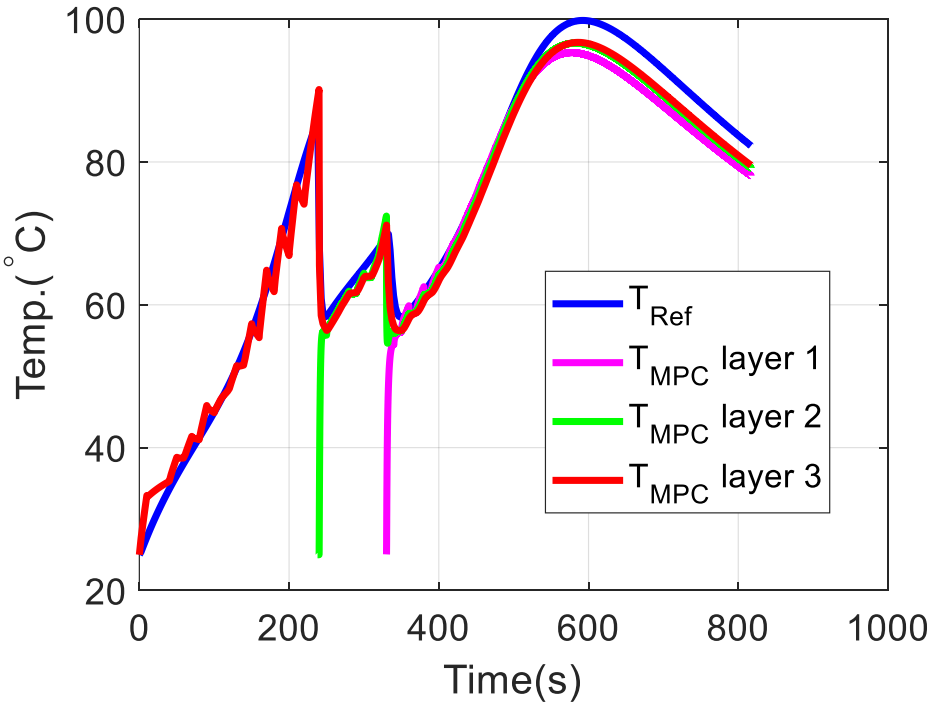


Figure 5.13: Comparison of three layers SNMPC temperature with bottom layer reference temperature

The results from case 1 are then compared with case 2. Figure 5.14 shows the SNMPC reference tracking case 1 and case 2. As one would expect at the interface case 1 has better tracking performance than that of case 2. Similarly, the middle and top layer reference temperature is compared with the corresponding SNMPC temperature evolution for both case1 and case 2. The results are shown in Fig. 5.15,5.16

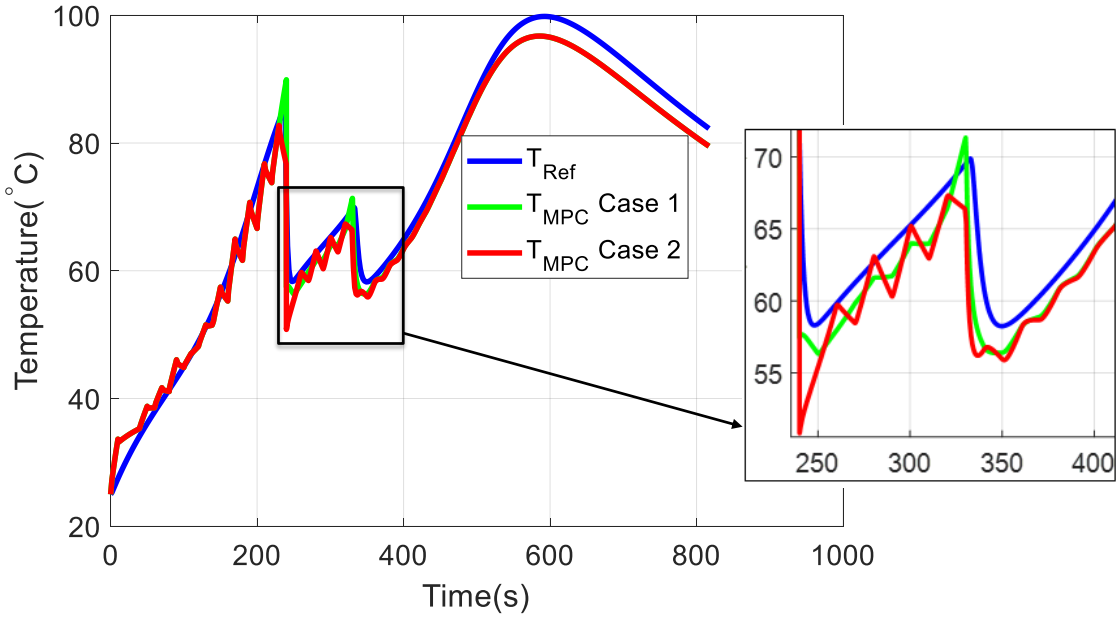


Figure 5.14: SNMPC reference temperature tracking for the bottom layer

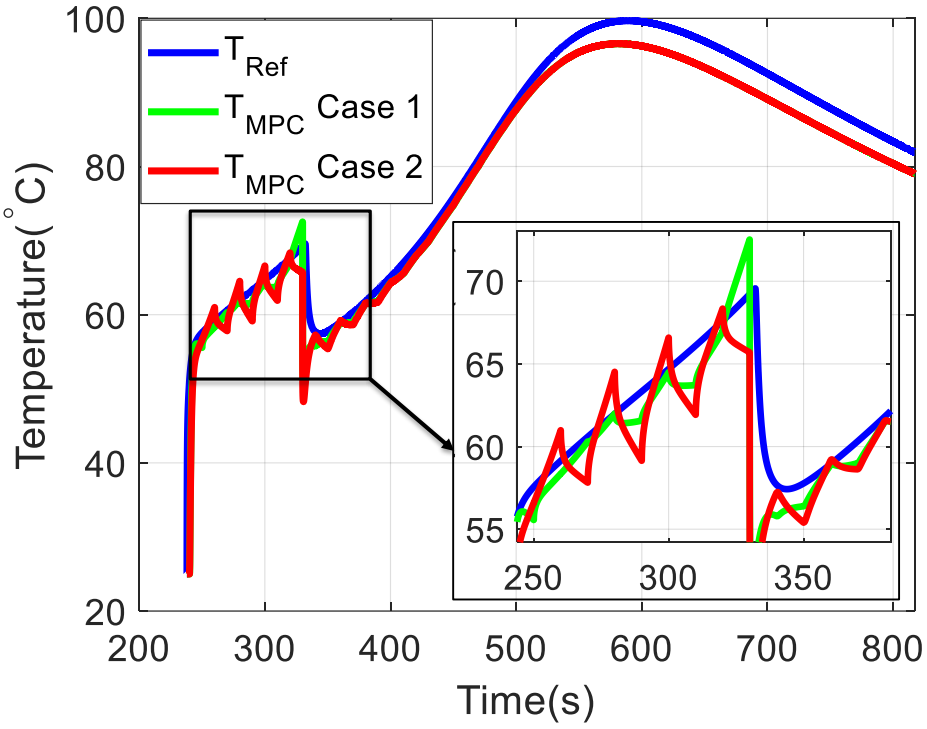


Figure 5.15: SNMPC reference temperature tracking for the middle layer

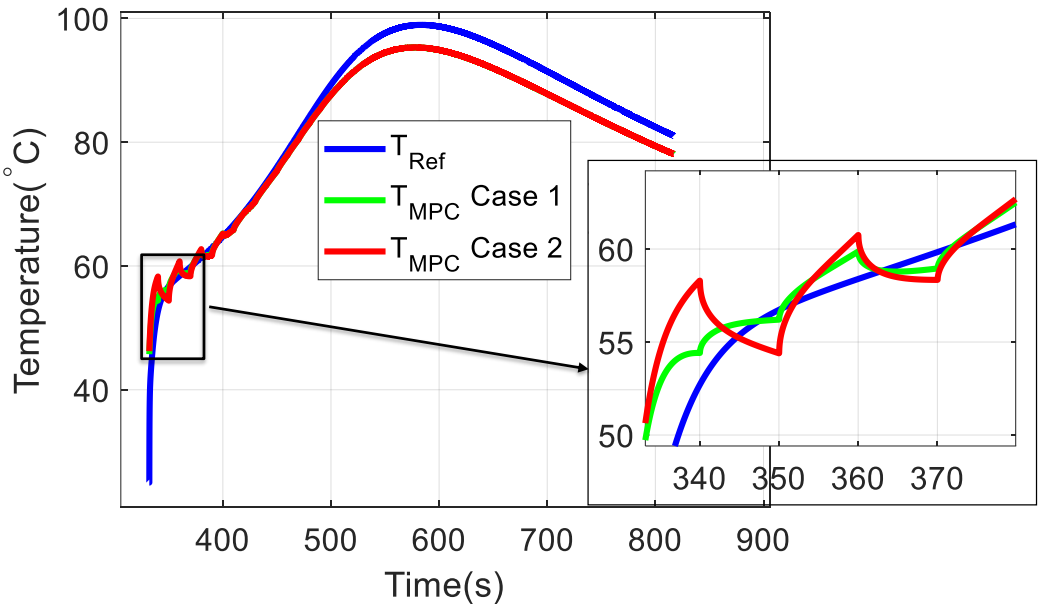


Figure 5.16: SNMPC reference temperature tracking for the top layer

Here the reference temperature is tracked

## 5.5 Conclusion

In this chapter, online control method with NMPC is proposed for both single layer of material and for multi-layer. First, a nonlinear model predictive control (NMPC) scheme is outlined for UV-induced acrylate-based curing of a single layer thick composite part. Then, the model is extended for switching nonlinear model predictive control (SNMPC) for layer-by-layer curing process. The key characteristic is that the processes model switches when a new layer is added to the existing layer. Open loop optimal control is used to determine the optimal layering time and temperature profile which give a nearly uniform cure distribution of a thick composite material. Once the temperature trajectory and optimal time sequences are found, the SNMPC is implemented for online control. The objective is to determine theoretical

optimal behavior which are then used for online SNMPC for tracking the reference temperature distribution. To demonstrate the effectiveness of the proposed approach a three-layer fiber-reinforced resin with two cases are considered and results show a very good agreement between the reference temperature distribution and SNMPC for both cases. However, as expected the interface the a cost function with switching cost has shown a better performance.

# Chapter 6

# Conclusions and Future Work

## 6.1 Conclusions

This dissertation documents an investigation into ultraviolet (UV) induced curing and layering processes including schemes for their optimization and control. First, a curing process model is developed that is comprised of the coupled cure-kinetics and thermal evolution for a cationic polymerization of a single layer of material. This model is then extended to the process of concurrent layering and curing of multiple layers. The model for processing multiple layers is characterized as a multi-mode system that switches modes both when the UV source is turned off and when a new layer is added. A computational framework is outlined for determining the optimal sequence of switching times that gives a minimal cure level deviation across all layers subjected to the multi-mode system model of the process. For validation purposes, a one layer material with two mode has been considered. Comparison of the hardness of a sample cured with optimal switching time versus another sample cured for a longer time showed similar hardness values while using energy/ total time.

To improve the inter-laminar shear strength, the effect of in-situ consolidation

pressure on the inter-laminar shear strength of the final product is assessed experimentally. Using the optimal time sequence, a fiber-reinforced composite is made with in-situ consolidation and curing. The results showed that thick composite parts fabricated with in-situ consolidation and UV curing process, with the optimal sequence, showed increased inter-laminar shear strength with increases of the consolidation pressure up to a certain point. An increase in consolidation pressure beyond this point decreased the inter-laminar shear strength. Scanning electron microscopy (SEM) is used to investigate the effect of compaction on the microstructure of the final cured product.

For online control, first, a nonlinear model predictive control (NMPC) scheme is outlined for UV-induced acrylate-based curing of a single layer thick composite part. Then, the model is extended for switching nonlinear model predictive control (SNMPC) for layer-by-layer curing process. The key characteristic is that the processes model switches when a new layer is added to the existing layer. Open loop optimal control is used to determine the optimal layering time and temperature profile which give a nearly uniform cure distribution of a thick composite material. Once the temperature trajectory and optimal time sequences are found, the SNMPC is implemented for online control. The objective is to determine theoretical optimal behavior which are then used for online SNMPC for tracking the reference temperature distribution. To demonstrate the effectiveness of the proposed approach a three-layer fiber-reinforced resin is considered and results show a very good agreement between the reference temperature distribution and SNMPC.

## 6.2 Future Works

The potential recommendations for future works are :

1. Development of measurement mechanism for degree of cure: Degree of cure state has been considered in many researchers as unmeasurable/difficult to measure. However, dielectric analysis (DEA) or dielectric cure monitoring is a thermal analysis technique for determining cure state. So the potential future work related to this dissertation is to develop /customize the already existing DEA to monitoring of UV-induced layer-by-layer cure process.

2. Robust switching nonlinear model predictive control for radiation induced layer-by-layer curing process for both cationic and free radical polymerization considering noise and/or parameter uncertainity.

# Appendices

# Appendix A

The state space model given in (2.18) is solved by converting the PDE to a set of ODEs indexed by the spatial discretization of the domain. This is done using the method of lines, with the central difference approach of approximating the spatial derivatives in the temperature PDE. Each layer discussed in Section 2.3 is discretized in the same manner. So, as a layer is added, the size of the state-space increases by twice the spatial discretization of each layer. The ODEs for the temperature state take the following form. Note that each equation is coupled to the local cure rates.

$$\dot{T}_j = \begin{bmatrix} -(C_T+2)a & 2a & 0 & ... & 0 & 0 & 0 \\ a & -2a & a & \cdots & 0 & 0 & 0 \\ 0 & a & -2a & \cdots & 0 & 0 & 0 \\ \vdots & \vdots & \vdots & \ddots & \vdots & \vdots & \vdots \\ 0 & 0 & 0 & \cdots & -2a & 0 & 0 \\ 0 & 0 & 0 & \cdots & a & -2a & a \\ 0 & 0 & 0 & \cdots & 0 & 2a & -2a \end{bmatrix} \begin{bmatrix} T_1 \\ T_2 \\ T_3 \\ \vdots \\ T_{n_j-2} \\ T_{n_j-1} \\ T_{n_j} \end{bmatrix} + b \begin{bmatrix} \dot{\alpha}_1 \\ \dot{\alpha}_2 \\ \dot{\alpha}_3 \\ \vdots \\ \dot{\alpha}_{n_j-2} \\ \dot{\alpha}_{n_j-1} \\ \dot{\alpha}_{n_j} \end{bmatrix} + a \begin{bmatrix} C_1 T_\infty \\ 0 \\ 0 \\ \vdots \\ 0 \\ 0 \\ 0 \end{bmatrix}$$

The local cure rates take different forms based on whether the UV is on or off.

Case 1: When UV is on

$$\dot{\alpha}_{2i-1} = d \begin{bmatrix} \exp(-E/RT_1)(1+\exp(-\phi I_0^p \exp(-\lambda \times 0))(1-\alpha_1) \\ \exp(-E/RT_2)(1+\exp(-\phi I_0^p \exp(-\lambda \times dz))(1-\alpha_2) \\ \vdots \\ \exp(-E/RT_{n_j-1})(1+\exp(-\phi I_0^p \exp(-\lambda \times (n_j-1))(1-\alpha_{n_j}) \\ \exp(-E/RT_{n_j})(1+\exp(-\phi I_0^p \exp(-\lambda \times n_j-1))(1-\alpha_{n_j}) \end{bmatrix}$$

Case 2: When UV is off

$$\dot{\alpha}_{2i} = d \begin{bmatrix} \exp(-E/RT_1)[1-\exp(-k_i t_s D)](1-\alpha_1) \\ \exp(-E/RT_2)[1-\exp(-k_i t_s D)](1-\alpha_2) \\ \vdots \\ \exp(-E/RT_{n_j-1})[1-\exp(-k_i t_s D)](1-\alpha_{n_j-1}) \\ \exp(-E/RT_{n_j})[1-\exp(-k_i t_s D)](1-\alpha_{n_j}) \end{bmatrix}$$

The above equations assume parameters such as density $\rho$, thermal conductivity $k_z$ and specific heat capacity $c_p$ to take on average constant values. The coefficients $a$, $b$ and $d$ are given as follows:

$$a = k_z/dz^2\rho c_p,\ \ b = \Delta H/c_p,\ \ C_T = 2dzh/k_z, C_I = 2dz\vartheta/kz,\ \ dz = l/(n_j-1),\ \ d = C_0 k_0.$$

# Bibliography


[1] P. K. Mallick, *Fiber-reinforced composites: materials, manufacturing, and design*. CRC press, 2007.

[2] H. Helms, U. Lambrecht, and U. Höpfner, "Energy savings by light-weighting final report," *Institute for Energy and Environmental Research (IFEU): Heidelberg, Germany*, 2003.

[3] D. L. Greene, "Commercial air transport energy use and emissions: Is technology enough?.," 1995.

[4] J. J. Lee, S. P. Lukachko, I. A. Waitz, and A. Schafer, "Historical and future trends in aircraft performance, cost, and emissions," *Annual Review of Energy and the Environment*, vol. 26, no. 1, pp. 167–200, 2001.

[5] E. Kroll and D. Artzi, "Enhancing aerospace engineering students' learning with 3d printing wind-tunnel models," *Rapid Prototyping Journal*, vol. 17, no. 5, pp. 393–402, 2011.

[6] K. V. Wong and A. Hernandez, "A review of additive manufacturing," *ISRN Mechanical Engineering*, vol. 2012, 2012.

[7] O. S. Carneiro, A. Silva, and R. Gomes, "Fused deposition modeling with polypropylene," *Materials & Design*, vol. 83, pp. 768–776, 2015.

[8] H. G. Kia, N. Huang, J. P. Spicer, and J. F. Arinez, "Additive manufacturing of a unibody vehicle," May 18 2017. US Patent App. 14/940,926.

[9] S. V. Murphy and A. Atala, "3d bioprinting of tissues and organs," *Nature biotechnology*, vol. 32, no. 8, p. 773, 2014.

[10] L. E. Murr, *Handbook of materials structures, properties, processing and performance*. Springer, 2015.

[11] L. E. Murr, "Frontiers of 3d printing/additive manufacturing: from human organs to aircraft fabrication," *Journal of Materials Science & Technology*, vol. 32, no. 10, pp. 987–995, 2016.

[12] M. Ashby, "The ces edupack resource booklet 2: Material and process charts," *Cambridge University, Cambridge, UK*, 2009.

[13] "UV induced polymerization." `https://www.globalspec.com/learnmore/optics_optical_components/light_sources/process_uv_lamps_systems`. Accessed: 2019-04-24.

[14] "Free radical polymerization mechanism." `https://www.pcimag.com/articles/85843-the-use-of-specialty-acrylic-esters-in-cure-in-place-coating-technology`. Accessed: 2019-04-24.

[15] R. Schwalm, *UV coatings: basics, recent developments and new applications*. Elsevier, 2006.

[16] A. Vitale, M. Sangermano, R. Bongiovanni, P. Burtscher, and N. Moszner, "Visible light curable restorative composites for dental applications based on epoxy monomer," *Materials*, vol. 7, no. 1, pp. 554–562, 2014.

[17] J. Lee, *Cationic polymerization of glycidyl ethers and furans: improved electron beam and UV cured epoxy networks*. PhD thesis, Drexel University, 2007.

[18] A. Endruweit, M. Johnson, and A. Long, "Curing of composite components by ultraviolet radiation: A review," *Polymer composites*, vol. 27, no. 2, pp. 119–128, 2006.

[19] A. Yebi and B. Ayalew, "A hybrid modeling and optimal control framework for layer-by-layer radiative processing of thick sections," in *American Control Conference (ACC), 2015*, pp. 3619–3624, IEEE, 2015.

[20] W. Shi and B. Rånby, "Uv curing of composites based on modified unsaturated polyester," *Journal of applied polymer science*, vol. 51, no. 6, pp. 1129–1139, 1994.

[21] C. Decker, "Uv-radiation curing chemistry," *Pigment & resin technology*, vol. 30, no. 5, pp. 278–286, 2001.

[22] J. M. Matias, P. J. Bartolo, and A. V. Pontes, "Modeling and simulation of photofabrication processes using unsaturated polyester resins," *Journal of applied polymer science*, vol. 114, no. 6, pp. 3673–3685, 2009.

[23] A. Yebi and B. Ayalew, "Feedback compensation of the in-domain attenuation of inputs in diffusion processes," in *American Control Conference (ACC), 2013*, pp. 2092–2097, IEEE, 2013.

[24] A. Yebi, B. Ayalew, and S. Dey, "Observer design for state estimation of uv curing processes," in *ASME 2014 Dynamic Systems and Control Conference*, pp. V002T24A005–V002T24A005, American Society of Mechanical Engineers, 2014.

[25] A. Yebi and B. Ayalew, "Partial differential equation-based process control for ultraviolet curing of thick film resins," *Journal of Dynamic Systems, Measurement, and Control*, vol. 137, no. 10, p. 101010, 2015.

[26] Y. Duan, J. Li, W. Zhong, R. G. Maguire, G. Zhao, H. Xie, D. Li, and B. Lu, "Effects of compaction and uv exposure on performance of acrylate/glass-fiber composites cured layer by layer," *Journal of Applied Polymer Science*, vol. 123, no. 6, pp. 3799–3805, 2012.

[27] I. Tena, J. Arakama, M. Sarrionandia, J. Aurrekoetxea, and J. Torre, "Effect of thickness on the interfacial strenght of layer by layer in situ uv curing," *European Conference on Composite Materials, Venice, Itly, 2012*, 2012.

[28] A. Yebi and B. Ayalew, "Optimal layering time control for stepped-concurrent radiative curing process," *Journal of Manufacturing Science and Engineering*, vol. 137, no. 1, p. 011020, 2015.

[29] A. Yebi, B. Ayalew, and S. Pilla, "Control-oriented model verification for uv processing of composite laminate," *Society for the Advancement of Material and Process Engineering (SAMPE), Baltimore, MD*, 2015.

[30] P. J. Bártolo, *Stereolithography: materials, processes and applications*. Springer Science & Business Media, 2011.

[31] B. A. Ficek, A. M. Thiesen, and A. B. Scranton, "Cationic photopolymerizations of thick polymer systems: Active center lifetime and mobility," *European polymer journal*, vol. 44, no. 1, pp. 98–105, 2008.

[32] M. Sangermano, N. Razza, and J. V. Crivello, "Cationic uv-curing: Technology and applications," *Macromolecular Materials and Engineering*, vol. 299, no. 7, pp. 775–793, 2014.

[33] M. Mascioni, N. N. Ghosh, J. M. Sands, and G. R. Palmese, "Electron beam and uv cationic polymerization of glycidyl ethers–part i: Reaction of monofunctional phenyl glycidyl ether," *Journal of Applied Polymer Science*, vol. 130, no. 1, pp. 479–486, 2013.

[34] A. Yebi and B. Ayalew, "Model-based optimal control of layering time for layer-by-layer uv processing of resin infused laminates," in *American Control Conference (ACC), 2016*, pp. 827–832, IEEE, 2016.

[35] D. E. Kirk, *Optimal control theory: an introduction*. Courier Corporation, 2012.

[36] T. R. Mehta, D. Yeung, E. I. Verriest, and M. Egerstedt, "Optimal control of multi-dimensional, hybrid ice-skater model," in *American Control Conference, ACC*, pp. 2787–2792, IEEE, 2007.

[37] Y. Wardi, M. Egerstedt, and M. Hale, "Switched-mode systems: gradient-descent algorithms with armijo step sizes," *Discrete Event Dynamic Systems*, vol. 25, no. 4, pp. 571–599, 2015.

[38] A. Yousefi, P. Lafleur, and R. Gauvin, "Kinetic studies of thermoset cure reactions: a review," *Polymer Composites*, vol. 18, no. 2, pp. 157–168, 1997.

[39] A. Kausar, "Role of thermosetting polymer in structural composite," *American Journal of Polymer Science & Engineering*, vol. 5, no. 1, pp. 1–12, 2017.

[40] J.-M. Raquez, M. Deléglise, M.-F. Lacrampe, and P. Krawczak, "Thermosetting (bio) materials derived from renewable resources: a critical review," *Progress in polymer science*, vol. 35, no. 4, pp. 487–509, 2010.

[41] A. Yebi and B. Ayalew, "Hybrid modeling and robust control for layer-by-layer manufacturing processes," *IEEE Transactions on Control Systems Technology*, vol. 25, no. 2, pp. 550–562, 2017.

[42] P. J. Biermann, J. H. Cranmer, C. A. Nove, and L. M. Brown, "End-of-cure sensing using ultrasonics for autoclave fabrication of composites," in *Nondestructive Evaluation for Process Control in Manufacturing*, vol. 2948, pp. 72–84, International Society for Optics and Photonics, 1996.

[43] D. Abliz, Y. Duan, L. Steuernagel, L. Xie, D. Li, and G. Ziegmann, "Curing methods for advanced polymer composites-a review," *Polymers & Polymer Composites*, vol. 21, no. 6, pp. 341–348, 2013.

[44] P. Garra, C. Dietlin, F. Morlet-Savary, F. Dumur, D. Gigmes, J.-P. Fouassier, and J. Lalevée, "Photopolymerization processes of thick films and in shadow areas: a review for the access to composites," *Polymer Chemistry*, vol. 8, no. 46, pp. 7088–7101, 2017.

[45] M. Atif, R. Bongiovanni, and J. Yang, "Cationically uv-cured epoxy composites," *Polymer Reviews*, vol. 55, no. 1, pp. 90–106, 2015.

[46] M. Sangermano, A. D'Anna, C. Marro, N. Klikovits, and R. Liska, "Uv-activated frontal polymerization of glass fibre reinforced epoxy composites," *Composites Part B: Engineering*, vol. 143, pp. 168–171, 2018.

[47] S. Parthasarathy, S. C. Mantell, and K. A. Stelson, "Estimation, control and optimization of curing in thick-sectioned composite parts," *Journal of Dynamic Systems, Measurement, and Control(Transactions of the ASME)*, vol. 126, no. 4, pp. 824–833, 2004.

[48] V. Voytekunas-Abadie and F. Ng, "Alternative curing methods for structural epoxy resins," tech. rep., SIMTech Technical Reports 2010, 2010.

[49] D. Kirk, "An introduction to optimal control theory," *Englewood Cliffs, NI Prentice Hall*, 1970.

[50] J.-P. Kruth, G. Levy, F. Klocke, and T. Childs, "Consolidation phenomena in laser and powder-bed based layered manufacturing," *CIRP annals*, vol. 56, no. 2, pp. 730–759, 2007.

[51] R. Mailunas, "Laminated object manufacturing-based design ceramic matrix composites," tech. rep., NORTHROP GRUMMAN CORP BETHPAGE NY, 2001.

[52] P. Parandoush and D. Lin, "A review on additive manufacturing of polymer-fiber composites," *Composite Structures*, vol. 182, pp. 36–53, 2017.

[53] D. Olivier, J. A. Travieso-Rodriguez, S. Borros, G. Reyes, and R. Jerez-Mesa, "Influence of building orientation on the flexural strength of laminated object manufacturing specimens," *Journal of mechanical science and technology*, vol. 31, no. 1, pp. 133–139, 2017.

[54] L. Esposito, L. Sorrentino, F. Penta, and C. Bellini, "Effect of curing overheating on interlaminar shear strength and its modelling in thick frp laminates," *The International Journal of Advanced Manufacturing Technology*, vol. 87, no. 5-8, pp. 2213–2220, 2016.

[55] X. Zhang, Y. Duan, X. Zhao, and D. Li, "Uv stepwise cured fabrication of glass fiber/acrylate composites: Effects of exposure dose on curing uniformity and interlaminar shear strength," *Journal of Composite Materials*, vol. 50, no. 10, pp. 1395–1401, 2016.

[56] A. Vlot and J. W. Gunnink, *Fibre metal laminates: an introduction*. Springer Science & Business Media, 2011.

[57] S. D. Beyene, B. Ayalew, and S. Pilla, "Optimal switching time control of uv induced cationic curing process," in *ASME 2018 Dynamic Systems and Control Conference*, pp. V002T23A004–V002T23A004, American Society of Mechanical Engineers, 2018.

[58] S. D. Beyene, B. Ayalew, and S. Pilla, "Effects of in-situ compaction and uv-curing on the performance of glass fiber-reinforced polymer composite cured layer by layer," in *Proceedings of the Solid Freeform Fabrication Symposium, Austin, TX, USA*, 2018.

[59] A. Mitchell and D. Griffiths, "The finite difference method in partial differential equations," *New York*, 1980.

[60] L. Nele, A. Caggiano, and R. Teti, "Autoclave cycle optimization for high performance composite parts manufacturing," *Procedia CIRP*, vol. 57, pp. 241–246, 2016.

[61] F. Sharafeddin, H. Nouri, and F. Koohpeima, "The effect of temperature on shear bond strength of clearfil se bond and adper single bond adhesive systems to dentin," *Journal of Dentistry*, vol. 16, no. 1, p. 10, 2015.

[62] L. Yang, J. Yang, J. Nie, and X. Zhu, "Temperature controlled cationic photocuring of a thick, dark composite," *RSC Advances*, vol. 7, no. 7, pp. 4046–4053, 2017.

[63] J.-D. Cho and J.-W. Hong, "Photo-curing kinetics for the uv-initiated cationic polymerization of a cycloaliphatic diepoxide system photosensitized by thioxanthone," *European Polymer Journal*, vol. 41, no. 2, pp. 367–374, 2005.

[64] S. D. Beyene, B. Ayalew, A. B. Kousaalya, and S. Pilla, "Model-based optimal switching time control of uv-induced cationic curing of diglycidyl ether bisphenol a," in *SAMPE 2018 Conference Proceedings*, Society for the Advancement of Material and Process Engineering North America, 2018. (Accepted).

[65] M. G. González, J. C. Cabanelas, and J. Baselga, "Applications of ftir on epoxy resins-identification, monitoring the curing process, phase separation and water uptake," in *Infrared Spectroscopy-Materials Science, Engineering and Technology*, InTech, 2012.

[66] A. Cherdoud-Chihani, M. Mouzali, and M. Abadie, "Study of crosslinking acid copolymer/dgeba systems by ftir," *Journal of applied polymer science*, vol. 87, no. 13, pp. 2033–2051, 2003.

[67] D. S. Achilias, M. M. Karabela, E. A. Varkopoulou, and I. D. Sideridou, "Cure kinetics study of two epoxy systems with fourier tranform infrared spectroscopy (ftir) and differential scanning calorimetry (dsc)," *Journal of Macromolecular Science, Part A*, vol. 49, no. 8, pp. 630–638, 2012.

[68] Y. Fu, D. Sun, X. Liu, X. An, and X. Zhang, "The curing kinetic analysis of epoxy base on ft-ir," in *3rd International Conference on Material, Mechanical and Manufacturing Engineering (IC3ME 2015)*, Atlantis Press, 2015.

[69] S. D. Beyene, B. Ayalew, and S. Pilla, "On the inter-laminar shear strength of composites manufactured via a stepped-concurrent uv curing and layering process," *Composite Materials*, 2019.

[70] E. C. Botelho, R. A. Silva, L. C. Pardini, and M. C. Rezende, "A review on the development and properties of continuous fiber/epoxy/aluminum hybrid composites for aircraft structures," *Materials Research*, vol. 9, no. 3, pp. 247–256, 2006.

[71] *Standard test method for short-beam strength of polymer matrix composite materials and their laminates*. ASTM International, 2006.

[72] Z. Fan, M. H. Santare, and S. G. Advani, "Interlaminar shear strength of glass fiber reinforced epoxy composites enhanced with multi-walled carbon nanotubes," *Composites Part A: Applied science and manufacturing*, vol. 39, no. 3, pp. 540–554, 2008.

[73] D.-J. Lee and I. Palley, "Simple model to predict the interlaminar shear strength of laminate composites," *Journal of Composite Materials*, vol. 46, no. 11, pp. 1357–1365, 2012.

[74] D. G. Lee and S. S. Cheon, "Impact characteristics of glass fiber composites with respect to fiber volume fraction," *Journal of Composite materials*, vol. 35, no. 1, pp. 27–56, 2001.

[75] W. J. Joost, "Reducing vehicle weight and improving us energy efficiency using integrated computational materials engineering," *Jom*, vol. 64, no. 9, pp. 1032–1038, 2012.

[76] D. Hrovat and J. Sun, "Models and control methodologies for ic engine idle speed control design," *Control Engineering Practice*, vol. 5, no. 8, pp. 1093–1100, 1997.

[77] J. R. Anderson, B. Ayalew, and T. Weiskircher, "Modeling a professional driver in ultra-high performance maneuvers with a hybrid cost mpc," in *2016 American Control Conference (ACC)*, pp. 1981–1986, IEEE, 2016.

[78] Q. Wang, T. Weiskircher, and B. Ayalew, "Hierarchical hybrid predictive control of an autonomous road vehicle," in *ASME 2015 Dynamic Systems and Control Conference*, pp. V003T50A006–V003T50A006, American Society of Mechanical Engineers, 2015.

[79] N. Slegers, J. Kyle, and M. Costello, "Nonlinear model predictive control technique for unmanned air vehicles," *Journal of guidance, control, and dynamics*, vol. 29, no. 5, pp. 1179–1188, 2006.

[80] N. Slegers and M. Costello, "Model predictive control of a parafoil and payload system," *Journal of Guidance, Control, and Dynamics*, vol. 28, no. 4, pp. 816–821, 2005.

[81] Q. Wang and R. F. Stengel, "Robust nonlinear control of a hypersonic aircraft," *Journal of guidance, control, and dynamics*, vol. 23, no. 4, pp. 577–585, 2000.

[82] X. Cao and B. Ayalew, "Multivariable predictive control of laser-aided powder deposition processes," in *2015 American Control Conference (ACC)*, pp. 3625–3630, IEEE, 2015.

[83] D. Hrovat, S. Di Cairano, H. E. Tseng, and I. V. Kolmanovsky, "The development of model predictive control in automotive industry: A survey," in *2012 IEEE International Conference on Control Applications*, pp. 295–302, IEEE, 2012.

[84] M. Pisaturo, M. Cirrincione, and A. Senatore, "Multiple constrained mpc design for automotive dry clutch engagement," *IEEE/ASME Transactions on Mechatronics*, vol. 20, no. 1, pp. 469–480, 2015.

[85] T. Weiskircher and B. Ayalew, "Predictive trajectory guidance for (semi-) autonomous vehicles in public traffic," in *2015 American Control Conference (ACC)*, pp. 3328–3333, IEEE, 2015.

[86] S. Gros, R. Quirynen, and M. Diehl, "Aircraft control based on fast non-linear mpc & multiple-shooting," in *2012 IEEE 51st IEEE Conference on Decision and Control (CDC)*, pp. 1142–1147, IEEE, 2012.

[87] J. B. Rawlings and D. Q. Mayne, *Model predictive control: Theory and design*. Nob Hill Pub. Madison, Wisconsin, 2009.

[88] C. Bordons and E. Camacho, "Model predictive control (advanced textbooks in control and signal processing)," 2004.

[89] P. D. Christofides, R. Scattolini, D. M. de la Pena, and J. Liu, "Distributed model predictive control: a tutorial review," *Proc. Chem. Process Control*, vol. 8, p. 22pp, 2012.

[90] I. Bonis, W. Xie, and C. Theodoropoulos, "A linear model predictive control algorithm for nonlinear large-scale distributed parameter systems," *AIChE Journal*, vol. 58, no. 3, pp. 801–811, 2012.

[91] H. Shang, J. F. Forbes, and M. Guay, "Characteristics-based model predictive control of distributed parameter systems," in *Proceedings of the 2002 American Control Conference (IEEE Cat. No. CH37301)*, vol. 6, pp. 4383–4388, IEEE, 2002.

[92] M. M. Thomas, J. Kardos, and B. Joseph, "Shrinking horizon model predictive control applied to autoclave curing of composite laminate materials," in *Proceedings of 1994 American Control Conference-ACC'94*, vol. 1, pp. 505–509, IEEE, 1994.

[93] P. Bartolo and G. Mitchell, "Stereo-thermal-lithography: a new principle for rapid prototyping," *Rapid Prototyping Journal*, vol. 9, no. 3, pp. 150–156, 2003.

[94] V. K. Pillai, A. N. Beris, and P. S. Dhurjati, "Implementation of model-based optimal temperature profiles for autoclave curing of composites using a knowledge-based system," *Industrial & engineering chemistry research*, vol. 33, no. 10, pp. 2443–2452, 1994.

[95] P. Dufour, F. Couenne, and Y. Touré, "Model predictive control of a catalytic reverse flow reactor," *IEEE Transactions on control systems technology*, vol. 11, no. 5, pp. 705–714, 2003.

[96] P. Dufour, D. J. Michaud, Y. Touré, and P. S. Dhurjati, "A partial differential equation model predictive control strategy: application to autoclave composite processing," *Computers & chemical engineering*, vol. 28, no. 4, pp. 545–556, 2004.

[97] V. Pillai, A. N. Beris, and P. Dhurjati, "Intelligent curing of thick composites using a knowledge-based system," *Journal of composite materials*, vol. 31, no. 1, pp. 22–51, 1997.